Title
New Development in the Calculation of Beta-Strength Functions

Authors
Moller, P.
Randrup, Jorgen

Publication Date
1989-08-01

LBL-27504
Preprint

Lawrence Berkeley Laboratory
UNIVERSITY OF CALIFORNIA

Submitted to Nuclear Physics A

New Developments in the Calculation of β—Strength Functions

P. Möller and J. Randrup

August 1989

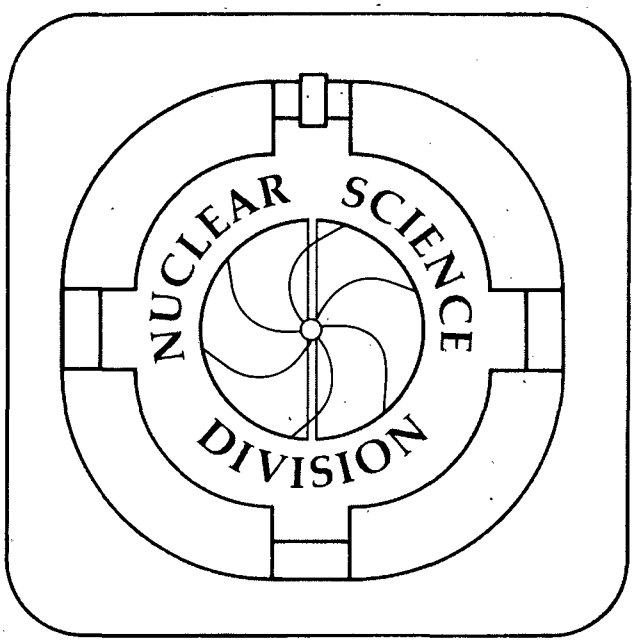

Prepared for the U.S. Department of Energy under Contract Number DE-AC03-76SF00098.

DISCLAIMER

LBL-27504

NEW DEVELOPMENTS IN THE CALCULATION OF β–STRENGTH FUNCTIONS*

PETER MÖLLER[1]
Idaho National Engineering Laboratory, EG&G Idaho, Inc., Idaho Falls, Idaho 83415

JØRGEN RANDRUP
Lawrence Berkeley Laboratory, Nuclear Science Division, University of California, Berkeley, California 94720

August 11, 1989

Abstract:

We have further developed a QRPA model that uses single-particle levels and wave-functions as the starting point for calculating Gamow-Teller β-strength functions. In our enhanced version Nilsson, Woods-Saxon, or folded-Yukawa wave functions and single-particle energies may serve as the starting point for determining the wave functions of the mother and daughter nuclei involved in the β decay. Pairing may be treated in either the BCS or the Lipkin-Nogami approximation. To account for the retardation of low-energy GT decay rates we add, as in the earlier model, a simple residual interaction specific to GT decay, namely $V_{GT} = :\beta^{1-} \cdot \beta^{1+}:$, to the Hamiltonian. This residual interaction is studied in the RPA approximation. In the case of odd-mass nuclei the $\Delta v = 0$ transitions are generally treated in a first-order perturbation expansion. We found that these expansions occasionally break down, and have modified them to avoid the singularities. The odd-odd case is treated in a way analogous to the odd-A case by considering one or the other of the odd particles as a spectator for $\Delta v = 0$ and both as spectators for $\Delta v = 2$. As a final extension of the earlier model, we also allow the unpaired odd particle to be in an excited state. We use the enhanced model to calculate Gamow-Teller β-strength functions, β-decay half-lives, and β-delayed neutron emission probabilities for nuclei in several regions of the periodic system, but with the main emphasis on the rare-earth region.

*This work has been carried out under the auspices of the US Department of Energy under DOE Contract No. DE-AC07-76IDO1570 (INEL) and was also supported by the Director, Office of Energy Research, Division of Nuclear Physics of the Office of High Energy and Nuclear Physics of the U.S. Department of Energy under contract No. DE-AC03076SF00098 (LBL).

[1]Present address: Theoretical Division, Los Alamos National Laboratory, Los Alamos, NM 87545

1. Introduction

The need to model astrophysical processes and the desire to understand how nuclear structure variations influence β-decay properties, are challenges that have stimulated the development of theoretical models for Gamow-Teller β-strength functions. For astrophysical applications it is necessary to model properties of a large number of nuclei, which limits the complexity of the models that can be considered. Earlier, many calculations of β-strength functions for astrophysical applications were based on the Gross Theory of β-decay [1]). Because this model is statistical in nature it describes only the average properties of the β-strength functions.

To account for structure in the β-strength function it is necessary to use a microscopic model of the nucleus as a starting point for constructing the wave functions and energy levels of the parent and daughter nuclei. Originally studies of this type were limited to spherical nuclei, see for example the studies by Hamamoto [2]), Halbleib and Sorensen [3]), Randrup [4]), and references quoted therein. These models were based on a spherical single-particle model with a pairing interaction treated in the BCS approximation and a residual GT interaction treated in the RPA approximation.

The model for spherical nuclei [2-4]) was extended to deformed nuclei by Krumlinde and Möller [5,6]) and simultaneously by Alkhazov *et al.* [7]). This extended model, which accounts for the effect of the microscopic structure of the nucleus on the shape of the β-strength function, is suitable for surveys of large numbers of nuclei since it allows one β-strength function to be calculated in about only 20 seconds on a CRAY-1 computer, in our implementation. Such studies of large regions of nuclei using this model and its associated computer code have, for example, been made by Kratz *et al.* [8]), Nitschke *et al.* [9]), and Meyer *et al.* [10]). Later, a very similar model has been employed by Bender *et al.* [11]).

The first version of the model developed by Krumlinde and Möller was based on the Nilsson single-particle model. Pairing was treated in the BCS approximation. Here we discuss several extensions of the model. We now have the possibility of basing the calculations on three different single-particle models, namely the Nilsson model, the Woods-Saxon model, or the folded-Yukawa model. Pairing may be treated in either the BCS or the Lipkin-Nogami approximation. The perturbation expressions for the $\Delta v = 0$ transitions have been modified to avoid a singularity. The β-strength functions may be calculated with the odd particle in an excited state, which means that we can study β-decay from a certain class of isomeric states. In sect. 2 we define and discuss these new enhancements of the model and in sect. 3 we apply the enhanced model to studies of some strength functions of particular interest. In sect. 3 we also make a systematic survey of β-decay half-lives in the rare-earth region.

2. Models

The β-strength function for a deformed nucleus can be calculated on the basis of transition matrix elements between intrinsic wave functions [6]). The complexity of the calculation depends essentially only on the model for the intrinsic nuclear wave function. In the approach we follow here, we construct the wave-functions by adding to a

pure single-particle model a pairing interaction and a residual Gamow-Teller interaction which is treated in the RPA approximation. A very simple model would be to treat β decay in the pure single-particle model only. An additional physical effect is added by taking into account the pairing interaction, and a third effect is treated by including a residual GT interaction. In the most simple version, the matrix elements would be calculated from the asymptotic quantum-number assignments in a Nilsson diagram. The admixtures of other wave functions would then be neglected. In our model these admixtures are taken into account, since we calculate all the components of the wave function corresponding to a particular state. In addition we consider the pairing and GT interactions. The addition of these residual interactions changes the complexity of the model from a model where the strength is simply given by selection rules involving the asymptotic quantum numbers to a more complex one. With the present model it takes 20 seconds on a CRAY-1 computer to calculate one strength function. In such a calculation the two RPA equations for σ_0 and $\sigma_\pm$ are each solved for about 1000 roots. We review the major changes and extensions of the model, relative to the earlier version [6]), employing the same notation. One may picture the model as a three-layered model, where each new layer takes into account new physical effects, but thereby increasing the complexity of the model. The three layers are, in increasing order of complexity, the deformed single-particle model, the pairing model, and the residual Gamow-Teller interaction, treated in the quasi-particle random-phase approximation (QRPA).

2.1. SINGLE-PARTICLE MODELS

The starting point of the calculation of the intrinsic nuclear wave-functions is a calculation of levels and wave-functions in a single-particle model. The properties of this underlying single-particle model are very important, because the positions of the peaks in the low-energy part of the β-strength function depend on the positions and the quantum numbers of the single-particle levels in the corresponding Nilsson diagram. Thus, a reliable calculation of the strength function requires that the positions of the single-particle levels are calculated accurately. No amount of refinement in the subsequent layers in the model can compensate for an inaccurate single-particle model. In order to obtain a β-strength model that is accurate over the entire nuclear chart it is therefore essential to employ a single-particle model that provides an accurate description of the band-head energies over the entire periodic system. The addition of pairing and Gamow-Teller residual interactions does not change the location of the peaks in the low-energy part of the spectrum significantly, only the magnitude of the strength is affected. These features are extensively illustrated in our earlier study [6]).

2.1.1. Nilsson modified-oscillator model

The use of the Nilsson model in the first version [6]) of the deformed quasi-particle

random-phase code was motivated both by its basic computational simplicity and the considerable experience accumulated from applications of the model to the calculation of a variety nuclear properties, such as ground-state spins and deformations for nuclei in several regions of the periodic system. In the Nilsson model the single-particle potential is given by

$$V = \frac{1}{2}\hbar\omega_0{\rho_t}^2\left[1-\frac{2}{3}\epsilon_2 P_2(\cos\theta_t)+2\epsilon_4 P_4(\cos\theta_t)\right]-V_{\rm corr}$$

$$V_{\rm corr} = \hbar\mathring{\omega}_0\left[2\kappa\,\boldsymbol{l}_t\cdot\boldsymbol{s}+\kappa\mu\left({\boldsymbol{l}_t}^2-<{\boldsymbol{l}_t}^2>_N\right)\right] \quad (1)$$

In this expression for the potential, κ is the spin-orbit strength parameter and the product $\kappa\mu$ is a diffuseness parameter. These parameters are determined by adjusting the positions of calculated single-particles levels to experimental band-head energies. A deficiency of the Nilsson model is that the potential goes to infinity at large distances and that the diffuseness of the single-particle potential is simulated, close to the Fermi surface, by the ${\boldsymbol{l}_t}^2$ term. These features are partly responsible for a somewhat unpredictable variation of the model parameters between different regions of the nuclear chart, a feature that makes it difficult to extrapolate the parameters to unknown regions of nuclei.

We have now acquired experience[12–14]) with applying the folded-Yukawa model to the calculation of nuclear properties such as deformation and ground-state masses throughout the periodic system. In order to overcome some of the deficiencies associated with the Nilsson model and to obtain a more unified description of nuclear-structure properties, we have incorporated the possibility of using folded-Yukawa single-particle levels and wave-functions as the starting point for generating the intrinsic nuclear wave functions. As a first step in this direction, a Woods-Saxon single-particle potential was included in our β-strength model a few years ago[15]).

2.1.2. Woods-Saxon model

We will only show a limited set of results obtained by use of a Woods-Saxon single-particle potential. Some preliminary results obtained with this code have been presented earlier[15]) and compared to results obtained with the Nilsson model. Here we will also compare with results obtained by use of the folded-Yukawa potential. We obtained the Woods-Saxon code from Nazarewicz and Dudek. It has been extensively discussed elsewhere. The results obtained here have been calculated with the universal parameter set[16]).

2.1.3. Folded-Yukawa model

Since the folded-Yukawa model has been extensively discussed in refs.[12,17]) and references quoted therein, we present here only the major features of the model.

In a nucleus consisting of Z protons and N neutrons the total number of nucleons is given by $A = Z + N$. The protons and neutrons move in different single-particle potentials. The single-particle potential felt by a nucleon is given by

$$V = V_1 + V_{\text{s.o.}} + V_{\text{C}} \tag{2}$$

The first term is the spin-independent nuclear part of the potential, for which we use the folded-Yukawa potential

$$V_1(\boldsymbol{r}) = -\frac{V_0}{4\pi {a_{\text{pot}}}^3} \int_{\text{V}} \frac{\mathrm{e}^{-|\boldsymbol{r}-\boldsymbol{r}'|/a_{\text{pot}}}}{|\boldsymbol{r}-\boldsymbol{r}'|/a_{\text{pot}}} d\boldsymbol{r}' \tag{3}$$

where the integration is over the domain enclosed by the generating shape, whose volume is held fixed at $\frac{4}{3}\pi {R_{\text{pot}}}^3$ as the shape is deformed. The range

$$a_{\text{pot}} = 0.8 \text{ fm} \tag{4}$$

of the Yukawa function in eq. (3) has been determined from an adjustment of calculated single-particle levels to experimental data in the rare-earth and actinide regions [18]). It is kept constant for nuclei throughout the periodic system [12,14]).

The spin-orbit potential is given by the expression

$$V_{\text{s.o.}} = -\lambda \left(\frac{\hbar}{2mc}\right)^2 \frac{\boldsymbol{\sigma} \cdot \nabla V_1 \times \boldsymbol{p}}{\hbar} \tag{5}$$

where λ is the spin-orbit interaction strength, m is the mass of either a neutron or a proton, $\boldsymbol{\sigma}$ is the Pauli spin matrix and $\boldsymbol{p}$ is the nucleon momentum. The spin-orbit strength has been determined from adjustments to experimental levels in the rare-earth and actinide regions. It has been shown [12,14,19]) that nuclear properties such as ground-state masses and deformations and fission barriers are well reproduced throughout the periodic system with λ given by a function linear in A through the values determined in these two regions. The linear expressions for λ_p and λ_n are

$$\lambda_{\text{p}} = 28.0 + 6.0 \frac{A}{240} \tag{6}$$

and

$$\lambda_{\text{n}} = 31.5 + 4.5 \frac{A}{240} \tag{7}$$

Finally, the Coulomb potential for protons is given by

$$V_{\text{C}}(\boldsymbol{r}) = e\rho_{\text{c}} \int_{\text{V}} \frac{d\boldsymbol{r}'}{|\boldsymbol{r}-\boldsymbol{r}'|} \tag{8}$$

where the charge density ρ_{c} is given by

$$\rho_{\text{c}} = \frac{Ze}{\frac{4}{3}\pi A {r_0}^3} \tag{9}$$

The above relations show that in the folded-Yukawa model the spin-orbit parameters decrease by about 20% and the diffuseness parameter $a_{\rm pot}$ remains constant if the region of study changes from the actinide region to the oxygen region. This is a very small variation over the periodic system compared to the variation of the spin-orbit and diffuseness parameters κ and $\kappa\mu$ in the Nilsson model. This gives us some confidence that the parameter choice in the folded-Yukawa model is reliable for extrapolations to unknown regions of nuclei. For the case of modelling β-strength functions it is of particular importance to correctly predict the level order in the single-particle diagram in the vicinity of the Fermi surface. Below, we will show how the model reproduces known ground-state spins of odd-A nuclei throughout the periodic system.

2.2. PAIRING MODELS

In the earlier version[6]) of the β-strength model and its numerical implementation a simple BCS model was used for the pairing model. In the present version of the model we have for testing and compatability reasons retained the initial BCS pairing model, but also introduced the possibility of using somewhat different formulations of the BCS model. However, the major extension in the calculation of pairing effects is that we now have the possibility of using the Lipkin-Nogami pairing model. This model avoids the collapse that occurs in the BCS model for large gaps in the single-particle spectrum.

In solving the pairing equations for neutrons or protons in either the BCS or Lipkin-Nogami model we consider a constant pairing interaction G acting between $N_2 - N_1 + 1$ doubly degenerate single-particle levels, which are occupied by $N_{\rm int}$ nucleons. This interaction interval starts at level N_1, located below the Fermi surface and ends at level N_2 located above the Fermi surface. With the definitions we use here, the levels are numbered consecutively starting with number 1 for the level at the bottom of the well. Thus, the last occupied level in the proton well is assigned number $Z/2$ for even proton number. Obviously, if the total number of neutrons or protons in the nucleus is $N_{\rm tot}$ we have

$$N_{\rm int} = N_{\rm tot} - 2N_1 + 2 \tag{10}$$

For even nucleon number, the number of level pairs included in the pairing calculation is often chosen symmetrically around the Fermi surface. In such a case

$$N_{\rm int} = N_2 - N_1 + 1 \tag{11}$$

However, for spherical nuclei it more reasonable to require that degenerate spherical states have equal occupation probability. This condition cannot generally be satisfied simultaneously with a symmetric choice of levels in the interaction region. We shall therefore give the equations for the more general case of arbitrary choice of N_2 and N_1, and with $N_{\rm int}$ obeying eq. (10).

2.2.1. BCS pairing model

In the BCS pairing model the pairing gap Δ, the Fermi energy λ, and the occupation probabilities ${v_k}^2$ are given by the set of $(N_2 - N_1 + 1) + 2$ coupled nonlinear equations

$$N_{\rm tot} = 2 \sum_{k=N_1}^{N_2} {v_k}^2 + 2(N_1 - 1) \tag{12}$$

$$\frac{2}{G} = \sum_{k=N_1}^{N_2} \frac{1}{\sqrt{(e_k - \lambda)^2 + \Delta^2}} \tag{13}$$

$${v_k}^2 = \frac{1}{2}\left[1 - \frac{e_k - \lambda}{\sqrt{(e_k - \lambda)^2 + \Delta^2}}\right], \quad k = N_1, N_1 + 1, \ldots, N_2 \tag{14}$$

where e_k are the single-particle energies. The quasi-particle energies E_k are given by the expressions

$$\begin{aligned} E_k &= [(e_k - \lambda)^2 + \Delta^2]^{1/2}, && k = N_1, N_1 + 1, \ldots, N_2 \\ E_k &= |e_k - \lambda|, && k < N_1 \text{ or } k > N_2 \end{aligned}$$

In order to calculate the potential energy in nuclear mass calculations, one also needs an expression for the pairing correction energy $E_{\rm pc} - \overline{E}_{\rm pc}$. The pairing correlation energy $E_{\rm pc}$ is given by

$$E_{\rm pc} = \sum_{k=N_1}^{N_2} (2{v_k}^2 - n_k)e_k - \frac{\Delta^2}{G} - \frac{G}{2}\sum_{k=N_1}^{N_2} (2{v_k}^4 - n_k) \tag{15}$$

where n_k, which have the values 2, 1 or 0, specify the sharp distribution of particles in the absence of pairing. The calculation of the pairing correlation energy $\overline{E}_{\rm pc}$ for an *average* nucleus will be discussed in section 2.2.2.

To solve eqs. (12–14) one must know either the pairing strength G or the microscopic pairing gap Δ. In the previous study [6]) a value for Δ was prescribed and the above equations were then solved for the occupation probabilities ${v_k}^2$ and the pairing strength G. For the microscopic pairing Δ the prescription $\Delta = 12/\sqrt{A}$ MeV was used. This approach was taken to avoid a collapse of the BCS equations for large gaps in the level spectra. The pairing strength G was obtained as a solution to the pairing equations, but not used for anything. An important deficiency in this approach is that variations in Δ due to the fluctuations in the nuclear level spectrum are absent. Such nonuniformities in the level spectrum coupled with changes in ground-state shapes can

lead to changes in Δ by a factor of two between close-lying nuclei. To better describe effects of microscopic structure on the pairing gap Δ we have included in our β-strength code: 1) a powerful method for determining the pairing matrix element G and 2) the Lipkin-Nogami pairing model. Both in the BCS and in the Lipkin-Nogami case we now normally prescribe G and calculate Δ.

2.2.2. Pairing model parameters and average pairing quantities

In order to incorporate the effects of the single-particle level structure on Δ we have added the possibility of solving the pairing equations for a prescribed value of G. One then needs an estimate of the pairing matrix element G, which together with the single-particle levels e_k are the input quantities. In some early approaches [20]), G was determined by solving the pairing equations for a region of nuclei and adjusting G so that calculated values of Δ optimally reproduced the odd-even mass differences. One should note that in such an approach the value of G depends on the region of nuclei considered and on N_1 and N_2, that is, on the number of levels above and below the Fermi surface that are included in the pairing calculation.

A more powerful approach that more simply leads to a prescription for the value of G, valid throughout the periodic system and for any resonable choice of the interaction region (N_1,N_2), is to consider the properties of an *average* nucleus and to determine a value of G from average macroscopic pairing gaps by use of macroscopic pairing equations. A conventional choice of macroscopic pairing gap has been $\overline{\Delta} = 12/\sqrt{A}$ MeV. In our study here we use new expressions for the nuclear neutron and proton average pairing gaps that have been derived by Madland and Nix [21]). They find

$$\overline{\Delta}_{\rm n} = \frac{rB_{\rm s}}{N^{1/3}} {\rm e}^{-sI-tI^2} \tag{16}$$

and

$$\overline{\Delta}_{\rm p} = \frac{rB_{\rm s}}{Z^{1/3}} {\rm e}^{+sI-tI^2} \tag{17}$$

with

$$I = \frac{N-Z}{N+Z} \tag{18}$$

Here I is the relative neutron excess and $B_{\rm s}$ is the ratio of the surface area of the nucleus at the deformation considered to the surface area of the spherical nucleus. In addition ref. [21]) introduced a new expression for the average residual n-p interaction energy δ appearing in the masses of odd-odd nuclei. They suggest

$$\delta = \frac{h}{A^{2/3}B_{\rm s}} \tag{19}$$

The four constants r, s, t and h are determined by a least-squares adjustment to experimental pairing gaps obtained from measured masses. The values obtained are $s = 0.118$, $t = 8.12$, $r = 5.72$ MeV and $h = 6.52$ MeV.

The dependence of G on the average pairing gaps $\overline{\Delta}_p$ and $\overline{\Delta}_n$ is obtained from the microscopic equations by assuming a constant level density for the average nucleus in the vicinity of the Fermi surface. This allows the sums to be replaced by integrals. The average level density of doubly degenerate levels may be taken to be

$$\bar{\rho} = \frac{1}{2}\bar{g}(\bar{\lambda}) \tag{20}$$

where $\bar{g}$ is the smooth level density that is obtained[17,22]) in the Strutinsky procedure. Thus, we can make the substitution

$$\sum_{k=N_1}^{N_2} f(e_k - \lambda) \Longrightarrow \bar{\rho} \int_{y_1}^{y_2} f(x)dx \tag{21}$$

where

$$\begin{aligned} y_1 &= \frac{-\frac{1}{2}N_{\rm tot} + N_1 - 1}{\bar{\rho}} \\ y_2 &= \frac{-\frac{1}{2}N_{\rm tot} + N_2}{\bar{\rho}} \end{aligned} \tag{22}$$

The gap equation eq. (13) may now be applied to an *average* nucleus with the result

$$\begin{aligned} \frac{1}{G} &= \frac{1}{2}\bar{\rho}\int_{y_1}^{y_2} \frac{dx}{\sqrt{x^2 + \overline{\Delta}^2}} \\ &= \frac{1}{2}\bar{\rho}\left[\log\left(\sqrt{{y_2}^2 + \overline{\Delta}^2} + y_2\right) - \log\left(\sqrt{{y_1}^2 + \overline{\Delta}^2} + y_1\right)\right] \end{aligned} \tag{23}$$

From this expression and from eqs. (16,17,22), G may be determined in any region of the nuclear chart.

The expression for the *average* pairing correlation energy $\overline{E}_{\rm pc}$ is obtained in a similar manner as the expression for the pairing matrix element G. The summations in eq. (15) are replaced by integrations according to the rule given by eqs. (21,22). For the first part of eq. (15) one obtains

$$\begin{aligned} &\sum_{k=N_1}^{N_2} (2{v_k}^2 - n_k)e_k - \frac{\overline{\Delta}^2}{G} \\ &= \sum_{k=N_1}^{N_2} 2{v_k}^2(e_k - \lambda) - \sum_{k=N_1}^{N_2} n_k(e_k - \lambda) - \frac{\overline{\Delta}^2}{G} \\ &= \bar{\rho}\int_{y_1}^{y_2}\left(x - \frac{x^2}{\sqrt{x^2 + \overline{\Delta}^2}}\right)dx - 2\bar{\rho}\int_{y_1}^{0} x\,dx - \frac{\overline{\Delta}^2}{G} \\ &= \bar{\rho}\left[\frac{{y_2}^2}{2} - \frac{y_2\sqrt{{y_2}^2 + \overline{\Delta}^2}}{2} + \frac{\overline{\Delta}^2}{2}\log\left(\sqrt{{y_2}^2 + \overline{\Delta}^2} + y_2\right)\right] \end{aligned}$$

$$-\bar{\rho}\left[\frac{{y_1}^2}{2}-\frac{y_1\sqrt{{y_1}^2+\overline{\Delta}^2}}{2}+\frac{\overline{\Delta}^2}{2}\log\left(\sqrt{{y_1}^2+\overline{\Delta}^2}+y_1\right)\right]+2\bar{\rho}\frac{{y_1}^2}{2}-\frac{\overline{\Delta}^2}{G} \quad (24)$$

For the second part of eq. (15) one obtains

$$\begin{aligned}
&-\frac{G}{2}\sum_{k=N_1}^{N_2}(2{v_k}^4-n_k)\\
&=-\frac{G}{2}\sum_{k=N_1}^{N_2}\left\{\frac{1}{4}\left[1-\frac{e_k-\lambda}{\left[(e_k-\lambda)^2+\overline{\Delta}^2\right]^{1/2}}\right]^2-n_k\right\}\\
&=-\frac{G}{4}\bar{\rho}\int_{y_1}^{y_2}\left[1+\frac{x^2}{x^2+\overline{\Delta}^2}-\frac{2x}{\left(x^2+\overline{\Delta}^2\right)^{1/2}}\right]dx+G\bar{\rho}\int_{y_1}^{0}x\,dx\\
&=-\frac{G}{4}\bar{\rho}\left[2y_2-2\sqrt{{y_2}^2+\overline{\Delta}^2}-\overline{\Delta}\tan^{-1}\left(\frac{y_2}{\overline{\Delta}}\right)\right]\\
&\quad+\frac{G}{4}\bar{\rho}\left[2y_1-2\sqrt{{y_1}^2+\overline{\Delta}^2}-\overline{\Delta}\tan^{-1}\left(\frac{y_1}{\overline{\Delta}}\right)\right]-G\bar{\rho}y_1 \quad (25)
\end{aligned}$$

Adding the various terms together leads to the following expression for the average pairing energy in the BCS model

$$\begin{aligned}
\overline{E}_{\rm pc} &= \frac{1}{2}\bar{\rho}\left[(y_2-G)\left(y_2-\sqrt{{y_2}^2+\overline{\Delta}^2}\right)+(y_1-G)\left(y_1+\sqrt{{y_1}^2+\overline{\Delta}^2}\right)\right]\\
&\quad+\frac{1}{4}G\bar{\rho}\overline{\Delta}\left[\tan^{-1}\left(\frac{y_2}{\overline{\Delta}}\right)-\tan^{-1}\left(\frac{y_1}{\overline{\Delta}}\right)\right] \quad (26)
\end{aligned}$$

In our computer codes we choose N_2 to correspond to the highest level in the range from the Fermi surface to +10 MeV above the Fermi surface, which energy range we designate by $E_{\rm int}^{\rm pair}$. By including an equal *number* of levels below the Fermi surface N_1 is defined. Thus, at this stage we have not implemented the possibility of a different number of levels above and below the Fermi surface, although our formulas are derived for this more general case.

We now solve the BCS pairing equations for a number of different choices of N_1 and N_2, for Nilsson-model proton single-particle levels with $\kappa_{\rm p}=0.0800$, $\mu_{\rm p}=0.300$, and $\epsilon_2=0.20$ for ^{94}Sr. For $Z=38$ and an energy interval of 7.0 MeV above the Fermi surface the code then chooses $N_1=10$ and $N_2=29$, that is 10 levels above and 10 levels below the Fermi surface. One then obtains $\bar{\Delta}=1.292$ MeV, $G=0.3028$ MeV and $\Delta_{\rm p}=1.54$ MeV. We also ran the pairing code for energy ranges of 5.0 and 9.0 MeV above the Fermi surface for the corresponding values of N_1 and N_2. The results corresponding to a choice of an equal number of levels above and below the Fermi surface constitute the first 3 lines in table 1. Further down in table 1 we study the results for

TABLE 1

Effect of changing the summation interval in a BCS pairing calculation for protons in ^{94}Sr. The number of particles is 38, so that the last occupied level is number 19.

$E_{\rm int}^{\rm pair}$ (MeV)	N_1	N_2	G (MeV)	$\Delta_{\rm p}$ (MeV)	$\overline{E}_{\rm pc}$ (MeV)	$E_{\rm pc}$ (MeV)
5.0	13	26	0.3532	1.581	−0.701	−1.80
7.0	10	29	0.3028	1.540	−0.749	−1.78
9.0	6	33	0.2666	1.519	−0.786	−1.78
	6	26	0.2923	1.453	−0.742	−1.57
	13	36	0.2923	1.630	−0.779	−2.04
	13	46	0.2679	1.711	−0.807	−2.31
	10	39	0.2655	1.615	−0.798	−2.04
	6	43	0.2431	1.600	−0.817	−2.04

other choices of N_1 and N_2. It is clear from table 1 that the method that we use here to determine G from the properties of an average nucleus works very well. The value of $\Delta_{\rm p}$ changes very little when the energy interval or N_1 or N_2 are changed and G is simultaneously readjusted. As a specific example let us consider the case of a 7-MeV energy interval which yields $N_1 = 10$ and $N_2 = 29$. Here $\Delta_{\rm p} = 1.540$ MeV. An increase of N_2 to 39 with a simultaneous corresponding adjustment of G gives a change in $\Delta_{\rm p}$ to 1.615 MeV, that is a change of only 5%. This should be compared to the value $\Delta_{\rm p} = 2.12$ MeV, an increase of 38%, which is obtained if G is not readjusted according to eq. (23) but held fixed at $G = 0.3028$ MeV. The pairing energy only changes by a maximum of 0.02 MeV for different choices of interaction interval, as long as an equal number of levels are chosen above and below the Fermi surface.

2.2.3. Lipkin-Nogami pairing model

In the Lipkin-Nogami pairing model [23–25]) the pairing gap Δ, the Fermi energy λ, the number-fluctuation constant λ_2, and the occupation probabilities ${v_k}^2$ are determined by the set of $2(N_2 - N_1 + 1) + 3$ coupled, nonlinear equations

$$N_{\rm tot} = 2 \sum_{k=N_1}^{N_2} {v_k}^2 + 2(N_1 - 1) \tag{27}$$

$$\frac{2}{G} = \sum_{k=N_1}^{N_2} \frac{1}{\sqrt{(\epsilon_k - \lambda)^2 + \Delta^2}} \tag{28}$$

$$v_k{}^2 = \frac{1}{2}\left[1 - \frac{\epsilon_k - \lambda}{\sqrt{(\epsilon_k - \lambda)^2 + \Delta^2}}\right], \quad k = N_1, N_1+1, \ldots, N_2 \tag{29}$$

$$\epsilon_k = e_k + (4\lambda_2 - G)v_k{}^2 \quad k = N_1, N_1+1, \ldots, N_2 \tag{30}$$

and

$$\lambda_2 = \frac{G}{4}\left[\frac{\left(\sum_{k=N_1}^{N_2} u_k{}^3 v_k\right)\left(\sum_{k=N_1}^{N_2} u_k v_k{}^3\right) - \sum_{k=N_1}^{N_2} u_k{}^4 v_k{}^4}{\left(\sum_{k=N_1}^{N_2} u_k{}^2 v_k{}^2\right)^2 - \sum_{k=N_1}^{N_2} u_k{}^4 v_k{}^4}\right] \tag{31}$$

where

$$u_k{}^2 = 1 - v_k{}^2 \ , \ k = N_1, N_1+1, \ldots, N_2 \tag{32}$$

Furthermore, the quasi-particle energies E_k of the odd nucleon in an odd-A nucleus are given by [24])

$$E_k = \left[(\epsilon_k - \lambda)^2 + \Delta^2\right]^{1/2} + \lambda_2, \quad k = N_1, N_1+1, \ldots, N_2 \tag{33}$$

In an exact treatment the presence of additional quasi-particles somewhat modify this expression [24]). However, for simplicity we have neglected such effects which are much smaller than effects of uncertainties in the calculated single-particle level spectrum and would be hardly noticeable on the calculated strength function. Of importance is that we in the Lipkin-Nogami formulation avoid the collapse of the pairing equations that occurs in the BCS formulations, and that we, as a consequence, obtain a more realistic value of the pairing gap Δ. Outside the interval $N_1 \leq k \leq N_2$ we use

$$E_k = |\epsilon_k - \lambda|, \qquad k < N_1 \ \text{ or } \ k > N_2 \tag{34}$$

We have developed a computer code to solve the Lipkin-Nogami pairing equations. We also use this code as part of a code to calculate nuclear potential-energy surfaces, from which we determine nuclear ground-state masses. Since we often survey large regions of nuclei, a particular goal in developing this code was to make it fast and reliable.

In particular we wanted to avoid crashes due to numerical difficulties. During the development effort we noticed that such difficulties sometimes would arise for small values of the pairing matrix element G and large gaps in the single-particle level spectrum at the Fermi surface, that is in situations where the BCS equations have *no* non-trivial solution. We eventually succeeded in overcoming the numerical difficulties.

For a test case of 328 nuclei in the Pb region ($200 \leq A < 220$), running on a CRAY-1 computer, the pairing part took 3 seconds longer with our Lipkin-Nogami code than in a BCS model, for which case the code took less than one second to execute. A preliminary version of another Lipkin-Nogami code that we had at our disposal took 235 seconds longer. Thus we achieved an enormous increase in speed relative to that code. Our code has two possibilities for the values of the parameters of the iteration towards the solution of the pairing equations. One we call "fast", the other "slow". The code will itself choose the "slow" mode if convergence is not achieved in the "fast" mode, which is always tried first.

We determine the three unknowns Δ, λ, and λ_2 by (damped) Newton-Raphson iteration. We calculate at each step numerically the 9 first-order derivatives. From the given initial set of values for Δ, λ, and λ_2 the next set of values are determined by use of these 9 derivatives by use of the damped Newton-Raphson method. However, we never allow more than a 40% change in Δ and λ_2 and never more than a 1 MeV change in λ at each step. Usually convergence is obtained in about 5 steps. We always choose the starting value of Δ to be 1 MeV, of λ to be the Fermi level of the sharp single-particle distribution, and of λ_2 to be $6 \times G/4$. This is the "fast" iteration mode. If convergence is not obtained after 30 steps we switch to the "slow" iteration mode, starting with the original initial values again. We now only allow up to a 20% change in Δ at each step, a 40% change in λ and a 0.5 MeV change in λ_2. However, the most important difference in the "slow" mode is that we in each iteration step first keep Δ fixed and solve for λ and λ_2. When these have been found we make one iteration in Δ, with λ and λ_2 fixed. In both of these steps we use the Newton-Raphson method. When we are close to the solution we have to switch to a simultaneous iteration in all three unknowns to obtain convergence, that is we again calculate all the 9 first-order derivatives and invert the full resulting matrix.

We have tested the code in a number of ways. In one test we made a careful comparison between the results of our code and the other code we had available, for 640 ground-state masses in the Pb region. This calculation considers nuclei from the proton to the neutron drip line. Our pairing code ran for this new set of nuclei in 55 seconds. Most of this computer time was spent calculating such quantities as shell corrections and Coulomb energies. All cases ran without a switch to the slow convergence mode in our code. A run with the other code took 872 seconds. There was no crash in this region of nuclei. Comparing the results of the two runs, we found that the maximum difference between calculated shell + pairing corrections was 0.024 MeV and between deltas 0.003 MeV.

In a calculation of nuclear masses for 8979 nuclei throughout the periodic system there was no crash of our code, despite rather extreme values of the neutron excess

and consequently very low values of the average pairing gaps and the corresponding pairing matrix element G. In this calculation the slow convergence mode was entered only about 20 times.

2.3. RPA MODEL

The calculated β-decay rates are sensitive to certain components of the residual interaction. As in our earlier treatment [6]) we add the so called Gamow-Teller force,

$$V_{\rm GT} = 2\chi_{\rm GT} : \boldsymbol{\beta}^{1-} \cdot \boldsymbol{\beta}^{1+} : \tag{35}$$

to the single-particle Hamiltonian, after pairing has already been incorporated. Here $\boldsymbol{\beta}^{1-} = \sum_i \boldsymbol{\sigma}_i \boldsymbol{t}_i^-$ is the Gamow-Teller β^--transition operator, so the correlations generated by the GT force are of specific importance to the Gamow-Teller decays, which are the dominant decay modes in many nuclei of astrophysical interest. Other types of residual interaction are of importance for other decay modes, but leave the Gamow-Teller decay rates unaffected, and can consequently be ignored in the treatment here. The only major changes in the RPA model relative to the earlier work [6]) involve the treatment of the transitions of the unpaired nucleons in odd-A and odd-odd nuclei.

It should be noted that the RPA treatment, as formulated by Halbleib and Sorensen [3]) incorporates only particle-hole corrections of specific importance to GT transitions. It has recently been found [26,27]) that the effect of neglected particle-particle terms may be significant for β^+ transitions. Moreover, the RPA treatment may not contain enough ground-state correlations [27]). However, in view of the present uncertainties regarding these points we leave possible further refinements for future consideration. Some additional comments are given in the presentation of the results of our β-decay half-life calculations, in section 3.4.

2.3.1. Odd-A nuclei

For odd-A nuclei there are two types of transition, $\Delta v = 2$ transitions and $\Delta v = 0$ transitions [6]). For the first type of transitions the RPA formalism for the even-even case may be used, since the odd particle only acts as a spectator. The $\Delta v = 0$ transitions involve the unpaired odd particle and are treated in first-order perturbation theory. For an odd-proton parent nucleus the $\Delta v = 0$ case may be treated by writing the wave function for the odd proton in the initial state as

$$|p_{\rm corr}> = \alpha_p^\dagger |{\rm GT0}> + \sum_{n\omega_{-K}} \alpha_n^\dagger \Gamma^{1\dagger}_{-K}(\omega_{-K})|{\rm GT0}><{\rm GT0}|\left[\alpha_n^\dagger \Gamma^{1\dagger}_{-K}(\omega_{-K})\right]^\dagger V_{\rm GT}^{0-K} \alpha_p^\dagger |{\rm GT0}> A_p(n\omega_{-K}) \tag{36}$$

and that of the odd neutron in the final state as

$$|n_{\rm corr}>= \alpha_n^\dagger|{\rm GT0}> + \sum_{p\omega_K} \alpha_p^\dagger \Gamma_K^{1\dagger}(\omega_K)|{\rm GT0}><{\rm GT0}|\left[\alpha_p^\dagger\Gamma_K^{1\dagger}(\omega_K)\right]^\dagger V_{\rm GT}^{0K}\alpha_n^\dagger|{\rm GT0}> A_n(p\omega_K) \tag{37}$$

In our earlier work [6]) and that of Halbleib and Sorensen [3])

$$A_p(n\omega) = \frac{1}{E_p - E_n - \omega} \tag{38}$$

Below we will show that this expression for $A_p(n\omega)$ has to be modified to avoid singularities in the expressions for the transition amplitudes that are obtained from the above first-order perturbation expansions for the odd-particle wave-functions. These transition amplitudes are:

$$\begin{aligned}
<n_{\rm corr}|\beta_K^{1+}|p_{\rm corr}> &= u_n u_p <n|\beta_K^{1+}|p> +2\chi <n|\beta_K^{1+}|p> R_1\,, \\
&\qquad \beta^+ \text{ decay of odd-proton nucleus} \\
<p_{\rm corr}|\beta_K^{1+}|n_{\rm corr}> &= v_n v_p <p|\beta_K^{1+}|n> +2\chi <p|\beta_K^{1+}|n> R_2\,, \\
&\qquad \beta^+ \text{ decay of odd-neutron nucleus} \\
<n_{\rm corr}|\beta_K^{1-}|p_{\rm corr}> &= v_n v_p <n|\beta_K^{1-}|p> +2\chi <n|\beta_K^{1-}|p> R_2\,, \\
&\qquad \beta^- \text{ decay of odd-proton nucleus} \\
<p_{\rm corr}|\beta_K^{1-}|n_{\rm corr}> &= u_n u_p <p|\beta_K^{1-}|n> +2\chi <p|\beta_K^{1-}|n> R_1\,, \\
&\qquad \beta^- \text{ decay of odd-neutron nucleus}
\end{aligned} \tag{39}$$

where R is given by

$$\begin{aligned}
R_1 &= \sum_{\omega_K} {X_{\omega_K}^K}^2 \left\{A_p(n\omega_K)\left[u_p u_n + C_{\omega_K}^K v_p v_n\right] + C_{\omega_K}^K A_n(p\omega_K)\left[v_p v_n + C_{\omega_K}^K u_p u_n\right]\right\} \\
R_2 &= \sum_{\omega_K} {X_{\omega_K}^K}^2 \left\{C_{\omega_K}^K A_p(n\omega_K)\left[u_p u_n + C_{\omega_K}^K v_p v_n\right] + A_n(p\omega_K)\left[v_p v_n + C_{\omega_K}^K u_p u_n\right]\right\}
\end{aligned} \tag{40}$$

and where we have used the fact that the various quantities are independent of the sign of K.

It was pointed out by Bender *et al.* [11]), that the terms linear in $C_{\omega_K}^K$ in eq. (40) should have a negative sign with the sign conventions for the quantities q_{iK} and $\tilde{q}_{iK}$ that were used in our original work [6]). We are grateful that this error in our original work, an error that was unfortunately present also in the computer code, was discovered. To correct the error one may either change the sign of the terms linear in $C_{\omega_K}^K$ in eq. (40) from plus to minus or change the sign of $\tilde{q}_{iK}$. We choose the latter possibility. Thus, the definitions of q_{iK} and $\tilde{q}_{iK}$ should be

$$\begin{aligned}
q_{iK} &= <p|\sigma_K|n> u_p v_n \\
\tilde{q}_{iK} &= -<p|\sigma_K|n> u_n v_p
\end{aligned} \tag{41}$$

As a test, we have run our code both with correct and incorrect sign. Fortunately, we find that the effect of the sign error on the calculated β-strength function is very small. For all practical purposes its effect on our earlier results can be neglected. In fact, for our standard test cases of β^--decay of ^{93}Rb and ^{95}Rb there is no visible difference in plots of the strength functions between results obtained with the different signs. Usually the difference between the two sign choices is a few percent in one or two peaks in the calculated β-strength function. The $\Delta v = 2$ transitions are of course not affected at all by this sign error.

2.3.2. Non-singular $\Delta v = 0$ transition-amplitude expressions

It was shown [15]) that the above expressions for the transition amplitudes occasionally exhibit a singular behavior, due to a breakdown of the perturbation expansion given in eqs. (36,37). However, the singularity may be removed by moving the pole at $E_p - E_n$ in the expression for $A_p(n\omega)$ from the real axis into the complex plane. This was accomplished [15]) by introducing a width d in the expression for $A_p(n\omega)$. One obtains the new expression

$$\begin{aligned} A_p(n\omega) &= \frac{1}{2}\left(\frac{1}{E_p - E_n + id - \omega} + \frac{1}{E_p - E_n - id - \omega}\right) \\ &= \frac{E_p - E_n - \omega}{(E_p - E_n - \omega)^2 + d^2} \end{aligned} \tag{42}$$

As an example of the singularities that may occur we show in fig. 1 the β-strength function for β^- decay of ^{160}Nd, calculated in our original model with the expansion coefficients A_p given by eq. (38). There is a huge singularity at about 3.0 MeV. With the generalized model for the expansion coefficients, given by eq. (42) the singularity is removed, as is seen in fig. 2. Results obtained using two values of the width d are given in the figure. The solid line corresponds to $d = 0.1$ MeV and the dashed line to $d = 1.0$ MeV. Strength above 9.0 MeV has not been plotted. As expected, we find that the results are very insensitive to the choice of d. As our standard choice for d we have selected $d = 0.5$ MeV.

2.3.3. Odd-odd nuclei

With certain assumptions, the odd-A case formalism may be used to calculate the strength function also in the odd-odd case. The possible transitions that can occur in β^- decay in the odd-odd case are shown schematically in fig. 3, in an extreme single-particle model. In the first case, $\Delta v = 2$ transitions to the upper left, the two odd particles act as spectators and the transition amplitudes are obtained from the solutions to the RPA equations [6]), just as in the case with no unpaired protons or neutrons.

There are two types of $\Delta v = 0$ transitions. In treating these two cases we disregard any residual interactions between the two odd particles and consider one or the other of the odd particles as a spectator. Thus, to the upper right the odd neutron is a spectator and the transition amplitudes are given by eq. (39), case 3. This approximation means that in our model the strength goes to a single state, but in an actual decay the strength would be distributed between states corresponding to some of the different orientations of the relative spins of the two unpaired neutrons in the final nucleus. These states would have energies that depend on residual interactions that are not included in our model. Our approximation here is somewhat similar to the approximation that the splitting of strength between rotational states is not treated in the model. Instead the strength is all collected in the band-head energy level [6]). The transition amplitudes for the case to the lower left in fig. 3 are given by eq. (39) case 4.

The ground-state to ground-state transition to the lower right is in our approximation also given by the same expression for the transition amplitude as is used for the case to the lower left, but the energy relative to the ground-state of the daughter is of course 0, which is $2\Delta_p$ lower than if we had ignored the fact that the two odd protons are paired in this state. For an odd-odd parent nucleus the ground-state to ground-state transition only takes place if the initial state has spin-parity 1^+. For other cases, the strength that we in our approximate treatment occasionally would assign to the ground state will in an actual nucleus decay into states $2\Delta_p$ and higher above the ground state.

To summarize, we find that for the $\Delta v = 2$ transitions the accuracy of our model is about the same as in the odd-A case. For $\Delta v = 0$ transitions we neglect the residual interaction between the two odd particles. Consequently we cannot obtain the distribution of strength between levels corresponding to the different relative orientations of the spins of the odd particles. Instead, this strength is collected in one state. It is of interest to observe that the first type of transitions that we treat more exactly than the other transition types are the more numerous, since the number of such transitions are proportional to $N \times Z$, whereas the latter type of transitions are only proportional to $Z + N$. The treatment of the ground-state to ground-state transition sometimes introduces errors of about $2\Delta_p$ in the location of the strength. This treatment of the odd-odd case is the standard one used in surveys over large regions of nuclei. However, the user of the β-strength code may of course use specific knowledge of the relative initial spin orientations of the odd neutron and odd proton to improve on the analysis of the odd-odd case, instead of accepting the standard output of the code. Below, when we study half-lives in the rare-earth region, we will analyze the difference in model accuracy between the odd-A and odd-odd case.

2.3.4. Gamow-Teller residual-interaction coupling constant

In the earlier work [6]) the choice

$$\chi_{GT} = 23/A \quad \text{MeV} \tag{43}$$

was made for the coupling constant for the residual Gamow-Teller interaction. This choice corresponds to a commonly accepted value [28]) and was derived by adjusting the position of the calculated giant Gamow-Teller resonance to the experimental data for ^{208}Pb. In a recent study Bender *et al.* [11]) obtained the value $\chi_{GT} = 15/A$ MeV by adjusting the calculated value of the giant GT resonance to its observed position for a number of cases in the Fe region. This latter value was also used by Bender *et al.* in a calculation of β-decay half-lives in this region of nuclei. The value of χ_{GT} influences both the magnitude of low-lying strength and the position of the giant GT resonance. We show here in fig. 4 the effect of the two values of χ on the position of the giant GT resonance in Pb in both the Nilsson modified-oscillator and the folded-Yukawa single-particle potential. The upper two strength functions correspond to the choice $\chi_{GT} = 23/A$ MeV and the lower two to the choice $\chi_{GT} = 15/A$ MeV. The notation (L-N) in fig. 4 and subsequent figures indicates that the Lipkin-Nogami pairing model was used. Comparing the upper left strength function to the similar calculation shown in fig. 1 in the earlier work [6]), we find that the centroid of the giant resonance in our earlier work is located at 15.73 MeV as compared to 16.3 MeV here. This difference is due to differences in the pairing models. It is found experimentally [28]) that the GT giant resonance is located at 19.2 MeV relative to the ground state of ^{208}Pb. Since the Q-value of the reaction is $Q_{pn} = 3.67$ MeV our calculated result here is that the location is at 19.97 MeV. With the lower value of $\chi_{GT} = 15/A$ MeV we find in the lower left diagram that the location of the resonance is about 13.25 + 3.67 MeV = 16.92 MeV. Thus, the calculated location of the giant resonance is too high by about 0.8 MeV with the conventional choice of χ and too low by about 2.3 MeV for the choice of $\chi_{GT} = 15/A$ MeV. In the folded-Yukawa model the calculated location of the resonance is too high by about 1.0 MeV and too low by about 1.8 MeV for these two cases, respectively. These results indicate that to reproduce the location of the giant resonance optimally in both the folded-Yukawa and the Nilsson modified-oscillator model one should choose χ_{GT} to be $21/A$ or $20/A$ MeV. However, the difference between any of these two values and the conventional choice for χ_{GT} as made in eq. (43) is so small that we continue to use in our calculations the value given in eq. (43). In this context one should observe that the calculated Gamow-Teller strength in the low-energy region usually is twice as large as the experimental results. This is the well-known problem of the missing GT strength [28–30]). To reproduce experimental half-lives the calculated strength is therefore in most investigations with models of the type we use here renormalized (multiplied) by a factor of about 0.5. Were we to use a lower value of χ_{GT} the suppression factor would have to be even smaller. We will comment more on this aspect when we discuss calculated β-decay half-lives below.

2.4. β-DECAY FROM EXCITED STATES

In our earlier treatment [6]) for Gamow-Teller β-strength decay we assumed that the mother nucleus decays from its ground state. However, in many experimental situations the nucleus undergoes β-decay from certain types of excited states. We have therefore

generalized our model to allow the description of decay from certain isomeric states and implemented these generalizations in our computer code. We only consider such isomeric states where the odd particle is in an excited state. Normally, when the nucleus is in its ground state the odd particle is in the lowest available orbital. To show that it is straightforward to consider also the more general case when the odd particle is in some other orbital we discuss below a few representative cases in greater detail.

2.4.1. Odd-A nuclei

In odd-A nuclei the excitation of the odd particle affects the $\Delta v = 2$ and the $\Delta v = 0$ transitions differently. Let us first study the $\Delta v = 2$ transitions. Specifically, let us consider $\Delta v = 2$, β^+-decay of an odd-proton nucleus, as shown in the upper left part of fig. 5. In this case, with the odd particle as a spectator, the solutions to the RPA equations for the transition energies ω remain unchanged. The only part of the calculation that changes is the calculation of the zero reference point of the energy scale. The energy of the β-strength function is given relative to the ground state of the daughter nucleus. The solutions ω to the RPA equations are obtained relative to the vacuum, which is the ground state of a neighboring even-even system. Now, relative to the even system the energy of the daughter configuration is $\omega + E_{\mathrm{p_{spect}}}$. However, the energy of the *ground state* of the daughter system is $E_{\mathrm{n_0}}$ relative to the even system, where $E_{\mathrm{n_0}}$ is the quasi-particle energy of the odd neutron in the lowest orbital. Thus, the energy E of the above daughter configuration relative to its ground state is

$$E = \omega + E_{\mathrm{p_{spect}}} - E_{\mathrm{n_0}} \tag{44}$$

The only change made in the present code relative to the original version[6]) is that $E_{\mathrm{p_{spect}}}$ is now allowed to be different from $E_{\mathrm{p_0}}$. Obviously, it has also been necessary to introduce a new variable to specify in which orbital the odd proton is initially located in the mother nucleus. In the $\Delta v = 2$ case just discussed it remains in that orbital in the daughter nucleus.

The above discussion shows that for $\Delta v = 2$ transitions there are the following relationships between the calculated spectra for decay from excited configurations and from the ground-state configuration: Precisely the same peaks that occur in decay from the ground state also occur in decay from excited states. The transitions have the same amplitude in both cases, but the positions of the transitions are displaced by the positive energy $E_{\mathrm{p_{spect}}} - E_{\mathrm{p_0}}$ in the decay from the excited configuration relative to the decay from the ground state.

We must also consider the $\Delta v = 0$ case. In this case only the odd, unpaired proton is involved in the decay. This is shown in the upper right part of fig. 5. In this case the only change that was made to the computer code was to allow for other initial states than the lowest unoccupied proton orbital. The expressions for the energies of the daughter configurations are unchanged relative to the previous model. For the energy

we obviously have

$$E = E_{\mathrm{n}} - E_{\mathrm{n}_0} \tag{45}$$

Here E_{n} is the quasi-particle energy for the configuration with the odd neutron in orbital n, and E_{n_0} is the lowest quasi-particle energy, corresponding to the ground state with the odd particle in the lowest possible energy state. Again we have of course introduced in our computer code a new variable that specifies the initial proton orbital.

Although the changes required in the computer code to treat decay from excited states are very minor for transitions of the $\Delta v = 0$ type, there are for this type of transitions important differences between the calculated spectra for decay from excited states and for decay from the ground state. These changes occur because the initial configuration of the odd particle is quite different in the two cases and *it is this odd-particle configuration that changes* for transitions of the $\Delta v = 0$ type. Thus, for transitions of the $\Delta v = 0$ type, peaks that are present in decay from the ground state will be absent in decay from excited states and new peaks will appear instead.

At present only a restricted class of excited states can be studied by the code. This can be understood by considering how the odd configurations are generated in the model and computer code. As a starting point one solves the single-particle, pairing, and RPA equations for an even-even nuclear system, which is called the vacuum nucleus. Both mother and daughter nuclei are generated from this vacuum nucleus. The proton and neutron numbers of the vacuum nucleus are selected such that the mother and daughter configurations deviate as little as possible from the vacuum, because the closer these configurations are to the vacuum the simpler the expressions for the energies, transition rates and other quantities of interest become. In addition, one obtains more accurate results from the perturbation expressions, the closer to the chosen vacuum the studied configurations are. In figs. 3 and 5 the dashed lines represent the positions of the Fermi surface for the vacuum nucleus, which has Z protons and N neutrons. It is easiest to understand how to select the vacuum by considering the $\Delta v = 0$ transitions. For β^+ decay it is clear that with the vacuum selected as in the upper right part of fig. 5 the parent configuration is constructed by creating a proton particle out of the vacuum and the daughter state by creating a neutron particle out of the vacuum. It is easy to verify that any other choice of vacuum would require either the mother or daughter configuration to be a three-quasiparticle state. In the case of β^+ decay of odd-proton nuclei this means that we can consider excited proton particle states in the mother nucleus as initial states. We show an example of β^- decay of an odd-proton nucleus in the lower left part of fig. 5. In this case it is clear that the initial states are of a hole type. A consideration of the various cases that can occur shows that our simple generalization of the code at this stage leads to the following restrictions on the type of initial, excited configurations that can be studied:

- β^+ decay from odd-proton nuclei: proton particle states
- β^- decay from odd-proton nuclei: proton hole states
- β^+ decay from odd-neutron nuclei: neutron hole states

- β^- decay from odd-neutron nuclei: neutron particle states

2.4.2. Odd-odd nuclei

A case of decay of an excited odd-odd system is shown in the lower, right part of fig. 5. As is seen in fig. 3 there are two types of $\Delta v = 0$ decay for an odd system. In the $\Delta v = 0$ decay shown in fig. 5, the odd particle that is in an excited state, in this case the odd neutron, is not involved in the transition. Instead it is the odd-hole state corresponding to the lowest-energy proton hole state that is involved in the transition shown. For this type of $\Delta v = 0$ transitions in the *odd-odd* system the transitions are identical to those that occur from the ground-state configuration but displaced in energy relative to the decay of the ground-state configuration by an amount that is equal to the excitation energy of the other odd, uninvolved particle. In the *odd-even* case $\Delta v = 0$ transitions always had to involve the excited odd particle, in which case the $\Delta v = 0$ transitions occurring from the ground-state configuration were replaced by completely different $\Delta v = 0$ transitions from the excited configuration. This situation also occurs in the *odd-odd* case for $\Delta v = 0$ transitions that do involve the excited odd particle.

The energy of the transition shown in the lower right part of fig. 5 is simply given by

$$E = E_{\mathrm{n}} + E_{\mathrm{n_{spect}}} \tag{46}$$

where E_{n} is the quasi-particle energy for the configuration with the odd neutron in orbital n, and $E_{\mathrm{n_{spec}}}$ is the quasi-particle energy of the spectator. In the case of decay from the ground-state configuration $E_{\mathrm{n_{spec}}} = E_{\mathrm{n_0}}$, where $E_{\mathrm{n_0}}$ corresponds to the case when the odd particle is in the lowest possible orbital. The rules above for the possible excited states that can be studied in the odd-even case may be carried over to the odd-odd case and in that case mean that for β^+ decay we may consider proton particle states or neutron hole states, and for β^- decay proton hole states or neutron particle states.

2.5. β-DECAY HALF-LIVES AND DELAYED NEUTRON-EMISSION PROBABILITIES

We here discuss the calculation of β-decay half-lives for Gamow-Teller decay and the related problem of calculating β-delayed neutron-emission probabilities. As a first step, we investigate a relatively simple model in order to gain some basic insight into how the half-life is calculated. In our discussion of the model we follow closely the presentation in the books by deShalit and Feshbach [31]) and Preston [32]). We develop a computer code based on this model and compare the results to a more exact model. Unless otherwise stated, we take the expressions in this section from the book by deShalit and Feshbach.

2.5.1. β decay

The β decay occurs from the ground state or an excited configuration in a mother nucleus to some state in the daughter nucleus, that is from an initial configuration to a final configuration. For β^- decay, the final configuration is a nucleus in some excited state or in a ground-state configuration, an electron (with energy E_e), and an antineutrino (with energy E_ν). The transition from the initial to the final state then involves an operator H, which is the weak-interaction Hamiltonian density. Once the operator H is known, the probability per unit time for emitting an electron between $\hbar\boldsymbol{k}_e$ and $\hbar(\boldsymbol{k}_e + d\boldsymbol{k}_e)$ and an antineutrino with a momentum between $\hbar\boldsymbol{k}_\nu$ and $\hbar(\boldsymbol{k}_\nu + d\boldsymbol{k}_\nu)$ is given by the well-known golden rule

$$dw_{fi} = \frac{2\pi}{\hbar}|H_{fi}|^2 \frac{d\boldsymbol{k}_e}{(2\pi)^3}\frac{d\boldsymbol{k}_\nu}{(2\pi)^3}\,\delta(E_0 - E_e - E_\nu) \tag{47}$$

where E_0 is the energy release in the decay.

In the above expression sums over the spins of the final states and averages over the initial spins should be performed. Our interest here is mainly to obtain the probability of decay to a specific final nuclear state f. To obtain this probability we observe that the matrix element $|H_{fi}|^2$ is a product of the antineutrino and electron level densities and nuclear matrix elements. One may obtain the probability distribution for the electrons from eq. (47) by summing over the appropriate spins and integrating over the direction of motion of the electron and over the antineutrino momentum. One must go through several lengthy steps to accomplish this. These steps are usually glossed over in discussions of these models but one extensive account of the steps involved is given in the book by Preston[32]). The resulting probability distribution of the electrons is

$$\frac{dw_{fi}}{d\epsilon} = \frac{m_0c^2}{\hbar}\,\frac{\Gamma^2}{2\pi^3}\,\rho(Z,R,\epsilon)\,|M_{fi}|^2(\epsilon_0-\epsilon)^2\epsilon(\epsilon^2-1)^{\frac{1}{2}} \tag{48}$$

where $\epsilon = E_e/m_0c^2$ and $\epsilon_0 = E_0/m_0c^2$, m_0 being the electron mass.

The nuclear matrix element $|M_{fi}|^2$ is the β-strength function. The dimensionless constant Γ is given by

$$\Gamma \equiv \frac{g}{m_0c^2}\left(\frac{m_0c}{\hbar}\right)^3 \tag{49}$$

Note that there is a misprint in the book[31]) by deShalit and Feshbach, where in chapter 9 eq. (2.11) the exponent is erroneously 2 instead of the correct value 3. The density ρ is in the relativistic limit given by

$$\rho = 2(2kR)^{2(s-1)}\,\frac{1+s}{s^2+\eta^2}\left|\frac{e^{\pi\eta/2}\Gamma(s+1+i\eta)}{\Gamma(2s+1)}\right|^2 \tag{50}$$

where

$$s^2 = 1-(\alpha Z)^2 \tag{51}$$

$$\eta = \pm\frac{\alpha Z E_e}{cp_e} = \pm\alpha Z\,\frac{E_e}{m_0c^2}\,\frac{m_0c}{p_e} \qquad \text{for} \quad e^{\mp} \tag{52}$$

and

$$\alpha = \frac{e^2}{\hbar c} \tag{53}$$

is the fine-structure constant.

The total probability for decay to one nuclear state is obtained by integrating eq. (48) to obtain

$$w_{fi} = \frac{m_0 c^2}{\hbar} \frac{\Gamma^2}{2\pi^3} |M_{fi}|^2 f(Z, R, \epsilon_0) \tag{54}$$

where

$$f(Z, R, \epsilon_0) = \int_1^{\epsilon_0} d\epsilon \, \rho(Z, R, \epsilon)(\epsilon_0 - \epsilon)^2 \epsilon(\epsilon^2 - 1)^{\frac{1}{2}} \tag{55}$$

The probability for β-delayed neutron emission, in percent, is given by

$$P_{\rm n} = 100 \frac{\sum\limits_{S_{\rm n} < E_f < Q_\beta} w_{fi}}{\sum\limits_{0 < E_f < Q_\beta} w_{fi}} \tag{56}$$

where we have assumed that decays to above the neutron binding energy $S_{\rm n}$ always lead to delayed neutron emission.

To obtain the half-life with respect to β-decay one sums up the decay rates w_{fi} to the individual nuclear states in the allowed energy window. The half-life is then related to the total decay rate by

$$t_{1/2} = \frac{\ln 2}{\sum\limits_f w_{fi}} \tag{57}$$

The above equation may be rewritten as

$$t_{1/2} = \frac{\hbar}{m_0 c^2} \frac{2\pi^3 \ln 2}{\Gamma^2} \frac{1}{\sum\limits_f |M_{fi}|^2 f(Z, R, \epsilon_0)} = \frac{B}{\sum\limits_f |M_{fi}|^2 f(Z, R, \epsilon_0)}$$

with

$$B = \frac{\hbar}{m_0 c^2} \frac{2\pi^3 \ln 2}{\Gamma^2} \tag{58}$$

In our half-life code we use for B the value

$$B = 4131 \text{ s} \tag{59}$$

for Gamow-Teller decay.

The above formulas apply to β^+ and β^- decay. However, for the purpose of calculating half-lives electron capture (EC) must also be considered.

2.5.2. Electron capture

The energy release in positron emission is

$$E_0^{\beta^+} = [M(Z,N) - M(Z-1,N+1) - 2m_0]\,c^2 \tag{60}$$

and in electron capture

$$E_0^{\mathrm{EC}} = [M(Z,N) - M(Z-1,N+1)]\,c^2 - \text{electron binding energy} \tag{61}$$

In fact

$$E_0^{\mathrm{EC}} = E_0^{\beta^+} + 2m_0c^2 - \text{electron binding energy} \tag{62}$$

which shows that for some decays electron capture will be possible although β^+ decay is energetically forbidden. The decay rate by electron capture is

$$dw_{fi}^K = \frac{2\pi}{\hbar}|H_{fi}|^2 \frac{d\boldsymbol{k}_\nu}{(2\pi)^3}\,\delta(E_0 - E_\nu) \tag{63}$$

After integrating over the neutrino wave vector $\boldsymbol{k}_\nu$ one obtains

$$w_{fi}^K = \frac{m_0c^2}{\hbar}\,\frac{\Gamma^2}{\pi}\left(\frac{\hbar}{m_0c}\right)^3 \rho|M_{fi}|^2{\epsilon_\nu}^2 \tag{64}$$

where K indicates electron capture and ϵ_ν is the neutrino energy in units of m_0c^2. The density ρ is different from the density entering in β^- or β^+ decay. In a nonrelativistic approximation it is given by

$$\rho = \frac{Z^3}{\pi {a_0}^3} \tag{65}$$

where a_0 is the Bohr radius. Thus

$$\left(\frac{\hbar}{m_0c}\right)^3 \rho = \frac{1}{\pi}(\alpha Z)^3 \tag{66}$$

The total half-life with respect to β^+ and EC decay is obtained through

$$t_{1/2} = \frac{\ln 2}{\sum_f (w_{fi}^K + w_{fi}^{\beta^+})} \tag{67}$$

As pointed out above, the energies involved in the two terms in the sum differ by $2m_0c^2$ and for some nuclear final states $w_{fi}^{\beta^+}$ may be zero (energetically forbidden) while w_{fi}^K is not.

However, to get reasonable accuracy it is necessary to use the relativistic expressions given by Preston[32]) and also to consider electron capture from both the K-shell and the L-shell. One then obtains

$$w_{fi}^{K+L_I} = \frac{m_0c^2}{\hbar}\,\frac{\Gamma^2}{\pi}|M_{fi}|^2 \frac{1}{4\pi}({g_{-1,K}}^2{q_K}^2 + {g_{-1,L_I}}^2{q_{L_I}}^2) \tag{68}$$

TABLE 2
Comparison of log f_0^- values calculated in two models

Z	A	ϵ_0 (MeV)	log f_0^- eq. (55)	log f_0^- ref. [33])
20	44	6.00	4.26	4.26
37	95	0.10	−2.19	−2.13
37	95	0.60	0.41	0.41
37	95	1.00	1.22	1.22
37	95	6.00	4.49	4.47
37	95	10.00	5.51	5.49
65	160	0.10	−1.57	−1.54
65	160	0.60	0.98	0.96
65	160	1.00	1.77	1.74
65	160	6.00	4.91	4.86
65	160	10.00	5.91	5.83

or equivalently

$$w_{fi}^{K+L_I} = \frac{m_0c^2}{\hbar}\frac{\Gamma^2}{2\pi^3}|M_{fi}|^2 f_{fi}^{K+L_I}(Z,R,\epsilon_0) \tag{69}$$

where

$$f_{fi}^{K+L_I}(Z,R,\epsilon_0) = \frac{\pi}{2}({g_{-1,K}}^2{q_K}^2 + {g_{-1,L_I}}^2{q_{L_I}}^2) \tag{70}$$

Here

$$\begin{aligned}
{g_{-1,K}}^2 &= \frac{2-B_K}{2\Gamma(2s+1)}(2\alpha Z_K)^3(2\alpha Z_K)^{2s-2}\left(\frac{m_0cR}{\hbar}\right)^{2s-2} \\
{g_{-1,L_I}}^2 &= \frac{(2-B_{L_I})(2s+1)(2s+2)^{-s}}{4\Gamma(2s+1)[(2s+2)^{1/2}+1]}(2\alpha Z_{L_I})^3(2\alpha Z_{L_I})^{2s-2}\left(\frac{m_0cR}{\hbar}\right)^{2s-2} \\
s &= (1-\alpha^2{Z_X}^2)^{1/2} \\
B_K &= 1-s \\
B_{L_I} &= 1-\left(\frac{1+s}{2}\right)^{1/2} \\
Z_K &= Z-0.35 \\
Z_L &= Z-4.15 \\
q_X &= [M(Z,N)-M(Z-1,N+1)]\,c^2 - B_X
\end{aligned} \tag{71}$$

Gove and Martin[33]) have tabulated $f(Z, R, \epsilon_0)$ in a treatment that is somewhat more exact than outlined above. In table 2 we compare results obtained from eq. (55) with the results of Gove[33]). The differences between the two models correspond to a difference in half-life of less than 20%. Despite the small differences we have obtained the computer code used to generate the tables of Gove and Martin and incorporated it into our programs. Most of the results presented here have been obtained with this more accurate treatment.

3. Calculations

Deformed single-particle models provide a starting point not just for calculations of β-strength functions but also for many other nuclear-structure quantities. Initially, deformed single-particle models were used to calculate the ground-state deformation and level structure of deformed nuclei. Since nuclear wave functions are also provided by these models, such quantities as electromagnetic moments and transition rates can also be calculated. In other applications, for example the macroscopic-microscopic approach, the potential energy of the nucleus is calculated as a function of its shape, and in this approach the shell correction is extracted from calculated single-particle spectra by use of Strutinsky's shell-correction method. In the macroscopic-microscopic approach nuclear ground-state shapes and masses may be determined, and by considering a larger set of shape variations one may also investigate the structure of the fission barrier. A knowledge of the ground-state shape is of course necessary to calculate the β-strength function.

A detailed knowledge of the low-energy part of the β-strength function is essential for the calculation of such quantities as the probability of β-delayed neutron and proton emission, the probability of β-delayed fission, and half-lives with respect to β-decay. Experimentally it has been known for some time that the low-energy part of the β-strength function exhibits a pronounced structure[34,35]), that is the strength is collected in a few well-localized peaks. For nuclei that are spherical in their ground state there are usually very few peaks within the Q_β window; for deformed nuclei the strength is more spread out, but still exhibits significant structure.

Theoretically these properties of the β-strength function can be understood in their main features in an extreme single-particle model. The peaks in the strength functions correspond to transitions between specific single-particle levels. In the spherical case the levels are highly degenerate and spaced far apart, which gives rise to the very few but strong peaks in the experimental strength function. For deformed nuclei the degeneracy is removed, allowing for significantly more transitions. Thus, compared to the spherical case, there are now more peaks in the experimental strength function, but the strength of each peak is lower.

Although an extreme single-particle model explains the origin of the structure in the β-strength function and the characteristic difference between strength functions associated with deformed and spherical nuclei, a more detailed description of the strength function requires the inclusion of the pairing and a Gamow-Teller interactions as discussed above. The inclusion of these terms in the potential reduces the calculated

strength in the low-energy part of the strength function to about 10% of what is obtained in an extreme single-particle model [6]). Because the pairing leads to a diffuse Fermi surface and consequently to some occupation probability above and to partially unfilled levels below the Fermi surface there are decay channels open in the more refined model that are blocked in the extreme single-particle model. One should also note that for deformed nuclei we often find considerable strength for transitions between Nilsson levels whose asymptotic quantum numbers do not allow for any transition probability, according to the GT selection rules. This result is due to the fact that the conventional asymptotic quantum number label gives the main component of the wave function corresponding to the level, but the transition strength is due to admixtures of wave-functions with other asymptotic quantum numbers. Since we perform a full diagonalization of the single-particle Hamiltonian we account for these admixtures in our model.

3.1. GLOBAL MODEL BEHAVIOUR

The above discussion makes clear that the positions of the peaks in the low-energy part of the β-strength function depend critically on the positions of the single-particle levels of the underlying single-particle model. In the deformed case one might expect a somewhat random distribution of strength because of the considerable number of levels available in the deformed region, and their seemingly irregular distribution. However, although the level distribution may seem random at a casual glance, the locations found experimentally for the low-lying bandhead energies and for the values of their quantum numbers are quite well described by calculations based on single-particle models. As an example we refer to the comparison [19]) of calculated and experimental levels in the deformed actinide region. For cases where the experimental level positions close to the Fermi surface are as well reproduced by the calculations as in this comparison, one expects that the β-transitions from mother to daughter also should be relatively well described by our model, with a structure of the calculated strength functions that reflects the structure of the underlying single-particle level diagram.

Since the β-strength function is a sensitive function of the underlying single-particle structure, a basic requirement in a calculation of a β-strength function is ideally that two conditions are fulfilled. First, the ground-state shape of the system of interest must be known. Second, the single-particle spectrum calculated at this shape must agree reasonably well with the experimental situation, in particular for the levels closest to the Fermi surface. Because we now use the folded-Yukawa single-particle potential, which has been used to calculate nuclear masses, shapes, and other ground-state quantities for nuclei throughout the periodic system [12,14]), we have extensive experience on how these requirements are met globally throughout the periodic system in this model. In general, very good agreement has been found between calculated and experimental ground-state masses [12]) and between calculated and experimental values for the ground-state quadrupole and hexadecapole shape coordinates [14]). More recently, we have, with only slight modifications of the model, performed a new calculation of ground-state masses

and shapes, now for nuclei from the proton to the neutron driplines, from oxygen to beyond $Z = 120$, altogether 8979 nuclei [36]). The masses were calculated in two different macroscopic approaches. In both approaches the microscopic correction was based on the folded-Yukawa single-particle model, but two alternative macroscopic models were used. One of the macroscopic models is the finite-range liquid-drop model (FR liquid-drop model). It corresponds to the model used in our original mass calculation [12]) and in a later calculation [37]). The second model is the finite-range droplet model (FR droplet model). This model was first used in a 1984 calculation [38]) (which reference unfortunately has numerous misprints). It was also used later in a contribution [39]) to the 1986–1987 Atomic Mass Prediction (this reference is devoid of misprints in the model specification). In our calculation of β-decay properties, the macroscopic model enters only in the calculation of Q_β values, neutron separation energies, and similar quantities. The theoretical values for these quantities also depend on the shell corrections. For the calculation of these quantities we use the Wapstra 1986–1987 experimental mass compilation [40]) and for the cases where experimental masses are not available, we use the 1988 mass calculation [36]) with the macroscopic model given by the FR droplet model.

In this latest mass calculation [36]) the calculated masses and ground-state deformations differ little from the results obtained in earlier calculations [12–14]). However, in contrast to the earlier calculation we have tabulated additional calculated ground-state properties in a form that can easily be used for further computer studies. We mentioned earlier the good agreement between calculated and measured ground-state deformations and the importance of using a correct ground-state deformation when calculating the β-strength function. We have now also tabulated the calculated levels with corresponding quantum numbers in the vicinity of the Fermi surface for all 8979 nuclear ground states. A good description of the low-lying level spectrum is also crucial for a reliable calculation of the β-strength function.

To investigate the global reliability of our calculated level spectrum close to the Fermi surface for our standard parameter choice we compare in figs. 6 and 7 calculated and experimental spin and parity assignments for odd-A nuclei for the light and heavy part of the periodic system, respectively. The calculated values are obtained from our 1988 tabulation [36]). The calculations very seldom predict that a nucleus is exactly spherical. To make a meaningful comparison between experimental spin and parity assignments and our calculated values for nuclei close to magic numbers we give a spherical level assignment to all nuclei whose calculated ground-state deformation ϵ_2 is less than 0.15. We obtain correct assignments in 60.0% of the cases. More specifically we found that the predictions were correct in 428 cases and incorrect in 285 cases. Our first aim in making this comparison was to check if there was any discrepancy that suggested an obvious improvement in our prescription in eqs. (6–7) for the spin-orbit strength. Since figs. 6 and 7 show excellent agreement at magic numbers throughout the periodic system it may be difficult to device a better prescription for the spin-orbit strengths than our chosen one. We have not concluded our analysis of the comparison between calculated and measured ground-state spin and parity assignments. However, it is clear that much of the disagreement occurs for transitional nuclei, where we have calculated the spin for

deformed shapes, but the experimental situation is that the nucleus remains spherical. One example of this type of disagreement is found in the region $84 \leq N \leq 89$ in the rare-earth region. Another example of a consistent disagreement is the region in the vicinity of $N = 56$. Experimentally $N = 56$ is a spherical subshell close to $Z = 40$, but the calculated result is that nuclei in this region are weakly deformed.

3.2. β-STRENGTH FUNCTIONS FOR Rb

Major new features in our β-strength code that were discussed above are, improved perturbation expressions for the $\Delta v = 0$ transition rates, the use of the Lipkin-Nogami pairing model that avoids the collapse that may occur in the usual BCS approximation, and the possibility of using the folded-Yukawa single-particle potential as the starting point for calculating the β-strength functions. To show the effects of some of these new features we display in figs. 8–10 β-strength functions for odd Rb isotopes from ^{89}Rb to ^{99}Rb. The calculations are based both on the Nilsson modified-oscillator and the folded-Yukawa single-particle potentials. The Nilsson-model results may be compared with the corresponding results obtained in the earlier model[6]). There are only very minor differences between the results of these two calculations for this sequence of nuclei. The main difference is that the two lowest peaks in the strength function are closer together in the new calculation than in the old one. This is an effect of the new pairing Δ values. In the new model the neutron and proton pairing gaps may be different, and we note in the figures the difference between the neutron and proton pairing gaps exceeds 0.5 MeV for ^{89}Rb.

A detailed comparison was made in our earlier work[6]) between measured and calculated strength functions for this sequence of nuclei. It was found that the low-energy peak in the calculated strength was about 1 MeV higher than the experimental result, but that the change in magnitude and location of the strength with neutron number was well reproduced by the calculation. That is, if the experiment showed an increase in the magnitude of the low-energy peak and a move towards lower excitation energy, as is the case when going from ^{93}Rb to ^{95}Rb, then the low-energy peak in the calculated strength shows the identical behavior, as we also see in fig. 9 for both the Nilsson and the folded-Yukawa potentials. In fact, it is interesting to observe that the differences between the Nilsson and folded-Yukawa models in figs. 8–10 are relatively minor. It is particularly noteworthy to observe how well both models reproduce the drastic change that occurs in the experimental strength function as the ground-state shape of the nucleus changes from spherical shape for ^{95}Rb to well-deformed for ^{97}Rb. For ^{95}Rb the experimental data[35]) show a sharp peak at about 4.5 MeV with no allowed strength below this peak, while for ^{97}Rb a radically different, much smoother strength function is observed, with some strength around 1 MeV, a window with no allowed strength in the interval 1.5 MeV to 3.5 MeV, and then a continuous distribution of strength above 3.5 MeV. The calculated strength functions reproduce this behavior very well.

A detailed interpretation of the calculated β-strength functions requires a knowledge

TABLE 3

Identification of major peaks in the ^{97}Rb β-strength function.

$E_{\rm exc}$ (MeV)	$\lvert M_{fi}\rvert^2$	$i_{\rm p}$	$i_{\rm n}$	$\Omega_{\rm p}^{\pi}$	$\Omega_{\rm n}^{\pi}$	Δv	I_β	$T_{1/2}$ (s)
0.01	0.0070	19	31	$3/2^+$	$3/2^+$	0	0.470	1.47
0.35	0.1156	19	28	$3/2^+$	$3/2^+$	0	6.632	0.10
0.78	0.0707	19	26	$3/2^+$	$1/2^+$	0	3.330	0.21
3.40	0.2018	19	23	$3/2^+$	$1/2^+$	0	2.253	0.31
3.63	0.0036	20	31	$5/2^+$	$3/2^+$	2	0.034	20.4
4.12	0.2125	20	28	$5/2^+$	$3/2^+$	2	1.461	0.47
4.36	0.0500	19	21	$3/2^+$	$5/2^+$	0	0.289	2.40

of the underlying neutron and proton single-particle level diagrams. We choose ^{97}Rb to illustrate some aspects of such an analysis. In figs. 11 and 12 we have plotted the corresponding Nilsson diagrams for neutrons and protons, respectively, for a folded-Yukawa single-particle potential. In table 3 we show some properties associated with the peaks seen in the folded-Yukawa β-strength function of ^{97}Rb shown in fig. 10. For each peak table 3 shows the energy of the peak, the nuclear matrix element for the transition, the number of the proton level involved in the transition counting from the bottom of the single-particle well, the number of the neutron level involved, the spin and parity of the proton level, the spin and parity of the neutron level, the difference Δv between the number of broken pairs in the daughter and mother nucleus, the intensity of the transition in arbitrary units, and the partial half-life of the transition, in seconds. Table 3 is very similar to a standard output that is obtained when the β-strength code is run. One immediately observes that the lowest few transitions are of the $\Delta v = 0$ type. The $\Delta v = 2$ transitions can only occur above $2\Delta_{\rm p}$, that is in this case above 2.58 MeV. Thus the lowest transitions involve a neutron changing into a proton in level 19, where there is already one unpaired proton. This situation is illustrated in the lower left graph in fig. 5, where we in this case should consider the unpaired proton to be just below the Fermi surface. In figure 12, we can identify the proton level involved in this transition. At $\epsilon_2 \approx 0.30$ the $i_{\rm p} = 19$ level is the $\Omega_{\rm p} = 3/2^+$ level emanating from the $g_{9/2}$ spherical level. The neutron level involved is the level $i_{\rm n} = 31$ which when filled corresponds to neutron number $N = 62$. In fig. 11 we see that this level is coming from the $g_{7/2}$ spherical shell. Since both the initial and the final state involve orbitals emanating from spherical g shells, one might wonder why the overlap is so small. The nuclear matrix element is only 0.007, but since the l quantum numbers at first sight seem to be the same one would naively expect a much larger overlap. A further inspection of the neutron level diagram resolves this paradox. At $\epsilon_2 \approx 0.13$ the $3/2^+$ levels coming out of the $g_{7/2}$ and

the $d_{5/2}$ spherical shells interact strongly and the quantum numbers are interchanged. Thus at $\epsilon_2 \approx 0.30$ level $i_n = 31$ has only a very small $l = 4$ component, which accounts for the small overlap. Instead, the large overlap occurs for level $i_n = 28$ as is seen in table 3. It is clear from inspecting fig. 11 that this level at $\epsilon_2 \approx 0.3$ is now mainly of $l = 4$ character. The first $\Delta v = 2$ transitions occur at 3.63 and 4.12 MeV. The relative magnitude of these two transitions can also be understood by again considering the interaction at $\epsilon_2 \approx 0.13$ between the levels coming out of the $g_{7/2}$ and the $d_{5/2}$ spherical shells and the exchange of quantum numbers that occurs.

As an example of results calculated with Woods-Saxon single-particle wave functions we show calculated strength functions in this model for four Rb isotopes in fig. 13. These results are fairly similar to the results obtained by use of folded-Yukawa wave functions. For instance, if we compare the results for ^{95}Rb we see that in both the Woods-Saxon and the folded-Yukawa calculation there are four prominent bins in the interval 4.75 MeV to 9.0 MeV. The slight difference in the location of the strength in the two models reflects small differences in the underlying single-particle potentials. A comparison of the results for ^{93}Rb in fig. 13 with the folded-Yukawa results in fig. 9 reveals that there seems to be one peak missing below 8 MeV in the Woods-Saxon results. An inspection of the single-particle level diagrams reveals the source of this difference in results. In the folded-Yukawa model we have immediately below the spherical $Z = 38$ gap in fig. 12 a $p_{3/2}$ level followed by a $f_{5/2}$ level further below. In the Woods-Saxon model the order of these two levels is reversed for ^{93}Rb. Thus in the folded-Yukawa model the ground-state of ^{93}Rb is $3/2^-$, whereas in the Woods-Saxon model it is $5/2^-$, with the universal parameter set. To see the result in the Woods-Saxon model with the unpaired proton in the $p_{3/2}$ level we have used the feature that allows us to study decay from excited states in the mother nucleus and calculated the strength function from the excited state where the odd particle is in the $p_{3/2}$ state. In the Woods-Saxon model the state is only about 50 keV below the $f_{5/2}$ state. With this initial state we obtain strength of magnitude 1.07, 0.94, 1.2, and 3.24 in the bins starting at 4.75, 5.50, 6.00, and 8.25 MeV, respectively. As expected, this result is indeed very similar to the folded-Yukawa result.

Experimentally, the ground-state spins and parities of the odd-A $^{89-95}$Rb sequence are $3/2^-$, $3/2^-$, $5/2^-$, and 5/2 (parity unknown), the folded-Yukawa result is $3/2^-$, $3/2^-$, $3/2^-$, and $3/2^-$, and the Woods-Saxon result is $5/2^-$, $5/2^-$, $5/2^-$, and $3/2^-$. We now understand the similarity for ^{95}Rb between the folded-Yukawa and the Woods-Saxon model; in this case both models place the unpaired odd proton in the same orbital. None of the models reproduce the experimental spin over the entire range of neutron numbers. The Nilsson model does give the correct ground-state spin in all four cases, but this was achieved through a change of parameters at $N = 93$. Such convenient parameter changes can usually not be invoked when the model is applied to unknown regions of nuclei, as in astrophysical applications, for example.

3.3. CALCULATED β-DECAY HALF-LIVES COMPARED TO OTHER MODELS

The calculated half-lives presented below are all based on the folded-Yukawa single-particle model. The deformations used in the calculation are taken from our most recent mass calculation[36]), except in special cases, such as when we compare to the results of other calculations, for example in fig. 14. The ground-state deformations obtained in this most recent calculation are usually very similar to values obtained in a previous calculation[13]). However, differences occur in transitional regions. Our most recent calculation has the advantage that it considers nuclei from the proton to the neutron drip lines, so we have available values of the ground-state deformations for all nuclei of astrophysical interest. The Q_β values are calculated from experimental mass differences[40]) where available, otherwise from our most recent mass calculation. In all our calculations of half-lives we multiply the calculated half-lives by a renormalization factor

$$r_{\rm re} = 2 \tag{72}$$

This is equivalent to dividing the calculated strength by $r_{\rm re}$. No strengths shown in any figure in this paper have been renormalized in this way; the renormalization is only carried out on the calculated half-lives.

As our first object of study, we select to calculate half-lives for the cases recently studied by Bender *et al.*[11]). In fig. 14 we compare half-lives calculated with a folded-Yukawa single-particle potential in our present model with the results of Bender *et al.*, and with experimental data[41–43]). Both calculations use ground-state deformations from ref.[13]). There are some differences between the results of the two calculations, but this is not unexpected since they do not employ the same single-particle potential; Bender *et al.* use a Nilsson potential in their calculation. In our calculation we have 3 cases out of 12 where the calculated result is more than a factor of 10 different from the experimental value. In this particular figure our calculated half-lives in this group of large deviations are all longer than experiment. Bender *et al.* have no case with an error larger than a factor of 10. As we will discuss in more detail below, there are experimental cases where β-decay from the ground-state and β-decay from a close-lying isomer have decay half-lives that differ by two orders of magnitude, or more. This large difference is due to the influence of the quantum numbers of the odd particle on the decay properties. Since we in our model do not always determine the ground-state shape and the corresponding odd-particle configuration correctly we expect that errors in the calculated half-lives of this order of magnitude will occur occasionally. This must obviously be the case in any model, with a frequency that depends on the accuracy of the model. For rare-earth nuclei we calculate below more than two hundred decay half-lives. We postpone further discussion of the magnitude of the error in β-decay half-life calculations until we present this larger sample.

The plot of the ratio $t_{\rm calc}/t_{\rm exp}$ shows that the points are approximately similarly distributed around the ratio 1 in both calculations. However, Bender *et al.* use $\chi_{\rm GT} = 15/A$ MeV. By using this value in test calculations we find that this choice decreases the half-lives to about half the value that is obtained with the choice $\chi_{\rm GT} = 23/A$ MeV,

which is the value we normally use. In our calculation we have multiplied the calculated half-lives by the renormalization factor $r_{\rm re} = 2$ to account for the fact that the strength obtained in models of the type we use, is about twice the experimental strength. Bender *et al.* use no renormalization factor. One would therefore expect that the half-lives calculated by Bender *et al.* would be about a factor of four shorter than the half-lives calculated by us. No such trend is seen in fig. 14. At this point we do not understand why the two calculations yield about the same half-lives with different choices of $\chi_{\rm GT}$ and renormalization factor $r_{\rm re}$. One possibility is that the sample of nuclei studied is too small for a systematic trend of this nature to be visible against a background of random fluctuations. We shall see in the further calculations presented below, that our calculated decay half-lives are centered on a line only slightly above the line representing the ratio 1. Our results thus are very consistent with results that have been obtained over recent years: a) to reproduce the position of the giant Gamow-Teller resonance one should choose $\chi_{\rm GT} = 23/A$ MeV and b) this choice leads to a calculated strength that is about twice as high as the observed experimental strength.

In fig. 15 we compare β-decay half-lives calculated in three different models to experimental data [44]) for nuclei in the beginning of the rare-earth region. All three calculations are about equally distributed on both sides of the line $t_{\rm calc}/t_{\rm exp} = 1$, if we ignore three points in our calculation with particularly large deviations. One sees that on the average the half-lives by Klapdor *et al.* [45]) are a little shorter and the half-lives by Takahashi *et al.* [1]) a little longer than experiment. The model used by Klapdor *et al.* in this figure is different from the model used by Bender *et al.* in fig. 14. To analyze the deviations between calculated and experimental β-decay half-lives in more detail than is possible for the data shown in figs. 14 and 15 a larger data set is needed. We have therefore performed a calculation of half-lives in the rare-earth region for all nuclei for which experimental half-lives are known and for which Q_β is larger than 1 MeV.

3.4. CALCULATED β-DECAY HALF-LIVES FOR RARE-EARTH NUCLEI

Our most extensive calculation of β-decay half-lives is in the rare-earth region. Here we have calculated the half-lives with respect to both β^+ and EC decay and with respect to β^- decay. To avoid lengthy constructions we will in our discussion in this section usually not distinguish between β^+ and EC decay and somewhat inexactly take Q_β to mean the maximum energy release in the decay. We have performed the calculation for all nuclei with Z between 62 and 76 for which the half-lives are known and for which Q_β is larger than 1 MeV. In figs. 16 and 17 we show the half-lives for combined β^+ and EC decay.

Cases that lie outside the scale of the figure have not been taken into account in our error analysis. Our conclusions below are not in any significant way affected by this selection of cutoff value for $t_{\rm calc}/t_{\rm exp}$. It is not our aim here to make a detailed analysis of each individual nucleus, but instead to present an overview of the rare-earth region and the model performance in a calculation of a large number of β-decay half-

lives. However, to get some understanding of what can be learned from a more detailed analysis we discuss briefly the cases that lie outside the window considered. There are nine such cases. In eight of those cases the experimental half-life is longer than 1 day, clearly cases where the decay usually should be dominated by forbidden transitions. In those eight cases we do not have any calculated strength below the Q_β value, and we are thus in agreement with the experimental situation for allowed decay. For ^{167}Yb the experimental half-life is 17.5 m but we calculate that the half-life is 1062 times longer, thus outside the window in the figure. For ^{167}Yb we have predicted a ground-state spin $5/2^+$, but experimentally the ground-state spin is $5/2^-$. (For ^{165}Yb we do predict a ground-state spin of $5/2^-$, in this case in agreement with the experimental situation.) In this particular case the large disagreement is probably due to the fact that the ground-state spin obtained in our model is incorrect.

In fig. 16 $t_{\rm calc}/t_{\rm exp}$ is plotted as function of Q_β with the aim of showing how the average error increases as Q_β decreases. It is obvious that errors in the location of the peaks in the calculated strength function have a larger effect on the calculated half-lives for small Q_β values than for larger ones. For a Q_β value of, say, 1 MeV the calculated half-life will be infinite if all the strength is above the Q_β window. Even if there experimentally is some strength in this window, very minor errors in the calculated level diagrams may have the effect that no strength is obtained in this window. Indeed, we see a fairly clear increase in the scatter of the points in fig. 16 as Q_β decreases. In fig. 17 the quantity $t_{\rm calc}/t_{\rm exp}$ is plotted as a function of the experimental half-life $t_{\rm exp}$. As a function of this quantity, one would expect the average error to increase as $t_{\rm exp}$ increases. This is also the case. In a visual inspection of fig. 17 one is left with the impression that the error in the calculation is fairly large. However, this is partly a fallacy, since for small errors there are many more points than for large errors. This is not clearly seen in the figure, since for small errors many points are superimposed on each other.

Normally one analyzes the error in a calculation by studying a root-mean square deviation, which in this case would be

$$\sigma_{\rm rms}{}^2 = \frac{1}{n}\sum_{i=1}^{n}(t_{\rm exp} - t_{\rm calc})^2 \qquad (73)$$

Such an error analysis is unsuitable here, for two reasons. First, the quantities studied vary by many orders of magnitude. In our case the variation is more than 10 orders of magnitude, from the millisecond range to years and beyond. Second, the calculated and measured quantities may differ by orders of magnitude, For quantities with this behaviour it is of interest to establish if the model reproduces measured values to within 2 orders of magnitude, to within 1 order of magnitude or perhaps to within a factor of 2. This can be established by studying the quantity $\log(t_{\rm calc}/t_{\rm exp})$, plotted in fig. 17, instead of $(t_{\rm exp} - t_{\rm calc})^2$. It is clear that this error definition is related to the distance of the points in fig. 17 from the line $t_{\rm calc}/t_{\rm exp} = 1$. Were all the points located on this line there would be perfect agreement between data and measured values. For the case all the points were grouped on the line $t_{\rm calc}/t_{\rm exp} = 10$ there would in all cases be an error

of a factor of 10. However, it is immediately clear that an error of this type could be entirely removed by changing the renormalization factor from the value given in eq. (72). In another extreme, suppose half the points were located on the line $t_{\rm calc}/t_{\rm exp} = 10$ and the other half on the line $t_{\rm calc}/t_{\rm exp} = 0.1$. In this case the average of $\log(t_{\rm calc}/t_{\rm exp})$ would be zero. We are therefore led to the conclusion that there are two types of errors that are of interest to study, namely the average position of the points in fig. 17, which is just the average of the quantity $\log(t_{\rm calc}/t_{\rm exp})$ and the spread of the points around this average. To analyze the error along the ideas above we therefore introduce the quantities

$$\begin{aligned} r &= t_{\rm calc}/t_{\rm exp} \\ r_1 &= \log_{10}(r) \\ M_{r_1} &= \frac{1}{n}\sum_{i=1}^{n} r_1^i \\ M_{r_1}^{10} &= 10^{M_{r_1}} \\ \sigma_{r_1} &= \left\{\frac{1}{n}\left[\sum_{i=1}^{n}\left(r_1^i - M_{r_1}\right)^2\right]\right\}^{1/2} \\ \sigma_{r_1}^{10} &= 10^{\sigma_{r_1}} \end{aligned} \tag{74}$$

where M_{r_1} is the average position of the points and σ_{r_1} the spread around this average. The spread σ_{r_1} can be expected to be related to uncertainties in the positions of the levels in the underlying single-particle model. The use of a logarithm in the definition of r_1 implies that these two quantities correspond directly to distances as seen by the eye in fig. 17, in units where one order of magnitude is 1. After the error analysis has been carried out we want to discuss the result of the error analysis in terms like "on the average the calculated half-lives are 'a factor of two' too long." To be able to do this we must convert back from the logarithmic scale. Thus, we realize that the quantities $M_{r_1}^{10}$ and $\sigma_{r_1}^{10}$ are conversions back to "factor of" units of the quantities $M_{r_1}^{10}$ and σ_{r_1}, which are expressed in distance or logarithmic units.

In table 4 we show the results of an evaluation of the expressions in eq. (75) for three different cutoff values of $t_{\rm exp}$. A reasonable cutoff value might be $t_{\rm exp} = 1000$ s. For longer half-lives one can expect forbidden decay to be dominating, as is also manifested by the increase of $\sigma_{r_1}^{10}$ for the o–e and o–o cases between the cutoffs 1000 s and 10000 s. We find that the average value of r, $M_{r_1}^{10}$, is about 1.5 in the o–e and e–e cases. This means that on the average our calculated half-lives are about 50% too long. One would thus in the o–e and e–e cases obtain better agreement between experimental and calculated values if the renormalization constant were 2/1.5 that is $r_{\rm re} = 1.33$ instead of the value 2 that we currently use. One interpretation why the renormalization constant should be 1.33 instead of the commonly accepted [28]) value 2 is, of course, that our calculated strength on the average is only 1.33 times the experimental strength instead of

TABLE 4

Analysis of the discrepancy between calculated and measured β-decay half-lives seen in fig. 17.

	n	M_{r_1}	$M_{r_1}^{10}$	σ_{r_1}	$\sigma_{r_1}^{10}$	$t_{\rm exp}^{\rm max}$ (s)
o-o	17	0.22	1.65	0.46	2.87	100
o-e	43	0.16	1.45	0.51	3.24	100
e-e	22	0.22	1.67	0.24	1.75	100
o-o	30	0.35	2.24	0.58	3.84	1000
o-e	69	0.17	1.48	0.60	3.96	1000
e-e	35	0.17	1.49	0.28	1.90	1000
o-o	35	0.34	2.19	0.60	4.03	10000
o-e	84	0.15	1.41	0.72	5.23	10000
e-e	41	0.17	1.48	0.28	1.92	10000

twice the experimental strength as is usually assumed. However, another interpretation is that the calculated locations of the peaks are somewhat too high on the average. To check how much the peaks have to be lowered to change the half-life by 1/1.5 we calculated the half-life of ^{95}Rb in the Nilsson model for the correct Q_β value of 9.28 MeV for which value we obtained the half-life 2.92 s. For the Q_β value 9.68 MeV we obtained 2.0 s. Thus, an increase in Q_β by 0.4 MeV, which simulates the effect on the half-life of lowering the location of the peaks in the strength distribution, decreased the half-life by about the same amount as multiplying the strength by 1.5.

In section 2.3.3 certain simplifications were made to allow the extension of the odd-A formalism to the odd-odd case. Were these simplifications inadequate one would expect to see a larger σ_{r_1} in the o-o case than in the o-e case. No such trend is seen in table 4.

An interesting observation that can be made in table 4 is that M_{r_1} is larger for o-o decay than for o-e and e-e decay. This supports our speculation above that the location of the peaks in our calculated β-strength functions may be consistently too high in energy and one may argue that the reason is that our calculated pairing Δ values are too high by ϵ_Δ, with the estimate that $\epsilon_\Delta = 200$ keV, on the average. First let us discuss the $\Delta v = 0$ transitions in o-o and o-e decay. In o-e decay the energies of the $\Delta v = 0$ transitions are given by the *difference* between the quasi-particle energy of the orbital to which a particular decay takes place and the quasi-particle energy of the ground-state level. The two quasi-particle energies both contain Δ, but the difference does not depend on Δ, to first order. Thus, these peaks should have approximately

correct location independently of reasonably small errors in Δ. The energies of the states populated by $\Delta v = 0$ transitions in the case of o-o decay are given by a *sum* of two quasi-particle energies. An error in ϵ_Δ in Δ would give an error of $2 \times \epsilon_\Delta$ in the location of these peaks.

For all three types of decays there is also strength due to the $\Delta v = 2$ transitions. For e-e decay these are the only transitions that occur. The energies of these transitions are given as roots to the RPA equations, where the asymptotes are sums of two quasi-particle energies. An error ϵ_Δ would increase the energy of these transitions by $2 \times \epsilon_\Delta$. The same types of transition occur in the o-e and o-o cases. Thus we may argue that the $\Delta v = 2$ transitions with the error $2 \times \epsilon_\Delta$ contribute about 0.15 to the error in M_{r_1} in all these three cases and that the additional error of $2 \times \epsilon_\Delta$ in the $\Delta v = 0$ transitions in the o-o case gives an additional contribution to M_{r_1} in this case.

The above analysis is somewhat incomplete in the sense that it failed to take into account how dominating the $\Delta v = 0$ transitions are over the $\Delta v = 2$ transitions in the o-e case. If most of the decay probability is due to the $\Delta v = 0$ transitions, then an error in the location of the $\Delta v = 2$ peaks would have very little effect. A detailed simulation of the effect of small changes in Δ in all three cases would provide the necessary information. A more extensive analysis of the source of the error in the mean M_{r_1} should consider the following sources: i) the overall renormalization $r_{\rm re}$ could be different from 2, ii) the location of the peaks may have systematic errors from other sources than from an incorrect pairing Δ, and iii) there may be a systematic error in the pairing Δ which manifests itself in the characteristic error pattern discussed above. From our mass calculation [36]) we have some indications that the calculated values of Δ are indeed too high. The resolution may be that a slightly different average pairing $\overline{\Delta}$ should be used in the Lipkin-Nogami case as compared to the BCS case (cf. sections 2.2.2 and 2.2.3).

In the beginning of section 2.3 it was mentioned that particle-particle correlations were not taken into account in our RPA treatment. These correlations are expected to strongly suppress β^+ transitions [11,26]), that is lead to longer half-lives than what is obtained in a model that does not consider these correlations. However, our results in fig. 17 and table 4 show that we in a standard treatment with a standard choice of $\chi_{\rm GT} = 23/A$ MeV and renormalization coefficient $r_{\rm re} = 2$ obtain β^+ decay rates that agree approximately with experiment. In fact, as discussed above, the calculated rates we obtain are somewhat suppressed relative to experiment, although we do not incorporate particle-particle correlations. The β^- decay rates presented below are calculated for too few nuclei to allow for any detailed conclusions, but show no clearly different characteristics from our results for β^+ decay.

Because of the phase-space factors $(Q_\beta - E_{\rm exc})^5$ for β-decay and $(Q_{\rm EC} - E_{\rm exc})^2$ for electron capture, where $E_{\rm exc}$ is the energy of the final state in the daughter nucleus relative to the ground state, β-decay and EC half-lives decrease rapidly with increasing Q values. In fig. 18 we display the correlation between Q_β values and experimental β-decay half-lives for β^+ decay. The relation between the experimental half-life and Q_β is approximately linear in the log-log representation of this figure, with even-even,

TABLE 5

Analysis of the discrepancy between schematically calculated and measured β-decay half-lives seen in fig. 20.

	n	M_{r_1}	$M_{r_1}^{10}$	σ_{r_1}	$\sigma_{r_1}^{10}$	$t_{\rm exp}^{\rm max}$ (s)
o-o	17	0.27	1.86	0.50	3.19	100
o-e	43	0.19	1.56	0.49	3.11	100
e-e	22	-0.07	0.85	0.30	1.99	100
o-o	29	0.41	2.56	0.67	4.67	1000
o-e	69	0.13	1.33	0.48	3.05	1000
e-e	35	0.01	1.02	0.33	2.14	1000
o-o	34	0.40	2.52	0.69	4.84	10000
o-e	85	0.16	1.44	0.60	3.96	10000
e-e	41	0.11	1.28	0.46	2.88	10000

odd-even and odd-odd nuclei grouped on three different lines. We define a schematic model for β^+ decay in which the calculated half-lives are related to Q_β by such linear relations. These postulated linear relationships were used to generate figs. 19 and 20. It would of course be possible to device a more refined schematic model, but our purpose is to compare the results of an almost trivial model to a refined calculation.

Figures 19 and 20 show that the discrepancies between the schematically calculated half-lives and the experimental half-lives are very similar to those in figs. 16 and 17, where the half-lives were calculated in the QRPA model. In table 5 we show the result of an analysis, similar to the one presented in table 4 for fig. 17, of the discrepancy between the schematic half-lives and the experimental data shown in fig. 20. We see that the results in tables 4 and 5 are very similar, as expected from the figures.

The fact that a simple schematic model leads to the same accuracy for the calculated β-decay half-lives as does the more refined QRPA calculation might lead to the reaction that it is not "necessary" to use a QRPA approach in the study of β-decay properties. However, our more detailed comparisons above and below, between calculations and experiment, show that the QRPA model, with its ability to take into account the effect of internal structure on the β-strength function, does lead to a much more detailed understanding of β-decay properties than approaches not incorporating the microscopic structure of the nucleus.

It obviously remains somewhat of a challenge to obtain better agreement between calculated and measured β-decay half-lives than what is obtained in the schematic

model. Part of the discrepancies present in figs. 16 and 17 may be due to the fact that a large part of our calculations involve nuclei in the transitional region around $N = 82$. In our calculations we used for the ground-state deformation precisely the shape that was obtained as the minimum in the potential-energy surface in our mass calculation. It is possible that a better approach would be to assume a spherical configuration whenever the calculated ground-state deformation ϵ_2 is less than, say, 0.15, as was done in the comparison between calculated and experimental ground-state spins. One should also note that one may have substantial errors in calculated decay half-lives even if the structure of the calculated β-strength function agrees very well with the measured strength function, because small errors in the calculated energy position of the peaks in the strength function give rise to large errors in the calculated half-lives.

We also investigated whether we would obtain much better agreement with data if we studied only those odd-A nuclei for which our calculated ground-state spin agree with data. We did see a trend in that direction, but the number of data points that could be used in this study were rather few, only 23 odd-even cases, compared to 104 in fig. 17. Thus, no firm conclusions could be drawn from this study.

In figs. 21 and 22 we show results obtained for β^- decay. The number of cases are too few to allow any detailed analysis of the results.

3.5. β-DECAY FROM EXCITED STATES

In section 2.4 we discussed how our model treats decay from excited states. As two illustrative examples of such decays we have selected the nuclei ^{102}Tc and ^{91}Mo, for which we calculate decay properties from the ground state and from one isomeric state. The results of this calculation are shown in fig. 23. The top two plots show the decay from the calculated ground-state and an excited state of the deformed nucleus ^{102}Tc. One should observe that the calculated ground state and excited state configurations are reversed relative to the experimental situation for this nucleus. Experimentally it is the ground state configuration that has spin $I^\pi = 1^+$. In the calculations this state is obtained as an excited state, and when discussing the *calculations* we therefore refer to this configuration as the excited state. In our model the calculated energy of the excited mother configuration we have selected in ^{102}Tc is 0.10 MeV above the ground-state energy. We mentioned above that the magnitude of the strength in each one of the $\Delta v = 2$ transitions would be the same in the decay from an excited configuration as in the decay from the ground-state configuration but that the location of these transitions would be shifted up in energy by the amount of excitation energy of the excited state. In the case of ^{102}Tc decay we find that there are no such transitions below 7.4 MeV. Above this energy it is difficult to study their behavior, because each bin contains a superposition of $\Delta v = 0$ and $\Delta v = 2$ transitions.

In section 2.4 we pointed out that for odd-odd nuclei the behavior of the $\Delta v = 0$ transitions is somewhat more complex than for the odd-even case. Figure 3 provides an illustration of the various types of decay that can occur from the ground-state configu-

ration of ^{102}Tc. The unpaired proton is in level 22 and the unpaired neutron in level 29. In our treatment of the excited state we have put the odd neutron in level 28. This is at variance with the rule we gave at the end of section 2.4, namely that we should not create excited states as particle states in levels below the Fermi surface, but since level 28 is so close to level 29 and just at the Fermi surface we may break this rule, since the probability of hole and particle states close to the Fermi surface both are close to 0.5. Our output that identifies the origin of the transitions in the β-strength function shows that the orbitals that are involved in the transition from the excited ^{102}Tc in the upper right of fig. 23 to the ground state of ^{102}Ru are the proton orbital 22 and the neutron orbital 28. It is clear that this is the only possibility; this transition corresponds to the type shown in the lower right part of fig. 3. Obviously the only way to obtain a transition below $\Delta_p + \Delta_n$ is through this transition.

Our code also identifies the large peak at about 3.5 MeV as a transition involving proton orbital 22 and neutron orbital 28. This may appear puzzling, since these are the orbitals involved in the decay to the ground state. The resolution is that the transition leading to the large peak at about 3.5 MeV is of the type shown in the lower right part of fig. 5. Thus, it is a paired neutron in level 28 that makes a transition to the proton orbit 22, where we initially had an unpaired proton, but as a final state have two paired protons. The same transition is present in the decay from the ground-state configuration of ^{102}Tc in the upper left part of fig. 23, but at a slightly lower energy. As discussed in sect. 2.4 in the case of a doubly odd system, the $\Delta v = 0$ transitions that do not involve the odd particle that is excited, in this case the odd neutron in levels 29 and 28 in the ground-state and excited-state configurations, respectively, will be present in the decays from both the ground-state and excited-state configurations. Just as is the case with the $\Delta v = 2$ transitions the energy of these $\Delta v = 0$ transitions from the excited configuration will be higher than the corresponding transitions from the ground-state by an amount that is equal to the difference in excitation energy of the quasi-particle that is not involved in the transition. In the case studied in the top part of fig. 23, the difference between the two neutron quasi-particle energies corresponding to levels 28 and 29 is 0.10 MeV which is consistent with the shift in location of the peak at about 3.5 MeV in the two top graphs in fig. 23.

Experimentally the ground-state decay of ^{102}Tc is from a 1^+ state with a half-life of 5.3 s. The excited state has spin 4 and decays with a half-life of 260 s. This is quite consistent with the calculated results, except that in the calculation the excited and ground states are interchanged, relative to the experimental situation. We see then, that in this particular case there is a change in experimental half-life by a factor 50 when the odd neutron is moved from a level $\Omega_n^\pi = 3/2^+$ to a level $\Omega_n^\pi = 3/2^-$ which is calculated to be only 100 keV away. This case clearly illustrates that it is impossible to guarantee small errors in the predictions of β-decay half-lives, even in a model that takes microscopic structure into account. Obviously one must expect occasional errors of up to two or more orders of magnitude even when decays in the range of a few seconds are considered.

The lower part of fig. 23 shows the decay of the spherical odd-even nucleus ^{91}Mo

from both a ground-state and an excited-state configuration. Experimentally the ground state of this nucleus has spin $\Omega_n^\pi = 9/2^+$ and a β-decay half-life of 15.5 m. There is an excited state at 0.65 MeV with a β-decay half-life of 1.1 m and with spin $\Omega_n^\pi = 1/2^-$.

In the calculation the excited state is located at an energy 1.76 MeV above the ground-state. The peaks between 0 and 1 MeV are of $\Delta v = 0$ character. The peaks that are present in this region in the decay of the ^{91}Mo ground-state configuration have been replaced by a completely different set of transitions in the decay of the excited configuration. However, the peak at about 7.5 MeV present in the decay of the ground-state configuration is of $\Delta v = 2$ character and is therefore present also in the decay of the excited configuration, but its position has moved up by an amount equal to the calculated excitation energy of the system, namely 1.76 MeV.

The fairly large difference between the calculated and experimental value for the energy of the excited state is due to several effects. The shape considered is a spherical shape, for which we predict the correct spin configuration of both the ground-state and the excited state. The splitting between the several spin-orbit partners that are present at spherical shape is in the model determined by a single spin-orbit parameter. In an actual nucleus there are additional residual interactions that cause deviations from this simple one-parameter model. The energy of the excited state is in the model given by the quasi-particle energy obtained from the pairing model. This energy depends not only on the position of the single-particle level in question but is also strongly dependent on the value that is obtained for the Fermi-surface parameter λ obtained by solving the equations in section 2.2.3. For situations where there are large gaps in the single-particle level spectrum this parameter is very sensitive to small changes in the positions of the calculated positions of the single-particle levels.

The calculated spins for the ground-state and excited-state configurations agree with measured values. In the calculation of half-lives the experimental Q_β values were used. The calculated half-life for decay from the ground state is 85 s and for the decay of the excited configuration 16 s which for the ground-state configuration is about a factor of 10 faster, and for the excited state about a factor of 4 faster than the experimental values. In our calculation of the β-decay properties of ^{91}Mo we have assumed that the nucleus is spherical. The calculated ground-state shape is actually slightly deformed, namely $\epsilon_2 = 0.05$. Experimentally, the $9/2^+$ and $1/2^-$ configurations are probably not as pure as is obtained with our assumption of a completely spherical configuration. This is probably the mechanism behind the slower experimental decay rates. It has previously [6]) been pointed out that one can expect that the model has its greatest difficulties in describing nuclei of transitional character.

3.6. β-DELAYED NEUTRON EMISSION AND HALF-LIVES FOR $^{25-35}$Na

In decay from the r-process line to the line of β-stability β-delayed neutron emission plays an important role in determining the isotopic abundances on the line of β-stability [8]). To show some examples of model predictions of β-delayed neutron emission

probabilities, P_n, and to gain insight into the interplay between β-strength functions, β-decay half-lives and P_n values, we have calculated these quantities for the sequence $^{25-35}$Na of sodium isotopes. In figs. 24 and 25 we display calculated strength functions for the eight lighter isotopes in this sequence. In fig. 26 we show the corresponding calculated β-decay half-lives and P_n values compared to experimental data[46-48]). The strength in the shaded triangular regions in figs. 24 and 25 has not been plotted, to avoid an unsuitable change of scale. The wide arrow indicates the neutron separation energy in the daughter and the thin arrow the Q value of the decay. In our simple model the decay to states above the wide arrow but below the Q_β value indicated by the thin arrow, will lead to delayed neutron emission.

In the calculations the ground-state deformation has been taken from the most recent mass calculation[36]), except for ^{31}Na. For this nucleus experimental data indicates deformation, but in the calculation we obtain the deepest minimum at spherical shape. However, as discussed in ref.[14]) one obtains in the potential-energy surface for this nucleus two minima of almost equal depth. Minor details in the calculations determine which is calculated to be the deeper one. We have therefore for ^{31}Na used a deformation corresponding to the deformed prolate minimum, although the spherical minimum is calculated[36]) to be the deeper minimum. In our earlier calculation[13,14]) the deformed minimum was calculated to be the deeper minimum.

On the logaritmic scale in fig. 26 the agreement between calculated quantities and experimental data looks fairly good. An interesting correlation is that the calculated half-lives and P_n values are either both below or both above the experimental data. A simple argument explains this correlation. Suppose the calculated P_n value is too low. This means that there is too much strength below the neutron binding energy, indicated by the wide arrow in the figures. But, too much strength at low energies also leads to increasing decay rates and consequently to too short half-lives compared to experiment. Thus excess strength at low energies leads both to too low P_n values and to too short β-decay half-lives relative to experiment.

It is clear that the β-decay half-lives are particularly sensitive to the strength at low excitation energy, because of the strong phase-space factor dependence. The P_n values are also affected by the strength in this region, since a large decay intensity to the low-lying energy levels would leave less decay intensity to levels above the neutron binding energy, the energy region from which β-delayed neutron emission occurs. However, the P_n values are particularly sensitive to the location of the strength in the vicinity of the neutron binding energy, indicated by the wide arrow in figs. 24 and 25. Obviously, strength below the neutron binding energy does not contribute to the delayed neutron emission rate, but strength above does. The strength function for ^{31}Na provides an interesting example of the sensitivity of the P_n value to the location of the strength in this region. As is seen in fig. 26 there is very good agreement between the calculated and experimental half-life for this nucleus. However, the calculated P_n value is 12% compared to the experimental[46]) value of 36%. An inspection of the calculated β-strength function for ^{31}Na in the lower left of fig. 25 shows that there is a huge peak in the strength function just below the neutron binding energy. To study the effect of

a small change in the location of this peak we have (by changing a number in one of the temporary files in the calculations) moved the location of this peak from 1.94 MeV to 2.06 MeV, just above the calculated location of the neutron binding energy. The effect on the calculated half-life is only 2%, but the calculated P_n value increases to 75%. This example illustrates the difficulty of consistently achieving high accuracy in P_n calculations.

Conceivably, the above described sensitivity of the P_n values to the exact locations of the sharp peaks in the calculated β-strength function can be reduced by performing a smearing. Such a procedure can be seen as an attempt to take a rough account of the remaining, non-specific residual interactions. The empirical fact that large jumps in P_n between neighboring nuclei appear to be absent lends further support for such an approach.

4. Summary

We have presented an improved model for the calculation of strength functions for Gamow-Teller β-decay. We have incorporated many significant enhancements over the original model for Gamow-Teller β-decay of deformed nuclei that was presented 6 years ago[6]). The most important are:

- In addition to the Nilsson modified-oscillator single-particle potential, we can now also use folded-Yukawa and Woods-Saxon potentials as starting points for determining the wave functions of the mother and daughter nuclei involved in the decay.

- The pairing part of the model has been improved. The pairing Δ_n and Δ_p values are determined in a microscopic model with the effect that the underlying level structure is reflected in the values obtained. We can use either a BCS pairing model or a Lipkin-Nogami model. The latter model avoids the collapses that occur in the BCS model. The strength G of the pairing interaction is determined by a method that is valid in any part of the nuclear chart.

- The perturbation treatment of $\Delta v = 0$ transitions in odd-even and odd-odd nuclei has been improved so that we now avoid the singularities that occurred in earlier treatments. Odd-odd nuclei are also treated.

- Decays from states where the unpaired odd particle is in an excited state can now be treated.

- Models for the calculation of half-lives with respect to β^- and β^+ decay and electron capture have been studied and incorporated into our computer codes.

Most of the enhancements described above were added to the model in 1988, but a few of the above features were incorporated earlier into the Nilsson model codes. In particular, the present treatment of the $\Delta v = 0$ transitions already was included already in 1985[15]). Our aim here has been to introduce, fully define, and discuss all the

enhancements relative to the earlier model [6]) in a consistent manner and to apply the model with several of its new features to a set of problems of current interest.

The initial applications of the enhanced model that we have introduced here, have been studies of Rb strength functions in all three single-particle models, calculations of rare-earth half-lives, calculations of decay properties from excited and ground-state configurations in ^{102}Tb and ^{91}Mo and the calculation of β-decay half-lives and P_n values for a sequence of neutron-rich sodium isotopes. Our general conclusion is that the model explains structure in the β-strength properties in terms of properties that we are able to understand and describe in our underlying nuclear-structure model. One illustration of a typical structure effect of this nature is the sudden change in the β-strength function and the β-decay half-life between ^{95}Rb and ^{97}Rb which is explained by the onset of deformation. Another example is the drastic difference in decay properties of the two lowest energy states in ^{102}Tc, which is explained by the different decay selection rules for the two odd-neutron orbitals.

A particular advantage of the current model is that the calculation of the β-strength functions is now based on the folded-Yukawa single-particle model. This model has been used in a microscopic-macroscopic approach in the calculation of nuclear structure quantities, such as ground-state masses, shapes, spins, level structure and pairing effects for 8979 nuclei between the proton and neutron drip lines from oxygen to the heaviest elements. This *unified* approach to the calculation of nuclear-structure quantities considerably enhances our capability to interpret the experimental data in terms of a consistent, underlying nuclear-structure picture. It should be recalled that the entire model for the Gamow-Teller strength function introduces few new free parameters. In principle only the renormalization parameter $r_{re} = 2$ and the strength χ_{GT} of the Gamow-Teller residual interaction are new parameters. Both may be determined from studies of the giant Gamow-Teller resonance in lead and, for greater accuracy, from resonances in other nuclei, without any consideration of low-energy β-decay properties. Other parameters in the model have been determined earlier, from studies not directly related to β decay, namely nuclear mass calculations and studies of ground-state single-particle level spectra.

Nuclear-structure models are of great importance in many astrophysical studies, for instance in studies of isotopic abundances produced in the decay from the r-process line to the line of β stability. Clearly, the introduction of realistic nuclear-structure models now significantly influences the conclusions that can be drawn in the modelling of astrophysical scenarios [8]). Nuclear mass models can now be used with some confidence outside the regions to which the model parameters were adjusted [12,37,39]). Many quantities associated with β-decay are, as we have seen above, quite well understood and described by the current model. However, occasionally small changes in deformation values, level order, or Q values will affect calculated β-decay rates and P_n values by several orders of magnitude. Such large uncertainties are of course undesirable and impair the confidence by which the model can be applied to unknown regions of nuclei in the study of problems of astrophysical interest. However, relative to earlier approaches that did not take full account of the effect of single-particle structure and nuclear deformation,

the present models represent an important step forward.

In the present version of our model, with its enhancements relative to the initial formulation [6]), in particular the use of the folded-Yukawa single-particle potential, we have achieved a unified model framework for the study of a large number of nuclear structure quantities within a single model and with a single, limited model parameter set. The model has, as mentioned above, already been applied to the calculation of a significant number of ground-state properties for 8979 nuclei, such as masses, shape, spin, level structure, and pairing properties. A detailed analysis of these results is now in progress. This analysis, together with more extensive studies of β-decay properties of known nuclei with the present model, now give us a better understanding of the properties of these nuclei and also the experience with the models that is required for extensive applications to regions far from stability.

Acknowledgments

We wish to acknowledge valuable discussions with R. C. Greenwood, C. W. Reich, M. W. Drigert, K. L. Kratz, D. J. Vieira, J. R. Nix, and W. Nazarewicz. Special thanks are due to J. Krumlinde who, despite other commitments, has continued to take an interest in this project; in particular, we wish to acknowledge that the method used to avoid the singularities in the $\Delta v = 0$ transitions was suggested by him. We are also grateful to E. Browne who provided us with a database of experimental β-decay properties.

One of us (PM) would like to thank the Idaho National Engineering Laboratory for the support that made this effort possible, the Lawrence Berkeley Laboratory for its hospitality during the project, and the Los Alamos National Laboratory where this manuscript was completed.

Most of the calculations in this study were carried out at the National Magnetic Fusion Energy Computer Center, (NMFECC), Lawrence Livermore National Laboratory. All the figures in this article were produced by Viking [49]), a computer graphics program for scientific-oriented publication-quality graphics for POSTSCRIPT output devices.

References

1) K. Takahashi and M. Yamada, Prog. Theor. Phys. **41** (1969) 1470.

2) I. Hamamoto, Nucl. Phys. **62** (1965) 49.

3) J. A. Halbleib, Sr., and R. A. Sorensen, Nucl. Phys. **A98** (1967) 542.

4) J. Randrup, Nucl. Phys. **A207** (1973) 209.

5) J. Krumlinde, P. Möller, C. O. Wene, and W. M. Howard, Proc. 4th Int. Conf. on nuclei far from stability, Helsingør, 1981 (CERN 81-09, Geneva, 1981) p. 260.

6) J. Krumlinde and P. Möller, Nucl. Phys. **A417** (1984) 419.

7) G. D. Alkhazov, A. A. Bykov, V. D. Vitman, Yu. V. Naumov, and S. Yu. Orlov, Proc. 4th Int. Conf. on nuclei far from stability, Helsingør, 1981 (CERN 81-09, Geneva, 1981) p. 238.

8) K. -L. Kratz, F. -K. Thielemann, W. Hillebrandt, P. Möller, V. Harms, A. Wöhr, and J. W. Truran, Proc. 6th Int. Symp. on capture gamma-ray spectroscopy, Leuven, 1987 (Inst. Phys. Conf. Ser. No. 88/J. Phys. G:Nucl. Phys. 14 Suppl. 1988) p. S331.

9) J. M. Nitschke, P. A. Wilmarth, J. Gilat, P. Möller, and K. S. Toth, Proc. Fifth. Int. Conf. on nuclei far from stability, Rosseau Lake, Ontario, Canada, 1987 (AIP, New York, 1988) AIP Conference Proc. **164** (1988) 403.

10) B. S. Meyer, W. M. Howard, G. J. Mathews, K. Takahashi, P. Möller, and G. A. Leander, Phys. Rev. C, (1989) in press.

11) E. Bender, K. Muto, and H. V. Klapdor, Phys. Lett. B **208** (1988) 53.

12) P. Möller and J. R. Nix, Nucl. Phys. **A361** (1981) 117.

13) P. Möller and J. R. Nix, ATOMIC DATA AND NUCLEAR DATA TABLES **26** (1981) 165.

14) R. Bengtsson, P. Möller, J. R. Nix, and Jing-ye Zhang, Phys. Scr. **29** (1984) 402.

15) K. L. Kratz, J. Krumlinde, G. A. Leander, and P. Möller, Proc. American Cemical Society Symp. on nuclie off the line of stability, Chicago, 1985 (American Chemical Society, Washington DC 1986, ACS Symposium Series 324, 1986) p. 159.

16) J. Dudek, Z. Szymanski, T. Werner, A. Faessler, and C. Lima, Phys. Rev. **C26** (1982) 1712.

17) M. Bolsterli, E. O. Fiset, J. R. Nix, and J. L. Norton, Phys. Rev. **C5** (1972) 1050.

18) P. Möller and J. R. Nix, Proc. Third IAEA Symp. on the physics and chemistry of fission, Rochester, 1973, vol. I (IAEA, Vienna, 1974) p. 103.

19) P. Möller, S. G. Nilsson, and J. R. Nix, Nucl. Phys. **A229** (1974) 292.

20) S. G. Nilsson, C. F. Tsang, A. Sobiczewski, Z. Szymański, S. Wycech, C. Gustafson, I.-L. Lamm, P. Möller, and B. Nilsson, Nucl. Phys. **A131** (1969) 1.

21) D. G. Madland and J. R. Nix, Nucl. Phys. **A476** (1988) 1.

22) J. R. Nix, Ann. Rev. Nucl. Sci. **22** (1972) 81.

23) H. J. Lipkin, Ann. of Phys. **9** (1960) 272.

24) Y. Nogami, Phys. Rev. **134** (1964) B313.

25) H. C. Pradhan, Y. Nogami, and J. Law, Nucl. Phys. **A201** (1973) 357.

26) J. Engel, P. Vogel, and M. R. Zirnbauer, Phys. Rev. **C37** (1988) 731.

27) B. Lauritzen, Nucl. Phys. **A489** (1988) 237.

28) C. Gaarde, J. S. Larsen, C. D. Goodman, C. C. Foster, C. A. Goulding, D. J. Horen, T. Masterson, J. Rapaport, T. N. Taddeucci, and E. Sugarbaker, Proc. 4th Int. Conf. on nuclei far from stability, Helsingør, 1981 (CERN 81-09, Geneva, 1981) p. 281.

29) A. Bohr and B. R. Mottelson, Phys. Lett. **100B** (1981) 10.

30) G. F. Bertsch and I. Hamamoto, Phys. Rev. **C26** (1982) 1323.

31) A. deShalit and H. Feshbach, in Theoretical physics, vol. I: Nuclear Structure (John Wiley & Sons, New York, 1974).

32) M. A. Preston, in Physics of the nucleus (Addison-Wesley, Reading, 1962).

33) N. B. Gove and M. J. Martin, NUCLEAR DATA TABLES **10** (1971) 205.

34) K.L. Kratz, H. Ohm, A. Schröder, H. Gabelmann, W. Ziegert, H. V. Klapdor, J. Metzinger, T. Oda, P. Pfeiffer, G. Jung, L. Alquist, and G. I. Crawford, Proc. 4th Int. Conf. on nuclei far from stability, Helsingør, 1981 (CERN 81-09, Geneva, 1981) p. 317.

35) K.-L. Kratz, Nucl. Phys. **A417** (1984) 447.

36) P. Möller, J. R. Nix, W. D. Myers, and W. J. Swiatecki, unpublished (1988).

37) P. Möller and J. R. Nix, ATOMIC DATA AND NUCLEAR DATA TABLES **39** (1988) 213.

38) P. Möller, W. D. Myers, W. J. Swiatecki, and J. Treiner, Proc. 7th Int. Conf. on nuclear masses and fundamental constants (AMCO-7), Darmstadt-Seeheim, 1984 (Lehrdruckerei, Darmstadt, 1984) p. 457.

39) P. Möller, W. D. Myers, W. J. Swiatecki, and J. Treiner, ATOMIC DATA AND NUCLEAR DATA TABLES **39** (1988) 225.

40) A. H. Wapstra, G. Audi, and R. Hoekstra, ATOMIC DATA AND NUCLEAR DATA TABLES **39** (1988) 281.

41) U. Bosch, W.-D. Schmidt-Ott, P. Tidemand-Petersson, E. Runte, W. Hillebrandt, M. Lechele, F.-K. Thielemann, R. Kirchner, O. Klepper, E. Roeckl, K. Rykaczewski, D. Schardt, N. Kaffrell, M. Bernas, P. Dessagne, and W. Kurcewicz, Phys. Lett. **164B** (1985) 22.

42) E. Runte, W.-D. Schmidt-Ott, P. Tidemand-Petersson, R. Kirchner, O. Klepper, W. Kurcewicz, E. Roeckl, N. Kaffrell, P. Peuser, K. Rykaczewski, M. Bernas, P. Dessagne, and M. Langevin Nucl. Phys. **A399** (1983) 163.

43) E. Runte, K.-L. Gippert, W.-D. Schmidt-Ott, P. Tidemand-Petersson, L. Ziegler, R. Kirchner, O. Klepper, P. O. Larsson, E. Roeckl, N. Kaffrell, P. Peuser, M. Bernas, P. Dessagne, M. Langevin, and K. Rykaczewski, Nucl. Phys. **A441** (1985) 237.

44) R. C. Greenwood, R. A. Anderl, A. J. Caffrey, J. D. Cole, M. W. Drigert, R. G. Helmer, M. A. Lee, C. W. Reich, and D. A. Struttmann, Proc. Int. Conf. on nuclear data for science and technology, Mito, Japan, 1988, ed. S. Igarasi (Saikon Publ. Co., Tokyo 1988) p. 359.

45) H. V. Klapdor, J. Metzinger, and T. Oda, ATOMIC DATA AND NUCLEAR DATA TABLES **31** (1984) 81.

46) P. G. Hansen and B. Jonson, in Charged particle emission from nuclei, ed. D. N. Poenaru and M. S. Ivaşcu, vol. III (CRC, Boca Raton, 1989) p. 157.

47) M. Langevin, C. Détraz, D. Guillemaud-Mueller, A. C. Mueller, C. Thibault, F. Touchard, and M. Epherre, Nucl. Phys. **A414** (1984) 151.

48) D. Guillemaud-Mueller, C. Détraz, M. Langevin, F. Naulin, M. de Saint-Simon, C. Thibault, F. Touchard, and M. Epherre, Nucl. Phys. **A426** (1984) 37.

49) P. Möller, J. R. Nix, and A. J. Sierk, (1989), unpublished.

Figure Captions

Fig. 1 β-strength function obtained from a calculation with expansion coefficients given by eq. (38). The breakdown of this expansion gives rise to the huge peak just below 3 MeV. The singularity was discovered in 1983 when only a simple pairing model had been incorporated in the code. In that pairing model the BCS equations are solved for externally fixed (FXD) Δ_p and Δ_n equal to $12/\sqrt{A}$ MeV.

Fig. 2 β-strength function obtained from a calculation with expansion coefficients given by eq. (42). The values of the width d are 0.1 MeV (solid line) and 1.0 MeV (dashed line). The singularity present in fig. 1 has disappeared. One also notes that the difference between the strength functions corresponding to the two d values is very small.

Fig. 3 Four different types of β^--decay of an odd-odd nucleus in an extreme single-particle model. The shaded circle in the daughter nucleus indicates which nucleon decayed. The dashed line shows the location of the Fermi surface for the even-even vacuum nucleus. It is for this nucleus that the pairing and RPA equations are solved.

Fig. 4 Calculated β^- Gamow-Teller strength functions based on two single-particle models and a Lipkin-Nogami (L-N) pairing model. The upper two strength functions are calculated for the choice $\chi_{GT} = 23/A$ MeV, the lower two for the choice $\chi_{GT} = 15/A$ MeV. The experimental location of the giant Gamow-Teller resonance corresponds to the excitation energy 15.5 MeV.

Fig. 5 Four different types of β-decay from excited states in odd-A and odd-odd nuclei in an extreme single-particle model. The different cases are discussed in the text.

Fig. 6 Comparison between calculated and measured ground-state spin-parity assignments for odd-A nuclei in the lighter part of the periodic system. There is excellent agreement for spherical and well-deformed regions, but disagreements in transitional regions such as $N \approx 56$ and $N \approx 87$.

Fig. 7 Comparison between calculated and measured ground-state spin-parity assignments for odd-A nuclei in the heavier part of the periodic system. The calculations in fig. 6 and this figure agree with data in 60% of the cases over the periodic system.

Fig. 8 Calculated β-strength functions for ^{89}Rb and ^{91}Rb in a Nilsson and a folded-Yukawa model. The difference in the Nilsson model calculation relative to our earlier work [6]) is that we use a Lipkin-Nogami pairing model and an improved perturbation treatment of the $\Delta v = 0$ transitions. The differences relative to the original work and between the two single-particle models are fairly minor.

Fig. 9 Calculated β-strength functions for ^{93}Rb and ^{95}Rb in a Nilsson and a folded-Yukawa model. The Nilsson κ and μ parameters are changed relative to fig. 8 (cf. discussion in ref. [6])). In agreement with experimental data the calculations show an increase in strength and a decrease in excitation energy for the low-energy peak for ^{95}Rb compared to ^{93}Rb.

Fig. 10 Calculated β-strength functions for ^{97}Rb and ^{99}Rb in a Nilsson and a folded-Yukawa model. A characteristic change in the structure has occurred in the β-strength function when compared to the calculations in figs. 8 and 9. This change in structure is seen experimentally and occurs because the ground-state shape of the nucleus has changed from spherical to deformed.

Fig. 11 Calculated neutron single-particle level diagram for ^{95}Rb for our standard parameter choice. The ϵ_4 parameter is kept fixed at $\epsilon_4 = 0$. As discussed in the text and illustrated in table 3, one may interpret peaks in the β-strength functions in terms of transitions between particular levels in this level diagram and the level diagram in fig. 12.

Fig. 12 Calculated proton single-particle level diagram for ^{95}Rb for our standard parameter choice. The ϵ_4 parameter is kept fixed at $\epsilon_4 = 0$.

Fig. 13 Calculated β-strength functions for ^{89}Rb, ^{91}Rb, ^{93}Rb and ^{95}Rb in a Wood-Saxon model. In the text these results are compared to the results presented in figs. 8 and 9.

Fig. 14 Measured β-decay half-lives compared to two RPA calculations in the $A = 60$ region. The calculation by Bender *et al.* [11]) is based on a Nilsson and our present calculation on a folded-Yukawa single-particle potential.

Fig. 15 Measured β-decay half-lives compared to three calculations in the beginning of the rare-earth region. Our present calculation is the only one that takes deformation fully into account.

Fig. 16 Ratios between calculated and measured half-lives for β^+ and electron capture decay as functions of Q_β. The discrepancy between calculated and experimental half-lives is expected to be larger for low Q_β values, because the calculated half-life is here most sensitive to errors in the calculated positions of the peaks in the strength functions. Q_β is the maximum energy release in the decay.

Fig. 17 Ratios between calculated and measured half-lives for β^+ and electron capture decay as functions of the experimental half-life for β^+ and EC decay. As expected, the error in the calculated half-life increases with increasing experimental half-life. An error analysis of the results in this figure is presented in table 4 and discussed in the text. Q_β is the maximum energy release in the decay.

Fig. 18 Correlation between Q_β value and measured β-decay half-life. Q_β is the maximum energy release in the decay.

Fig. 19 Ratios between schematically calculated and measured half-lives for β^+ and electron capture decay as functions of Q_β. The schematic model is a linear approximation to the correlation between $t_{\rm exp}$ and Q_β found in fig. 18. Q_β is the maximum energy release in the decay.

Fig. 20 Ratios between schematically calculated and measured half-lives for β^+ and electron capture decay as functions of the experimental half-life for β^+ and EC decay. Q_β is the maximum energy release in the decay.

Fig. 21 Ratios between calculated and measured half-lives for β^- decay as functions of Q_β. The number of cases in the figure are too few for revealing systematic trends.

Fig. 22 Ratios between calculated and measured half-lives for β^- decay as functions of the experimental half-life for β^- decay. The number of cases in

the figure are too few for revealing systematic trends. In particular, there are very few cases corresponding to short half-lives.

Fig. 23 Decays from the ground state compared to decay from excited states. For Tc the calculated energy of the excited state is only 0.1 MeV above the ground state, but the half-life is about 100 times shorter. The large difference in decay half-lives between configurations that are so close in energy shows that one has to expect errors in the calculated half-lives that occasionally are of this or larger magnitude. In the calculation the excited and ground state are reversed, relative to the experimental situation.

Fig. 24 Strength functions for β^--decay of four neutron-rich sodium isotopes. The wide arrow gives the neutron binding energy in the daughter nucleus and the narrow arrow the Q_β value of the decay. In the two lower strength functions the neutron binding energy is lower than the Q_β value, thus β-delayed neutron emission is possible. Strength above 15 MeV in the triangular shaded regions of ^{25}Na and ^{27}Na is not plotted.

Fig. 25 Strength functions for β^--decay of four very neutron-rich sodium isotopes. The wide arrow gives the neutron binding energy in the daughter nucleus and the narrow arrow the Q_β value of the decay. Experimentally the delayed neutron-emission probability P_n is above 20% for all four nuclei. Strength above 15 MeV in the triangular shaded region of ^{29}Na is not plotted.

Fig. 26 Calculated β-decay half-lives and delayed neutron-emission probabilities compared to experiment for neutron-rich sodium isotopes. If the calculated half-life is lower than the experimental value, then there is too much strength at low energies, possibly below the neutron binding energy; therefore the calculated P_n value can be expected to be lower than experiment in these cases. The plot shows that this expected correlation usually holds. The calculated half-lives and P_n values are either simultaneously both lower or both higher than experiment.

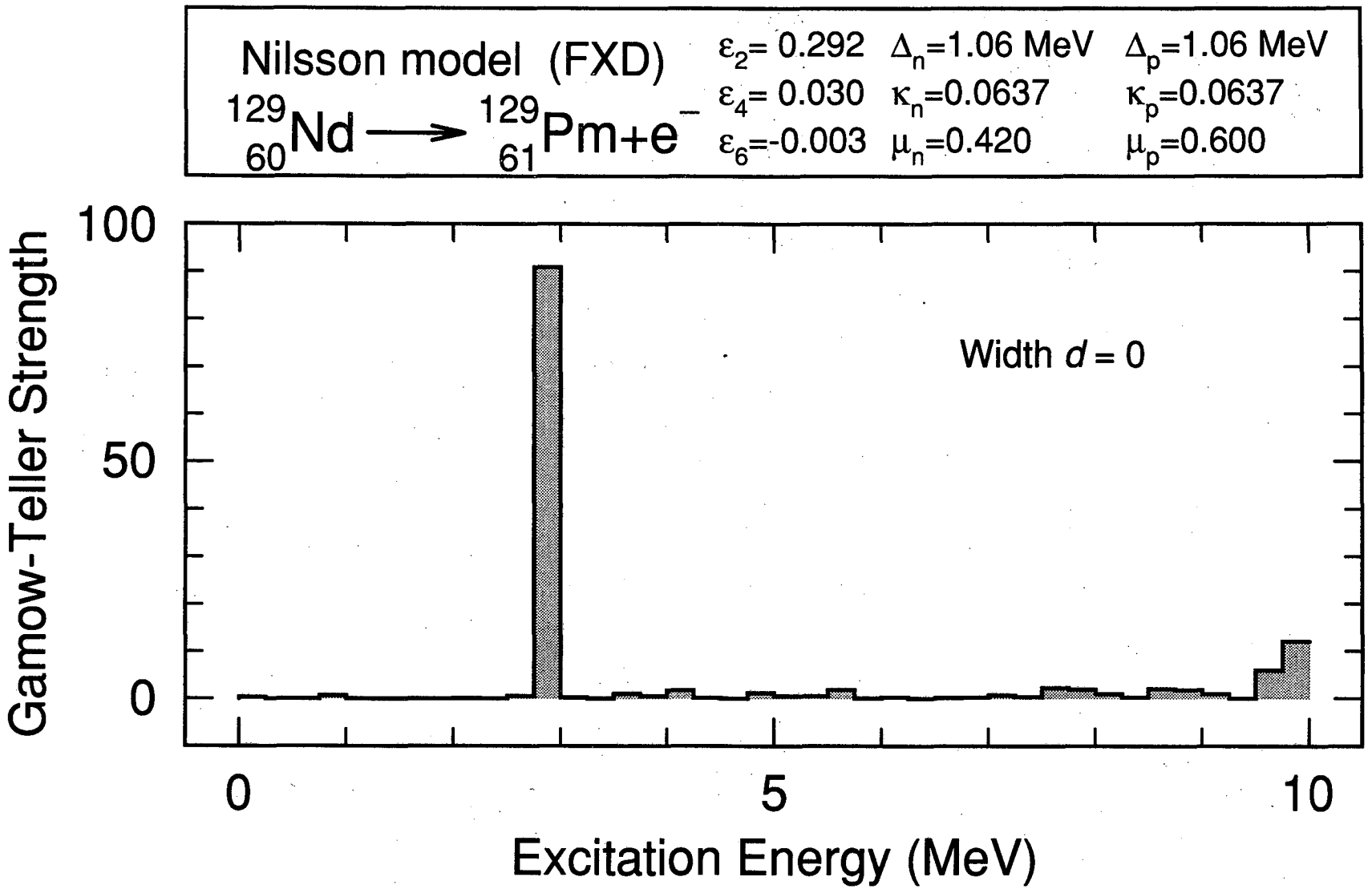
Nilsson model (FXD)
$^{129}_{60}Nd \longrightarrow {}^{129}_{61}Pm+e^-$
ε_2= 0.292 Δ_n=1.06 MeV Δ_p=1.06 MeV
ε_4= 0.030 κ_n=0.0637 κ_p=0.0637
ε_6=-0.003 μ_n=0.420 μ_p=0.600
Gamow-Teller Strength
100
50
0
Width d = 0
0
5
10
Excitation Energy (MeV)

Figure 1

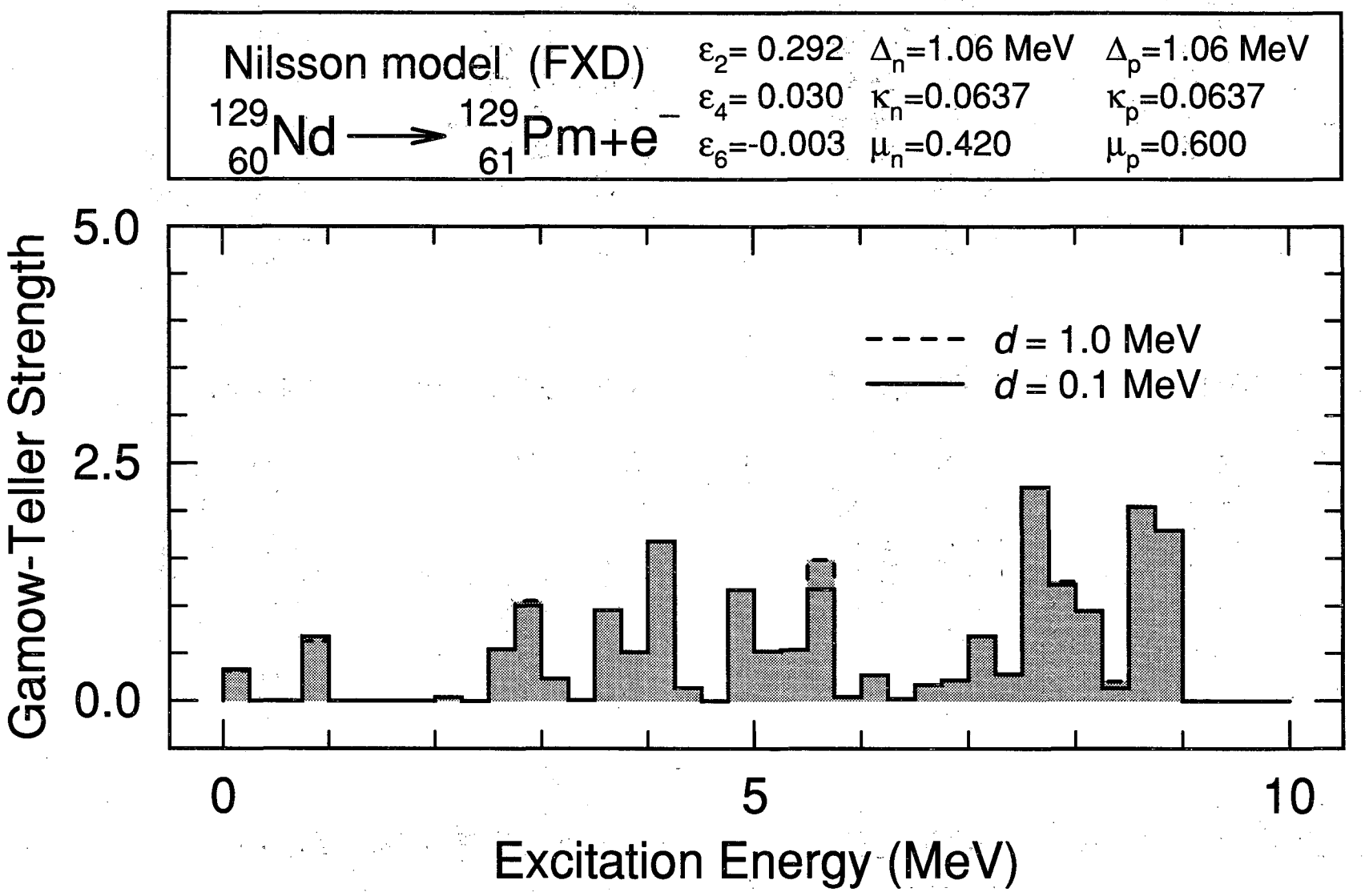
Nilsson model (FXD)
$^{129}_{60}Nd \longrightarrow {}^{129}_{61}Pm+e^-$
ε_2= 0.292 Δ_n=1.06 MeV Δ_p=1.06 MeV
ε_4= 0.030 κ_n=0.0637 κ_p=0.0637
ε_6=-0.003 μ_n=0.420 μ_p=0.600
Gamow-Teller Strength
5.0
2.5
0.0
d = 1.0 MeV
d = 0.1 MeV
0
5
10
Excitation Energy (MeV)

Figure 2

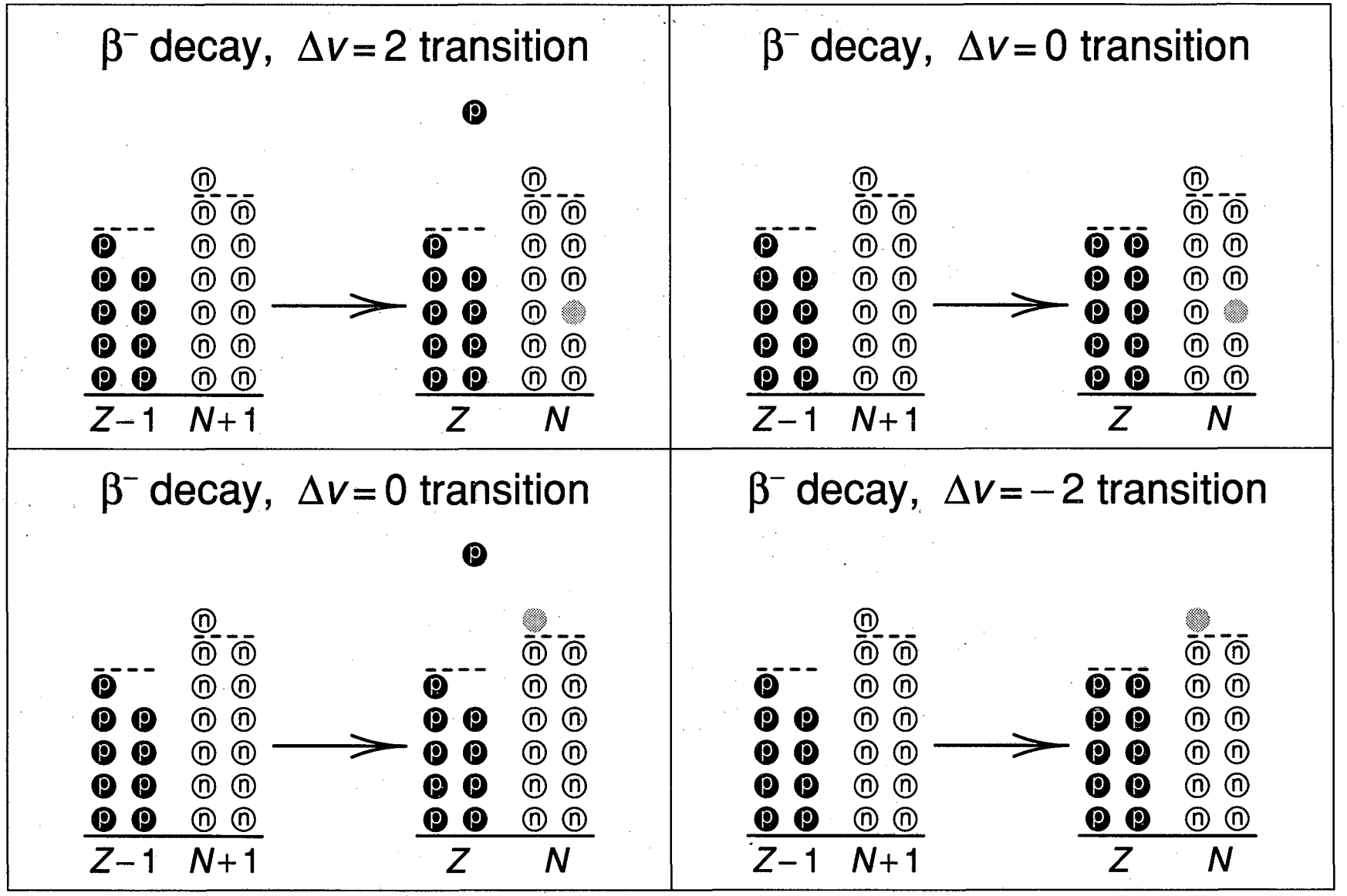
β⁻ decay, Δv = 2 transition
β⁻ decay, Δv = 0 transition
β⁻ decay, Δv = 0 transition
β⁻ decay, Δv = −2 transition
Z−1
N+1
Z
N

Figure 3

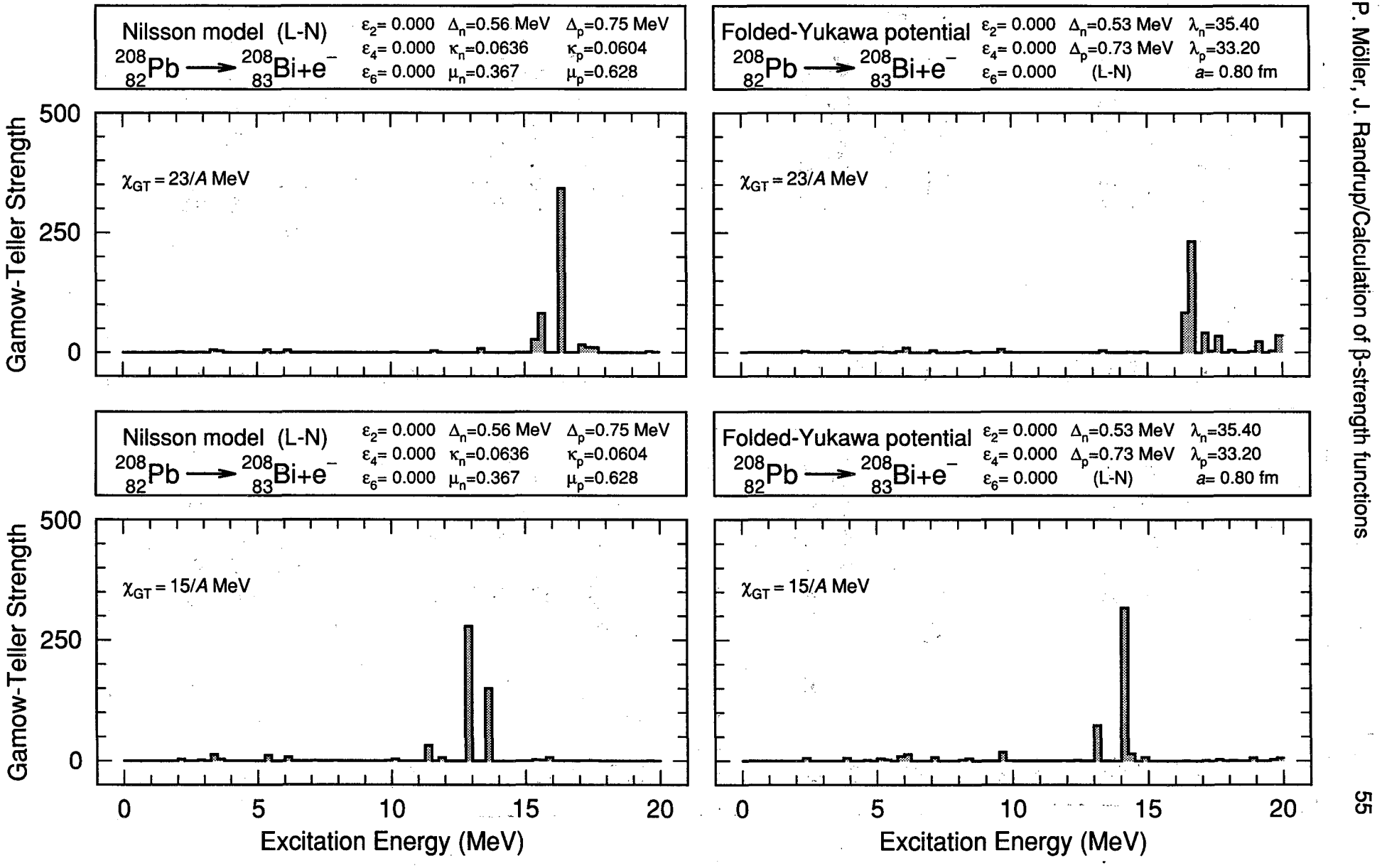
Nilsson model (L-N)
$^{208}_{82}Pb \rightarrow {}^{208}_{83}Bi+e^-$
ε_2= 0.000 Δ_n=0.56 MeV Δ_p=0.75 MeV
ε_4= 0.000 κ_n=0.0636 κ_p=0.0604
ε_6= 0.000 μ_n=0.367 μ_p=0.628
Folded-Yukawa potential
$^{208}_{82}Pb \rightarrow {}^{208}_{83}Bi+e^-$
ε_2= 0.000 Δ_n=0.53 MeV λ_n=35.40
ε_4= 0.000 Δ_p=0.73 MeV λ_p=33.20
ε_6= 0.000 (L-N) a= 0.80 fm
$\chi_{GT} = 23/A$ MeV
$\chi_{GT} = 15/A$ MeV
Gamow-Teller Strength
500
250
0
0
5
10
15
20
Excitation Energy (MeV)

Figure 4

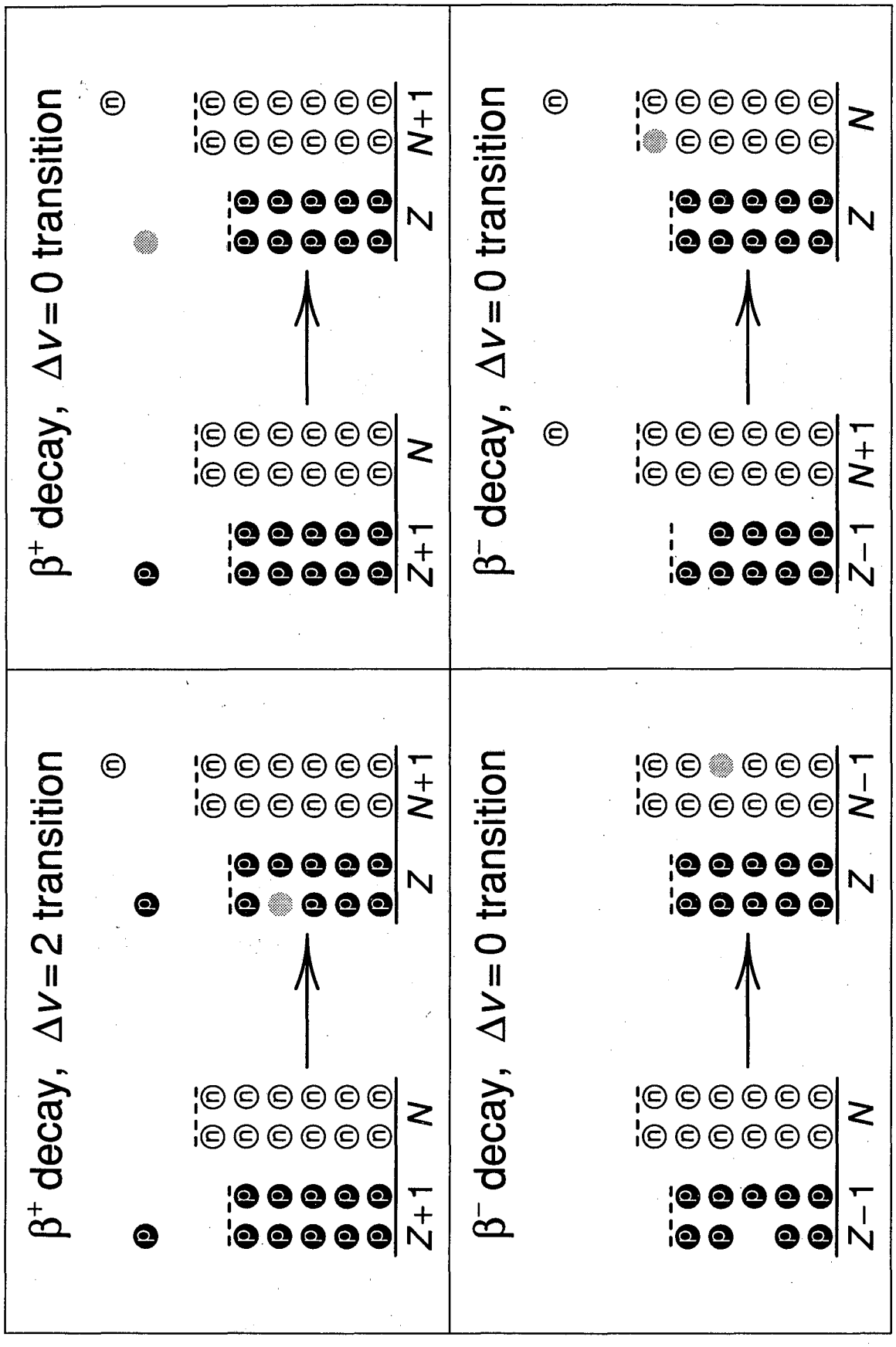
β+ decay, Δν=2 transition
β+ decay, Δν=0 transition
β− decay, Δν=0 transition
β− decay, Δν=0 transition
Z−1 N
Z N+1
Z+1 N
Z N−1
Z+1 N
Z N+1
Z−1 N+1
Z N

Figure 5

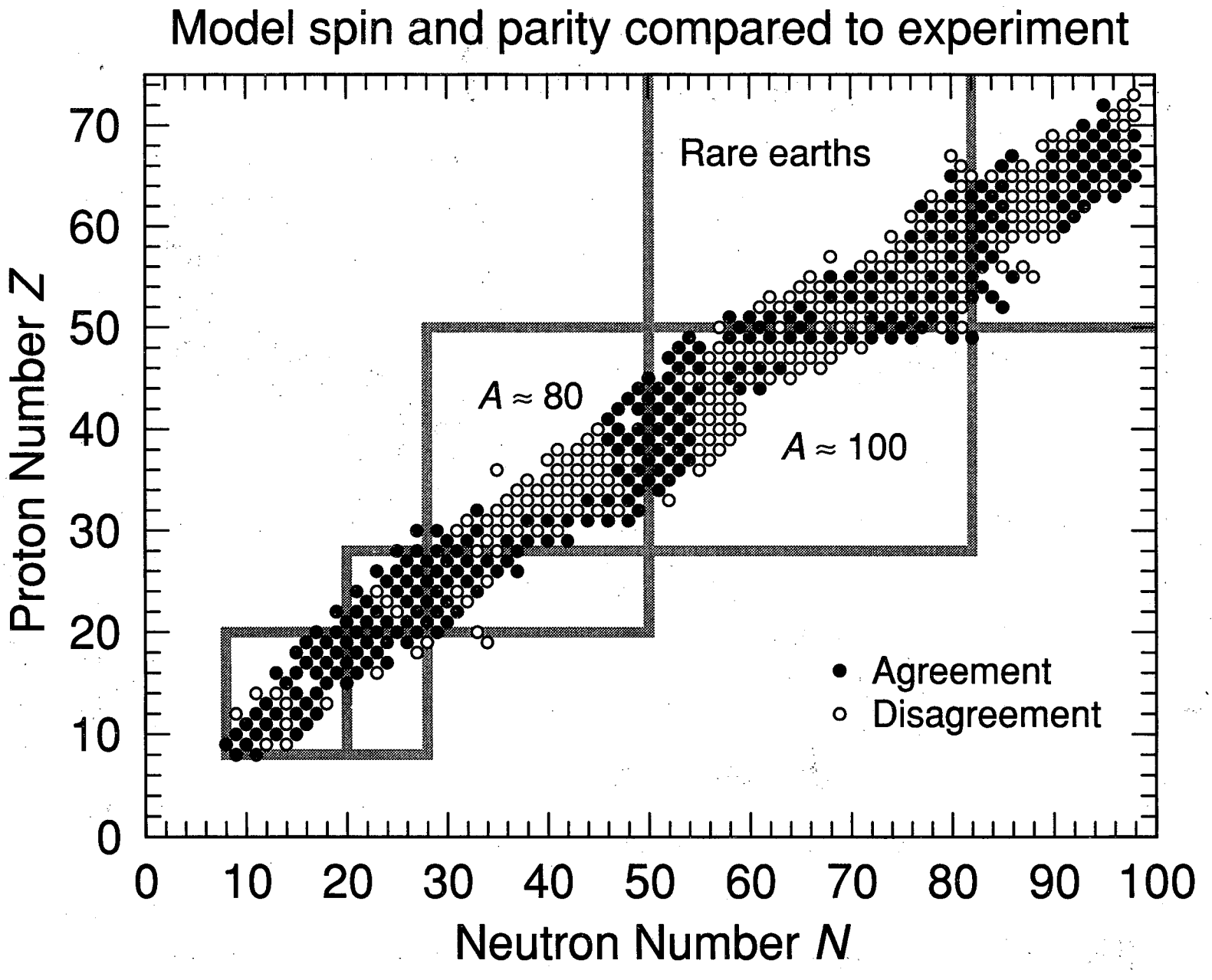
Model spin and parity compared to experiment
Rare earths
A ≈ 80
A ≈ 100
Agreement
Disagreement
Proton Number Z
Neutron Number N
0
10
20
30
40
50
60
70
80
90
100

Figure 6

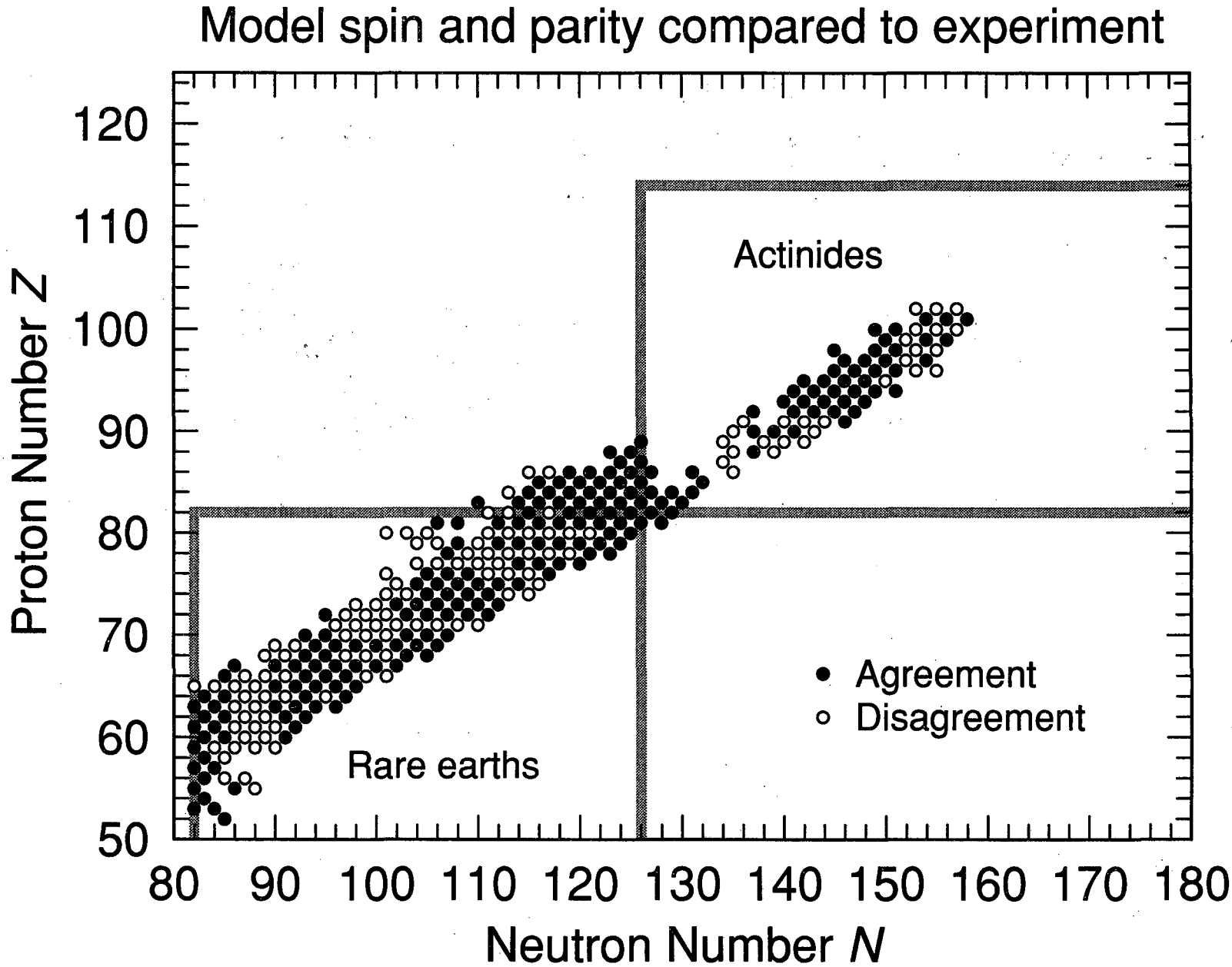
Model spin and parity compared to experiment
Proton Number Z
Neutron Number N
120
110
100
90
80
70
60
50
80
90
100
110
120
130
140
150
160
170
180
Actinides
Rare earths
Agreement
Disagreement

Figure 7

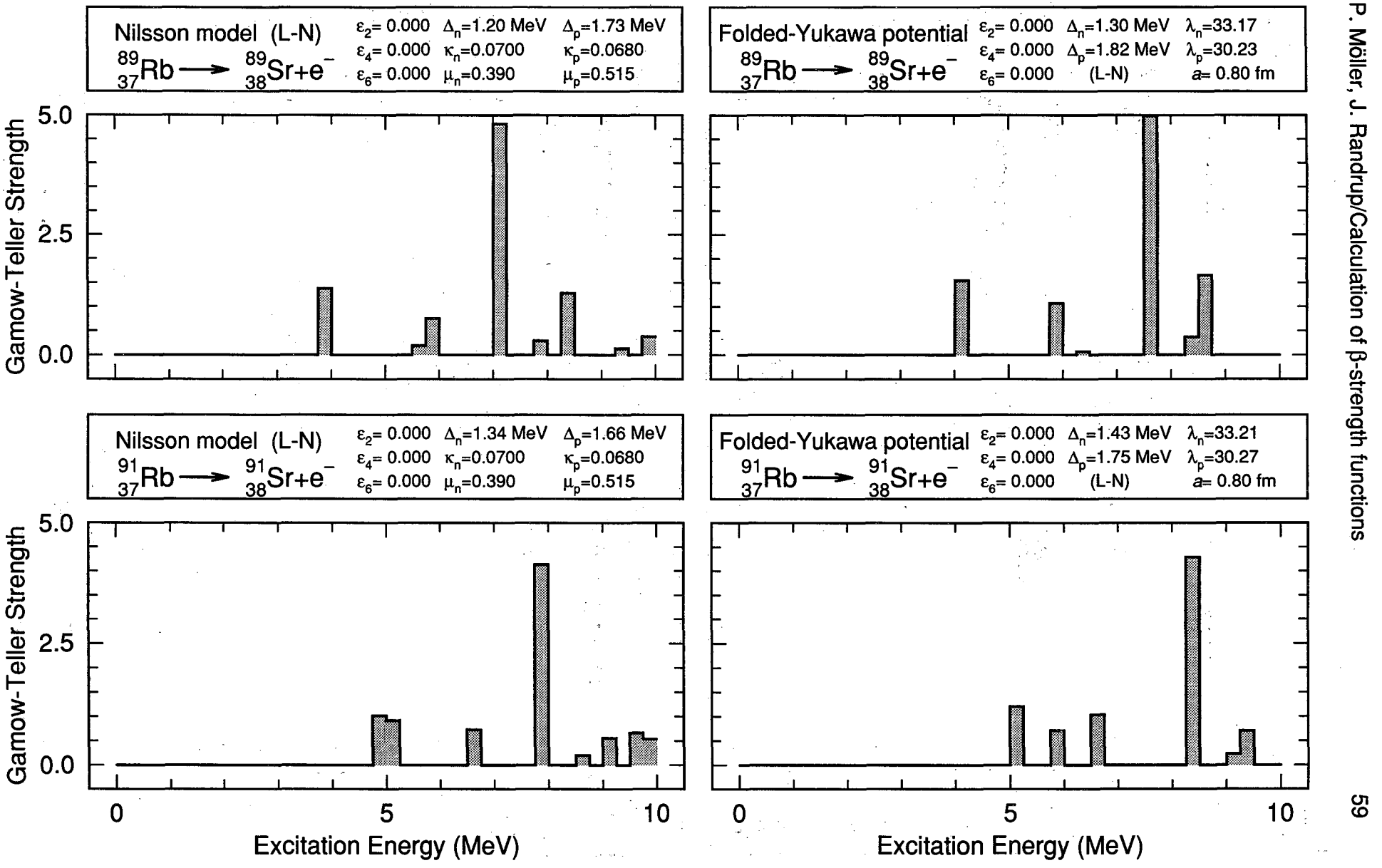
Nilsson model (L-N)
$^{89}_{37}Rb \rightarrow {}^{89}_{38}Sr+e^-$
ε_2= 0.000 Δ_n=1.20 MeV Δ_p=1.73 MeV
ε_4= 0.000 κ_n=0.0700 κ_p=0.0680
ε_6= 0.000 μ_n=0.390 μ_p=0.515
Folded-Yukawa potential
$^{89}_{37}Rb \rightarrow {}^{89}_{38}Sr+e^-$
ε_2= 0.000 Δ_n=1.30 MeV λ_n=33.17
ε_4= 0.000 Δ_p=1.82 MeV λ_p=30.23
ε_6= 0.000 (L-N) a= 0.80 fm
Nilsson model (L-N)
$^{91}_{37}Rb \rightarrow {}^{91}_{38}Sr+e^-$
ε_2= 0.000 Δ_n=1.34 MeV Δ_p=1.66 MeV
ε_4= 0.000 κ_n=0.0700 κ_p=0.0680
ε_6= 0.000 μ_n=0.390 μ_p=0.515
Folded-Yukawa potential
$^{91}_{37}Rb \rightarrow {}^{91}_{38}Sr+e^-$
ε_2= 0.000 Δ_n=1.43 MeV λ_n=33.21
ε_4= 0.000 Δ_p=1.75 MeV λ_p=30.27
ε_6= 0.000 (L-N) a= 0.80 fm
Gamow-Teller Strength
5.0
2.5
0.0
0
5
10
Excitation Energy (MeV)

Figure 8

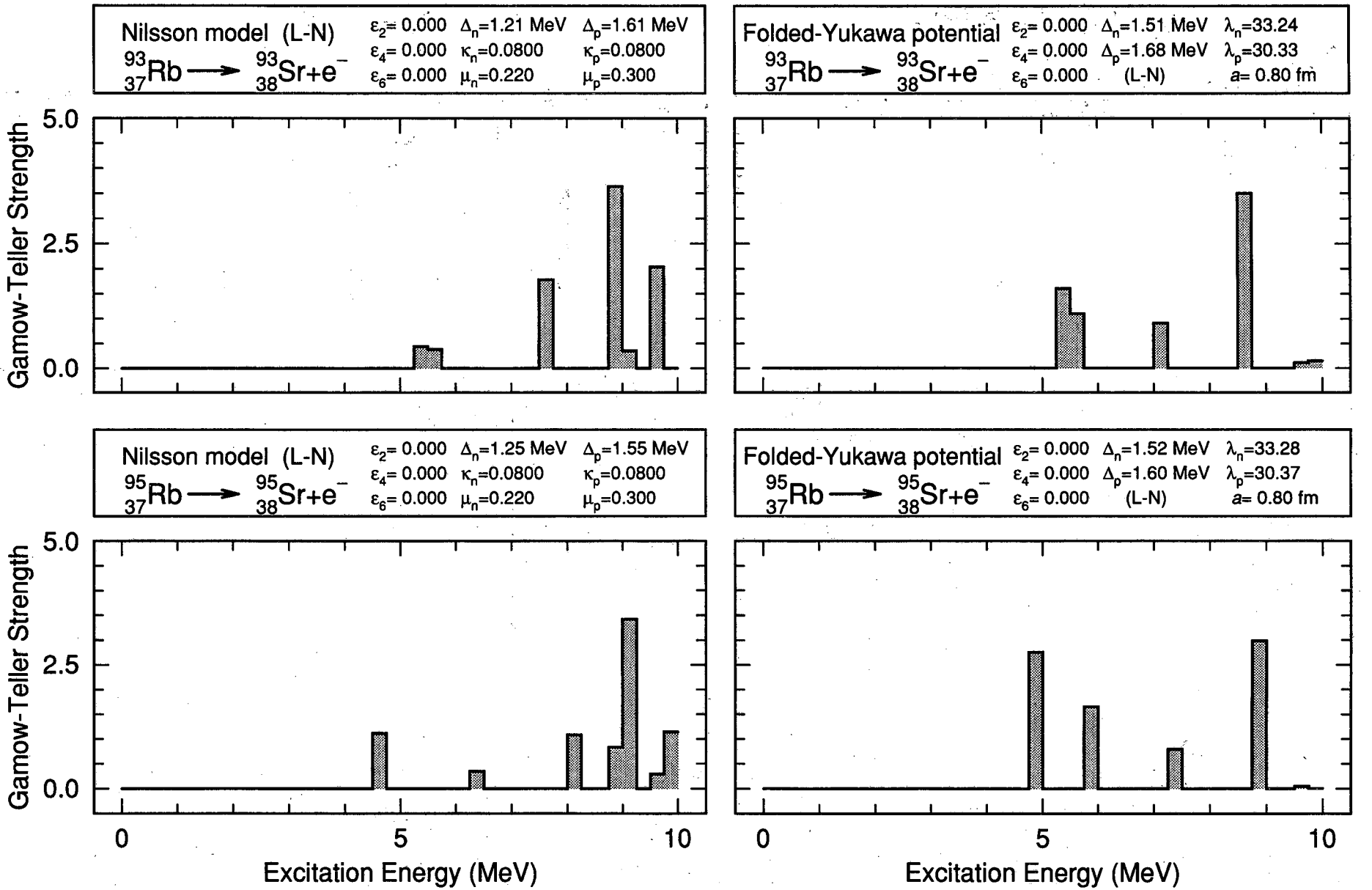
Nilsson model (L-N)
$^{93}_{37}Rb \rightarrow {}^{93}_{38}Sr+e^-$
ε_2= 0.000 Δ_n=1.21 MeV Δ_p=1.61 MeV
ε_4= 0.000 κ_n=0.0800 κ_p=0.0800
ε_6= 0.000 μ_n=0.220 μ_p=0.300
Folded-Yukawa potential
$^{93}_{37}Rb \rightarrow {}^{93}_{38}Sr+e^-$
ε_2= 0.000 Δ_n=1.51 MeV λ_n=33.24
ε_4= 0.000 Δ_p=1.68 MeV λ_p=30.33
ε_6= 0.000 (L-N) a= 0.80 fm
Nilsson model (L-N)
$^{95}_{37}Rb \rightarrow {}^{95}_{38}Sr+e^-$
ε_2= 0.000 Δ_n=1.25 MeV Δ_p=1.55 MeV
ε_4= 0.000 κ_n=0.0800 κ_p=0.0800
ε_6= 0.000 μ_n=0.220 μ_p=0.300
Folded-Yukawa potential
$^{95}_{37}Rb \rightarrow {}^{95}_{38}Sr+e^-$
ε_2= 0.000 Δ_n=1.52 MeV λ_n=33.28
ε_4= 0.000 Δ_p=1.60 MeV λ_p=30.37
ε_6= 0.000 (L-N) a= 0.80 fm
Gamow-Teller Strength
5.0
2.5
0.0
0
5
10
Excitation Energy (MeV)

Figure 9

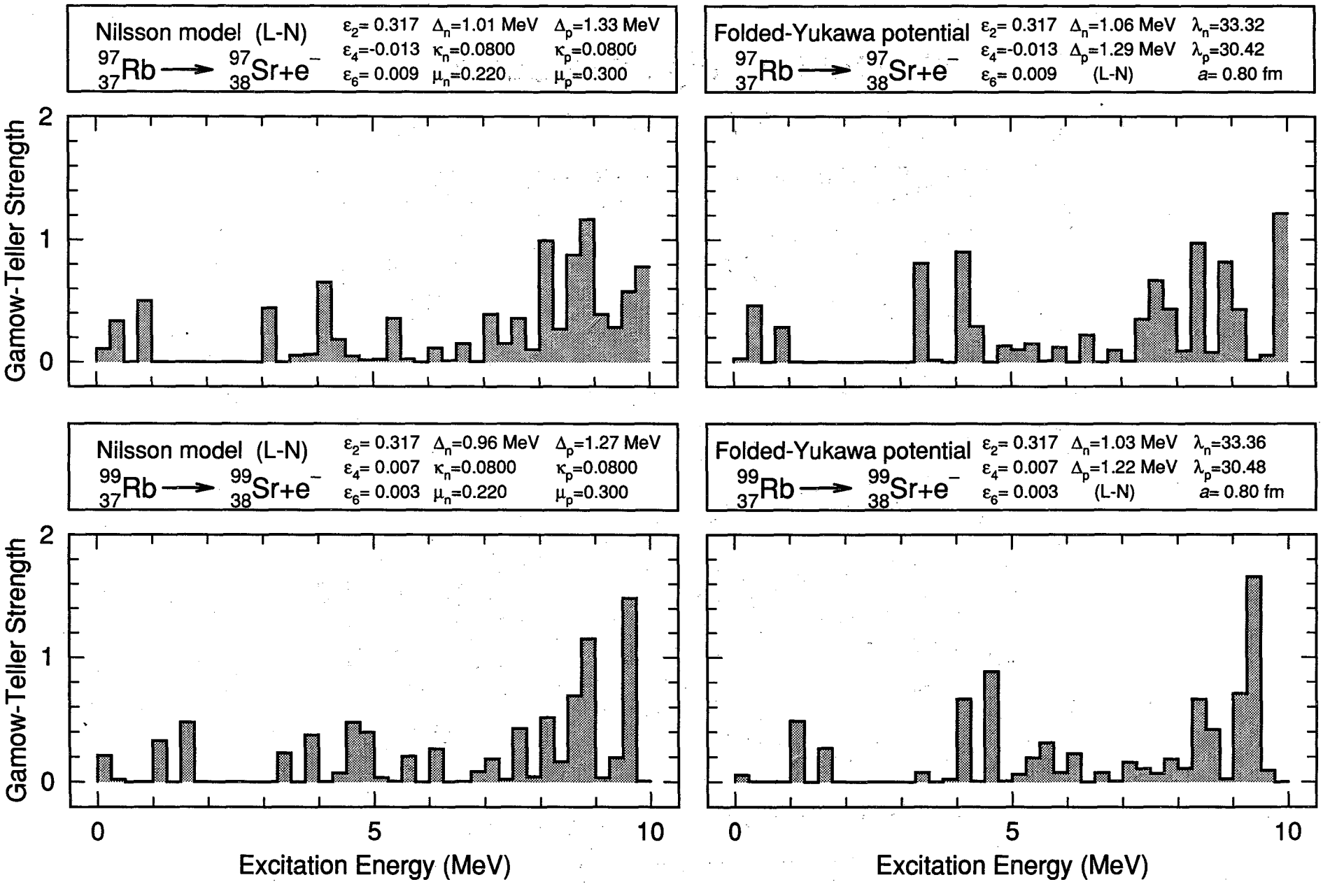
Nilsson model (L-N)
$^{97}_{37}Rb \rightarrow {}^{97}_{38}Sr+e^-$
ε_2= 0.317 Δ_n=1.01 MeV Δ_p=1.33 MeV
ε_4=-0.013 κ_n=0.0800 κ_p=0.0800
ε_6= 0.009 μ_n=0.220 μ_p=0.300
Folded-Yukawa potential
$^{97}_{37}Rb \rightarrow {}^{97}_{38}Sr+e^-$
ε_2= 0.317 Δ_n=1.06 MeV λ_n=33.32
ε_4=-0.013 Δ_p=1.29 MeV λ_p=30.42
ε_6= 0.009 (L-N) a= 0.80 fm
Nilsson model (L-N)
$^{99}_{37}Rb \rightarrow {}^{99}_{38}Sr+e^-$
ε_2= 0.317 Δ_n=0.96 MeV Δ_p=1.27 MeV
ε_4= 0.007 κ_n=0.0800 κ_p=0.0800
ε_6= 0.003 μ_n=0.220 μ_p=0.300
Folded-Yukawa potential
$^{99}_{37}Rb \rightarrow {}^{99}_{38}Sr+e^-$
ε_2= 0.317 Δ_n=1.03 MeV λ_n=33.36
ε_4= 0.007 Δ_p=1.22 MeV λ_p=30.48
ε_6= 0.003 (L-N) a= 0.80 fm
Gamow-Teller Strength
0
1
2
0
5
10
Excitation Energy (MeV)

Figure 10

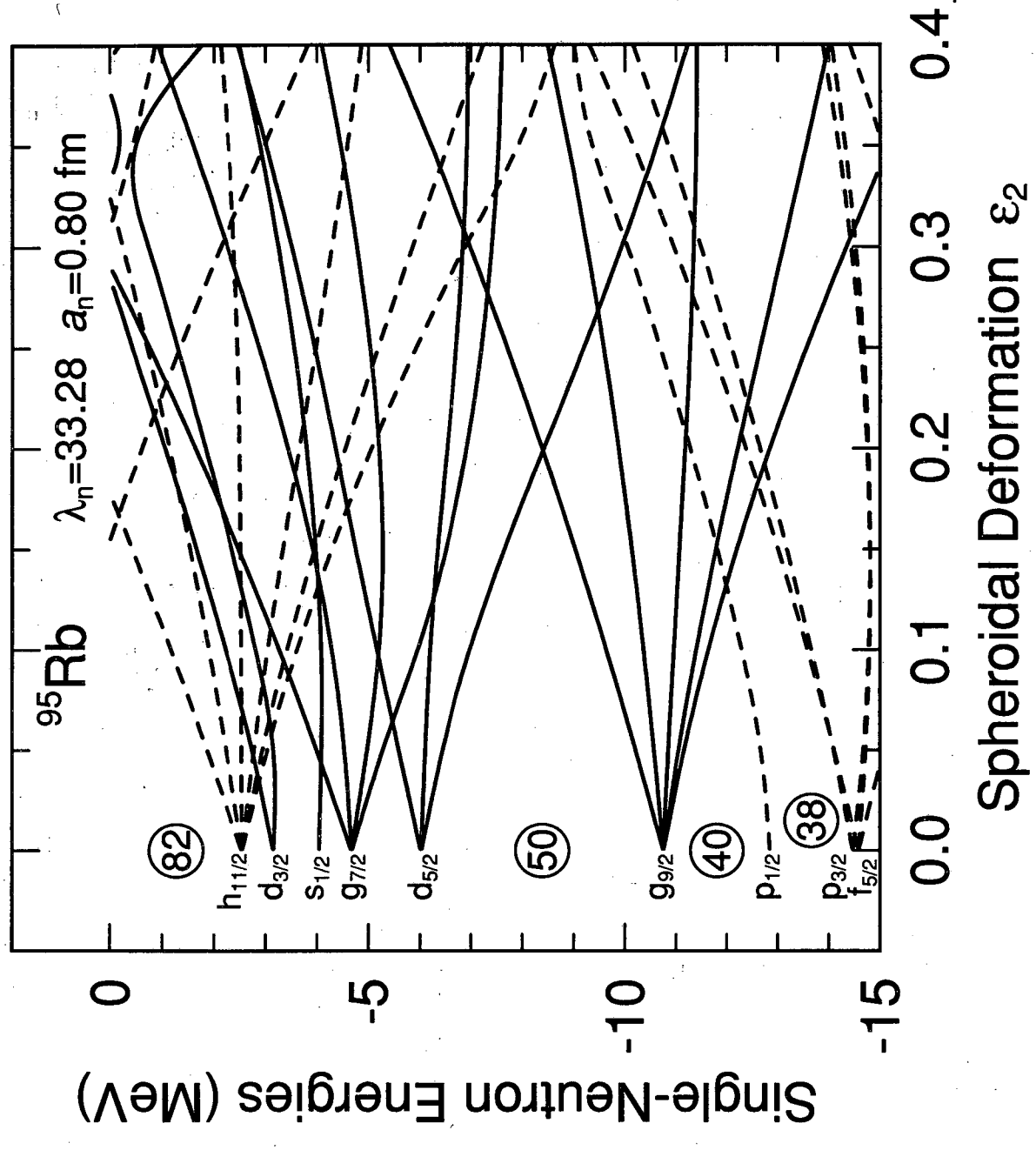
^{95}Rb
λ_n=33.28 a_n=0.80 fm
82
50
40
38
$h_{11/2}$
$d_{3/2}$
$s_{1/2}$
$g_{7/2}$
$d_{5/2}$
$g_{9/2}$
$p_{1/2}$
$p_{3/2}$
$f_{5/2}$
Single-Neutron Energies (MeV)
0
-5
-10
-15
0.0
0.1
0.2
0.3
0.4
Spheroidal Deformation ε_2

Figure 11

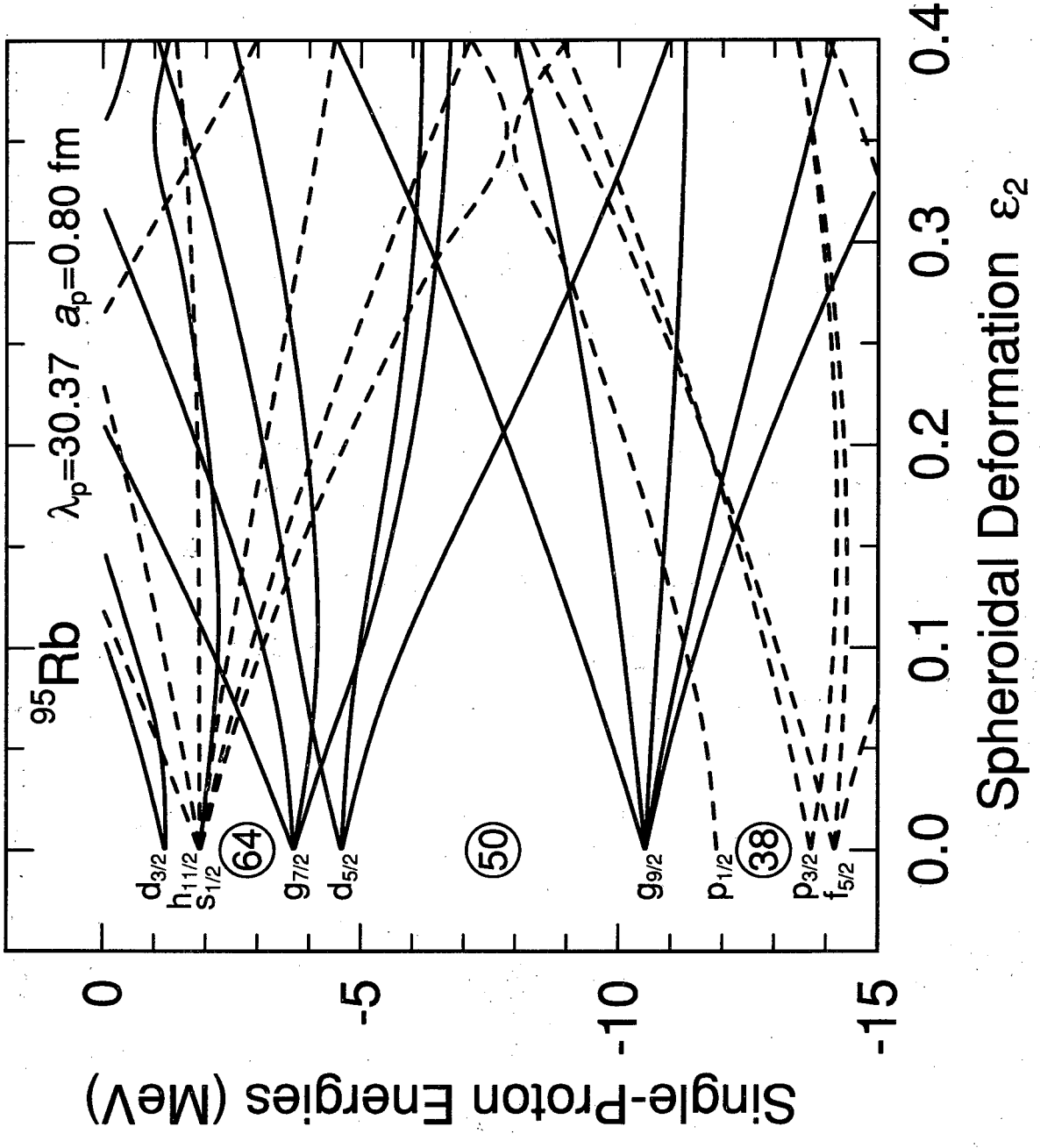
^{95}Rb
λ_p=30.37 a_p=0.80 fm
Single-Proton Energies (MeV)
Spheroidal Deformation ε_2
0
-5
-10
-15
0.0
0.1
0.2
0.3
0.4
$d_{3/2}$
$h_{11/2}$
$s_{1/2}$
64
$g_{7/2}$
$d_{5/2}$
50
$g_{9/2}$
$p_{1/2}$
38
$p_{3/2}$
$f_{5/2}$

Figure 12

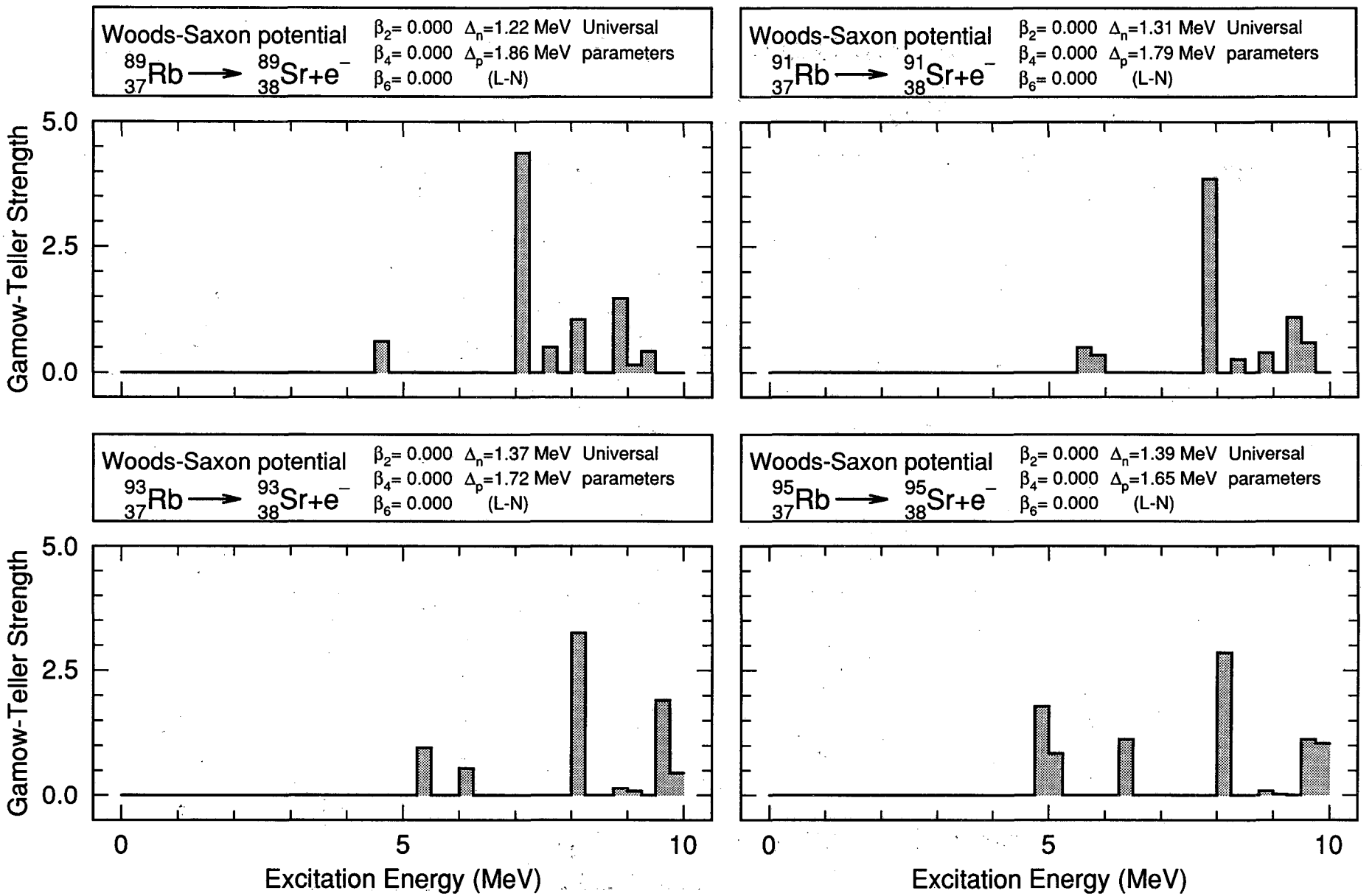
Woods-Saxon potential
$^{89}_{37}Rb \longrightarrow {}^{89}_{38}Sr+e^-$
β_2= 0.000 Δ_n=1.22 MeV Universal
β_4= 0.000 Δ_p=1.86 MeV parameters
β_6= 0.000 (L-N)
Woods-Saxon potential
$^{91}_{37}Rb \longrightarrow {}^{91}_{38}Sr+e^-$
β_2= 0.000 Δ_n=1.31 MeV Universal
β_4= 0.000 Δ_p=1.79 MeV parameters
β_6= 0.000 (L-N)
Woods-Saxon potential
$^{93}_{37}Rb \longrightarrow {}^{93}_{38}Sr+e^-$
β_2= 0.000 Δ_n=1.37 MeV Universal
β_4= 0.000 Δ_p=1.72 MeV parameters
β_6= 0.000 (L-N)
Woods-Saxon potential
$^{95}_{37}Rb \longrightarrow {}^{95}_{38}Sr+e^-$
β_2= 0.000 Δ_n=1.39 MeV Universal
β_4= 0.000 Δ_p=1.65 MeV parameters
β_6= 0.000 (L-N)
Gamow-Teller Strength
5.0
2.5
0.0
0
5
10
Excitation Energy (MeV)

Figure 13

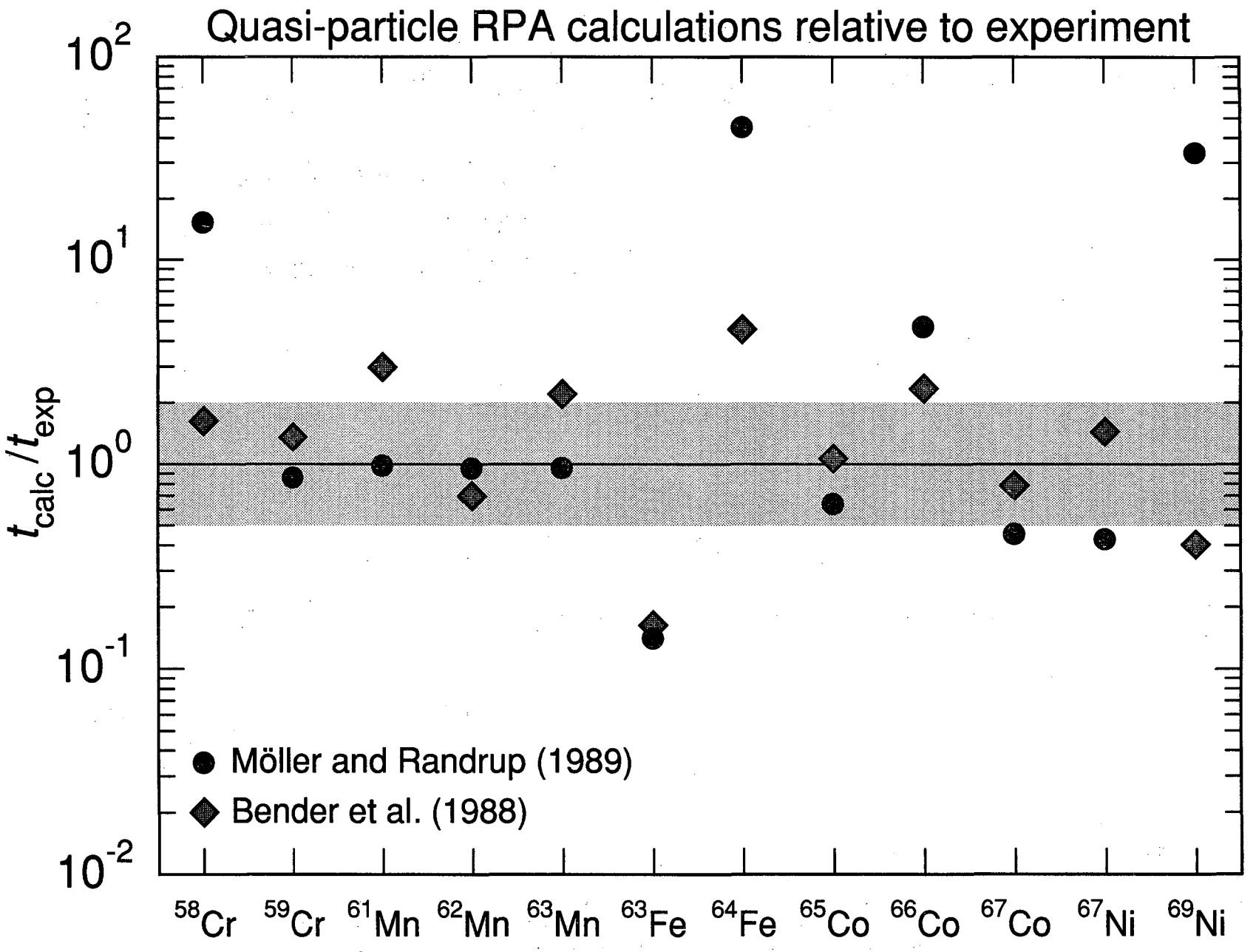
Quasi-particle RPA calculations relative to experiment
10^2
10^1
10^0
10^{-1}
10^{-2}
t_{calc}/t_{exp}
Möller and Randrup (1989)
Bender et al. (1988)
^{58}Cr
^{59}Cr
^{61}Mn
^{62}Mn
^{63}Mn
^{63}Fe
^{64}Fe
^{65}Co
^{66}Co
^{67}Co
^{67}Ni
^{69}Ni

Figure 14

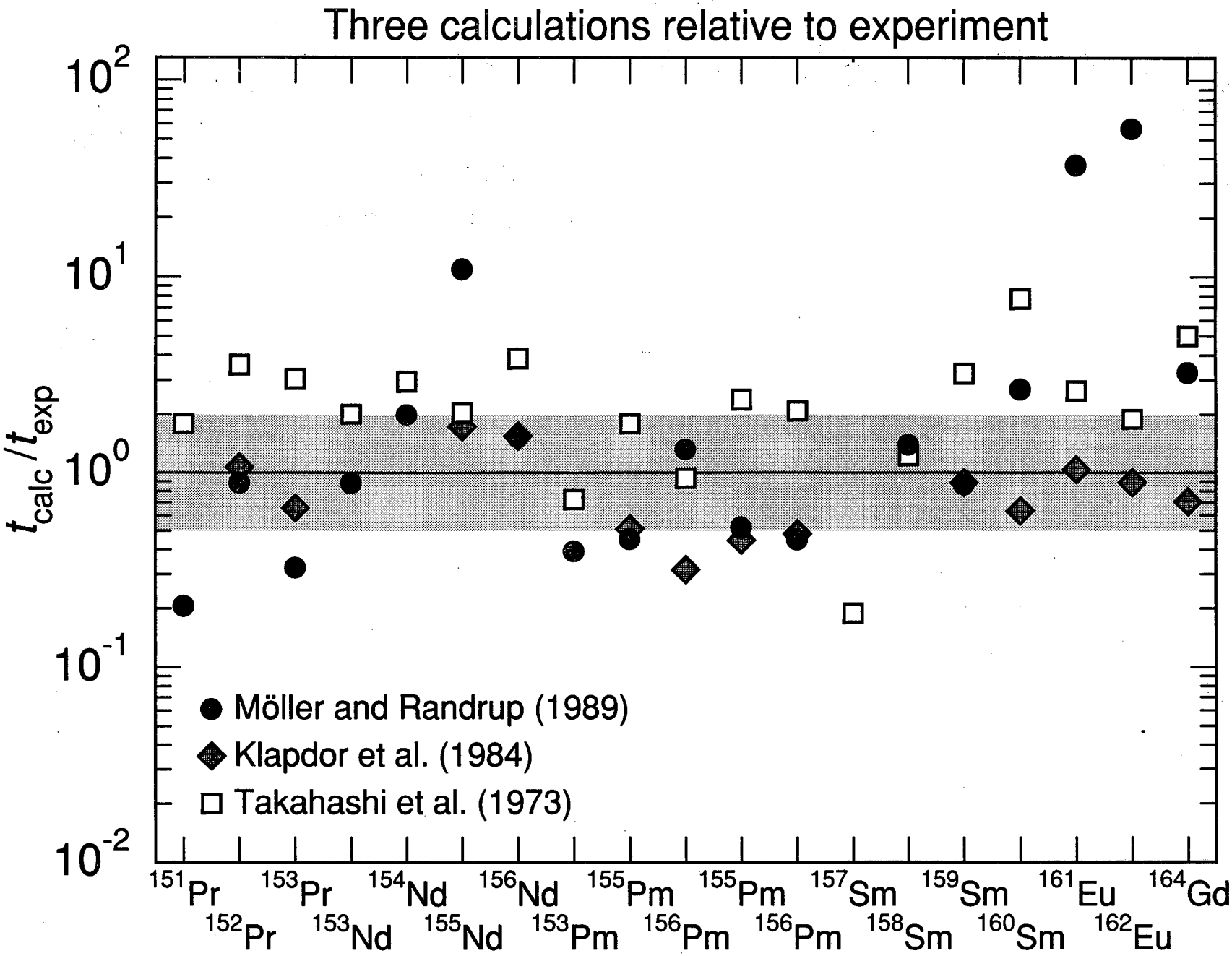
Three calculations relative to experiment
t_{calc}/t_{exp}
10^2
10^1
10^0
10^{-1}
10^{-2}
Möller and Randrup (1989)
Klapdor et al. (1984)
Takahashi et al. (1973)
^{151}Pr
^{152}Pr
^{153}Pr
^{153}Nd
^{154}Nd
^{155}Nd
^{156}Nd
^{153}Pm
^{155}Pm
^{156}Pm
^{155}Pm
^{156}Pm
^{157}Sm
^{158}Sm
^{159}Sm
^{160}Sm
^{161}Eu
^{162}Eu
^{164}Gd

Figure 15

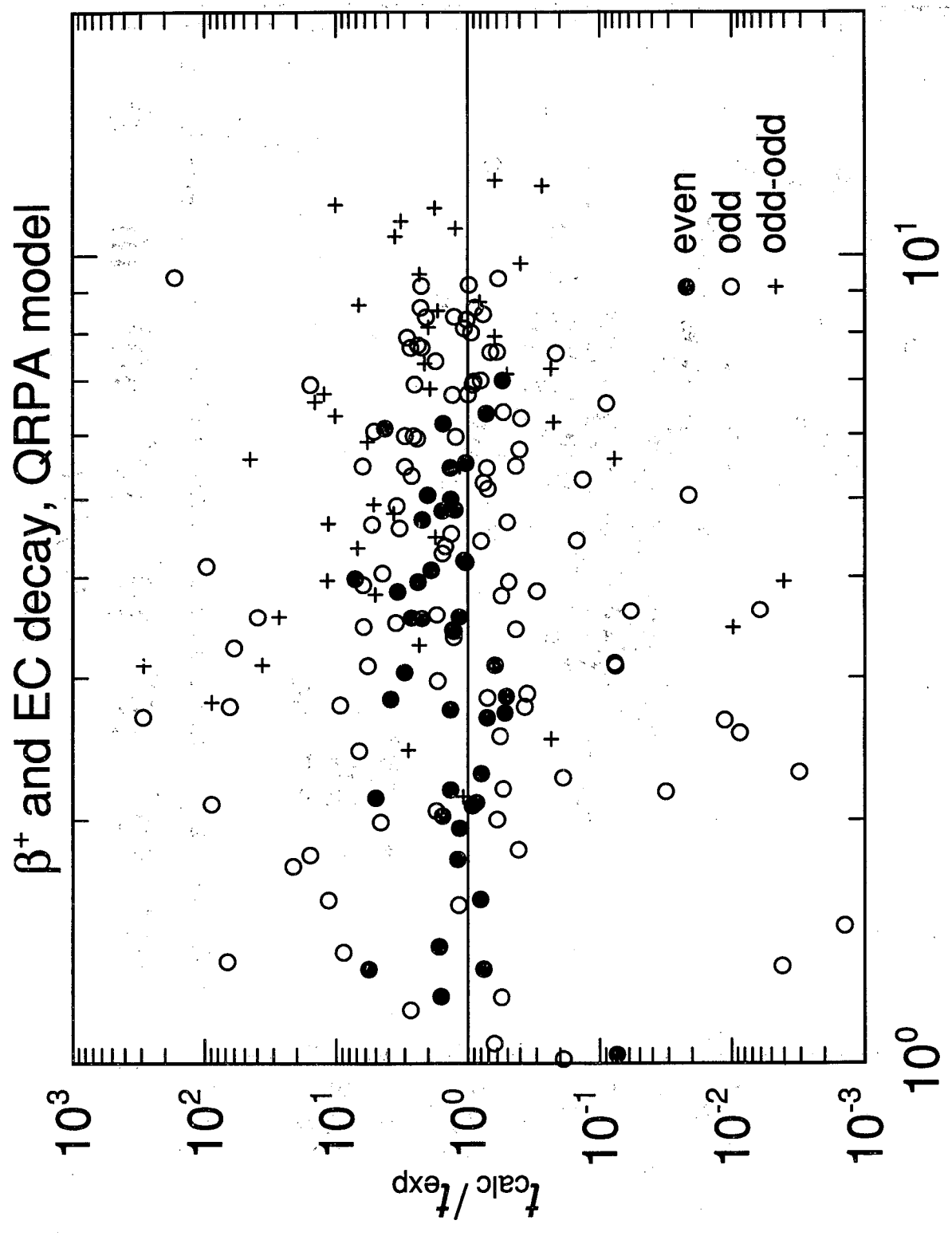
β+ and EC decay, QRPA model
even
odd
odd-odd
t_{calc}/t_{exp}
Q_β (MeV)
10^3
10^2
10^1
10^0
10^{-1}
10^{-2}
10^{-3}
10^0
10^1

Figure 16

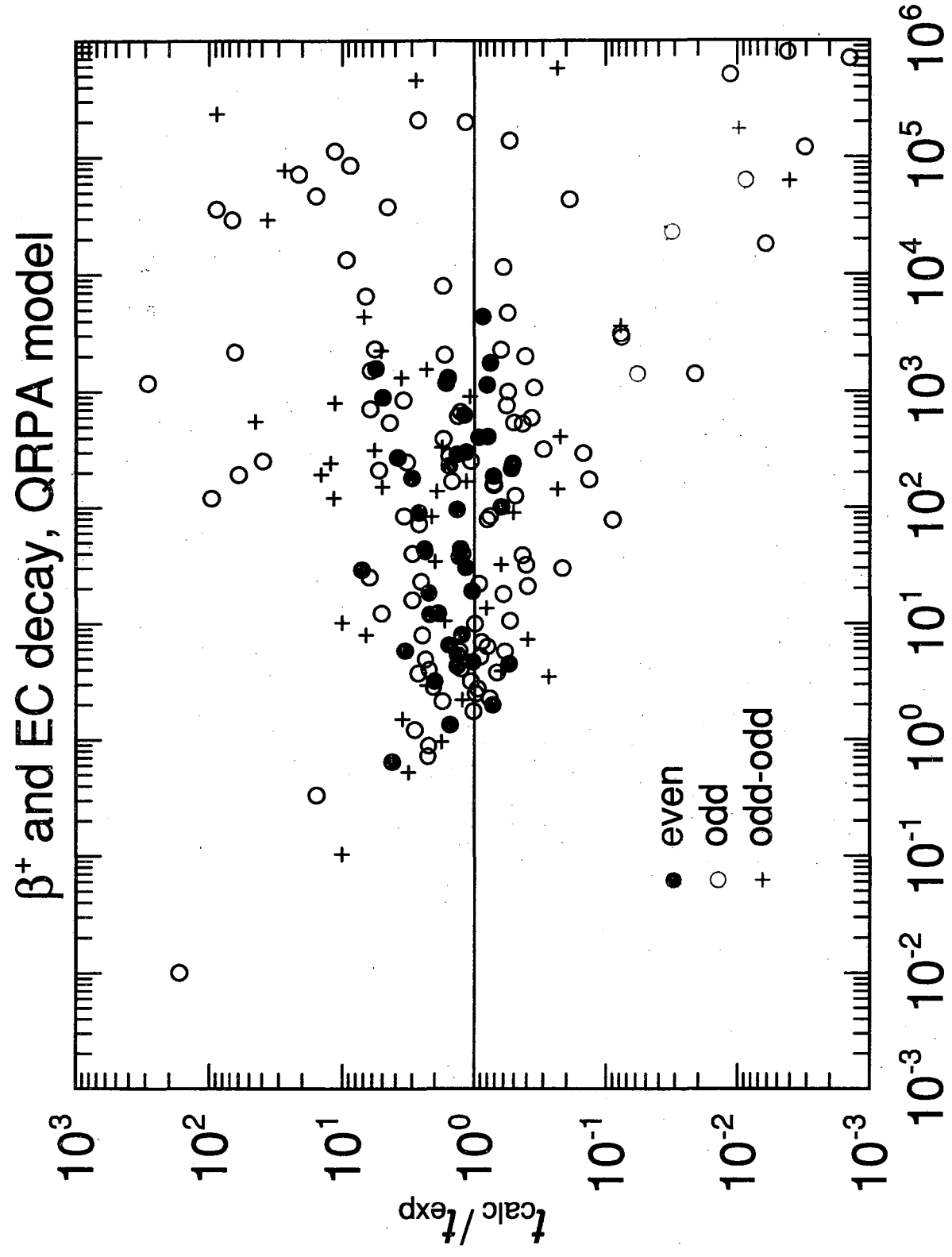
β+ and EC decay, QRPA model
even
odd
odd-odd
t_{calc}/t_{exp}
t_{exp} (s)
10^{-3}
10^{-2}
10^{-1}
10^{0}
10^{1}
10^{2}
10^{3}
10^{4}
10^{5}
10^{6}

Figure 17

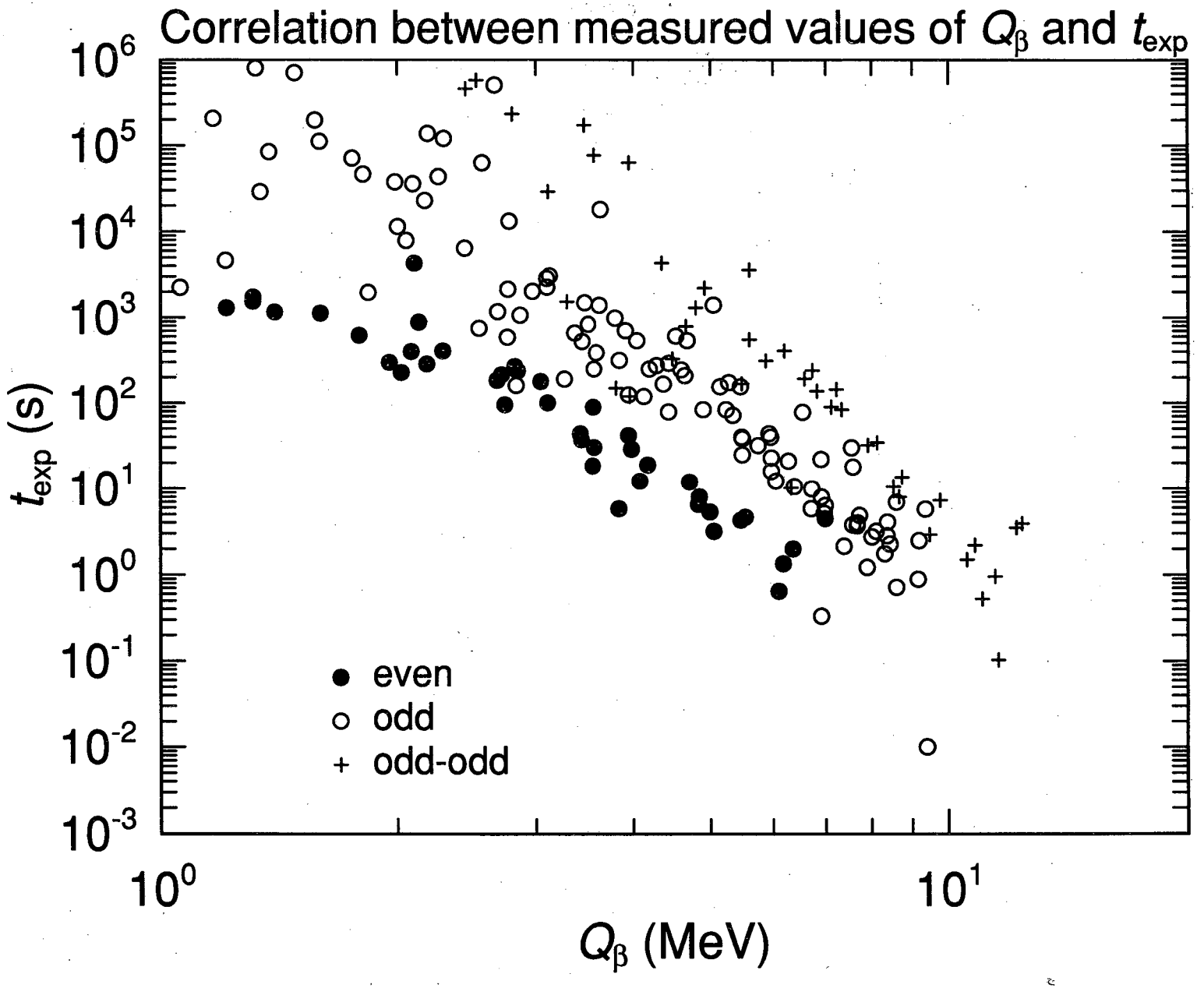
Correlation between measured values of Q_β and t_{exp}
t_{exp} (s)
10^6
10^5
10^4
10^3
10^2
10^1
10^0
10^{-1}
10^{-2}
10^{-3}
even
odd
odd-odd
10^0
10^1
Q_β (MeV)

Figure 18

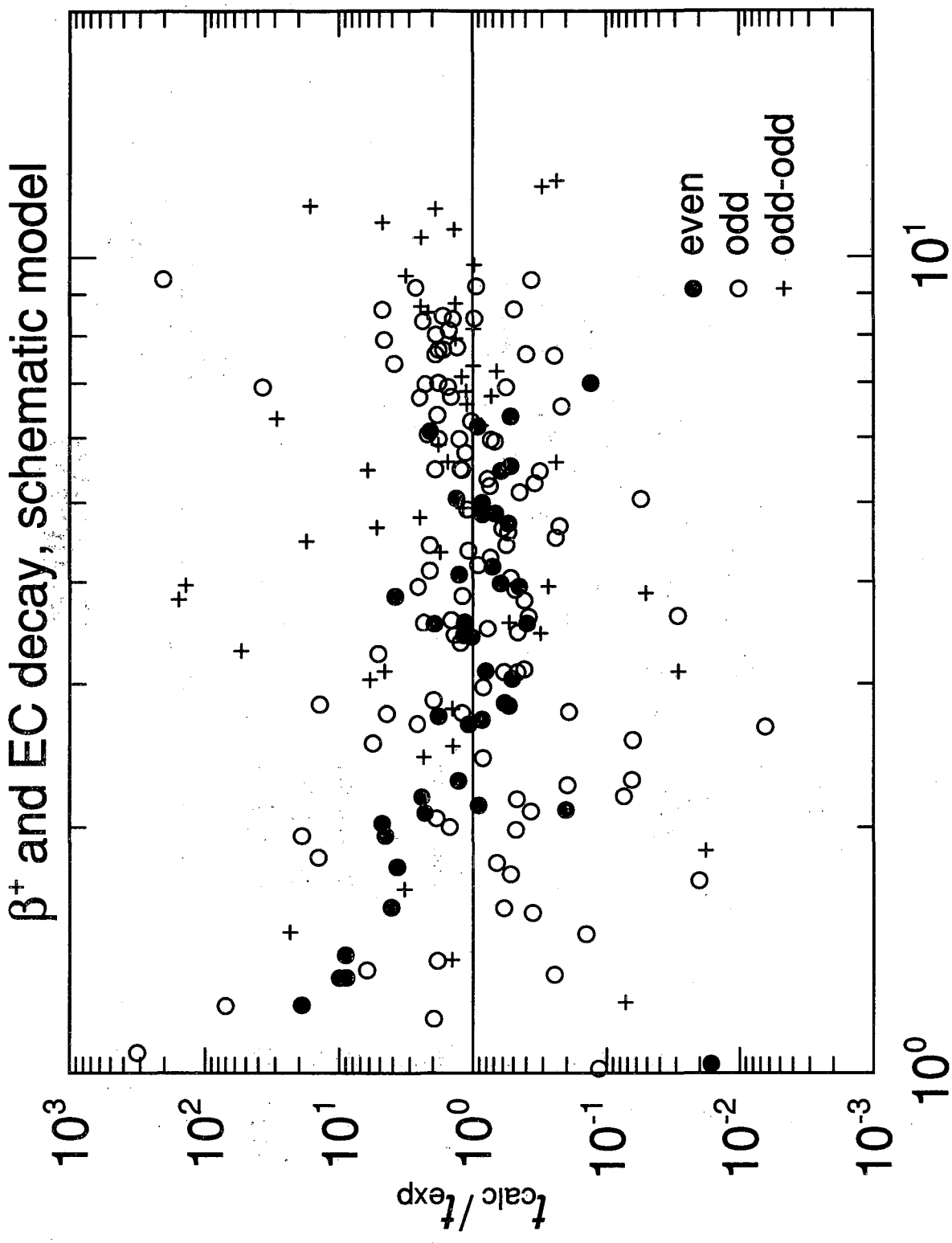
β+ and EC decay, schematic model
even
odd
odd-odd
t_{calc}/t_{exp}
Q_β (MeV)
10^3
10^2
10^1
10^0
10^{-1}
10^{-2}
10^{-3}
10^0
10^1

Figure 19

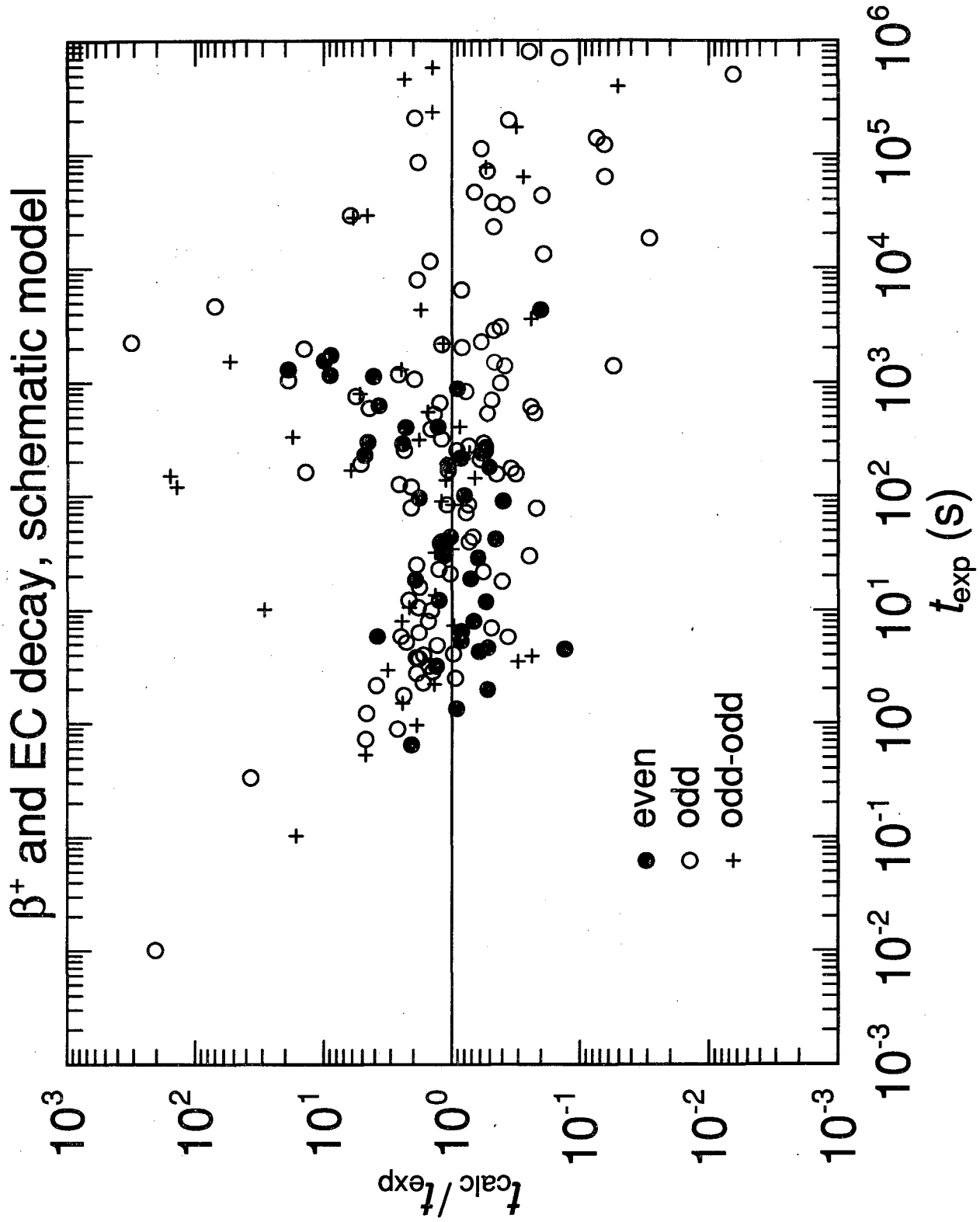
β+ and EC decay, schematic model
t_{calc}/t_{exp}
t_{exp} (s)
even
odd
odd-odd
10^{-3}
10^{-2}
10^{-1}
10^{0}
10^{1}
10^{2}
10^{3}
10^{4}
10^{5}
10^{6}

Figure 20

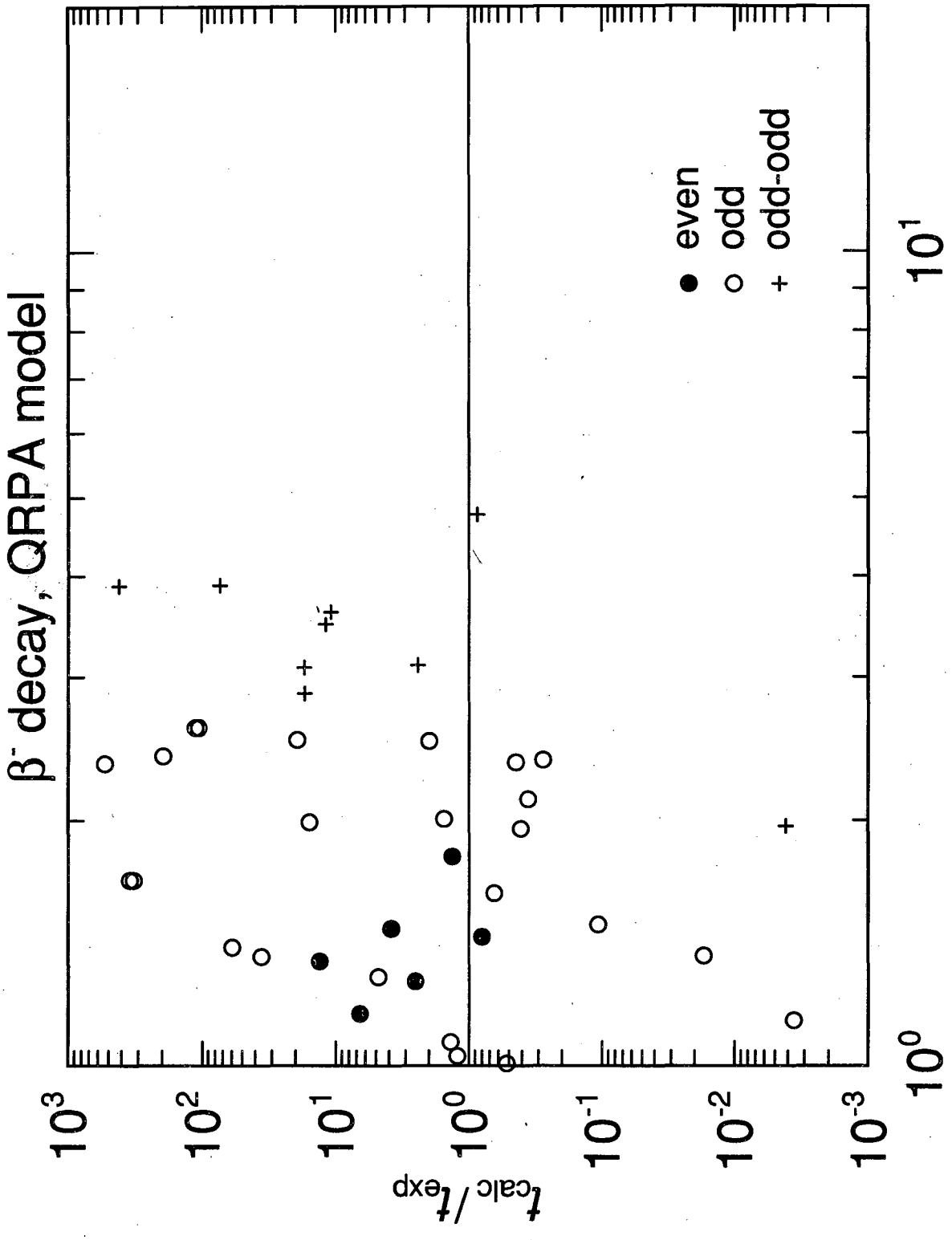
β⁻ decay, QRPA model
even
odd
odd-odd
t_{calc}/t_{exp}
Q_β (MeV)
10^3
10^2
10^1
10^0
10^{-1}
10^{-2}
10^{-3}
10^0
10^1

Figure 21

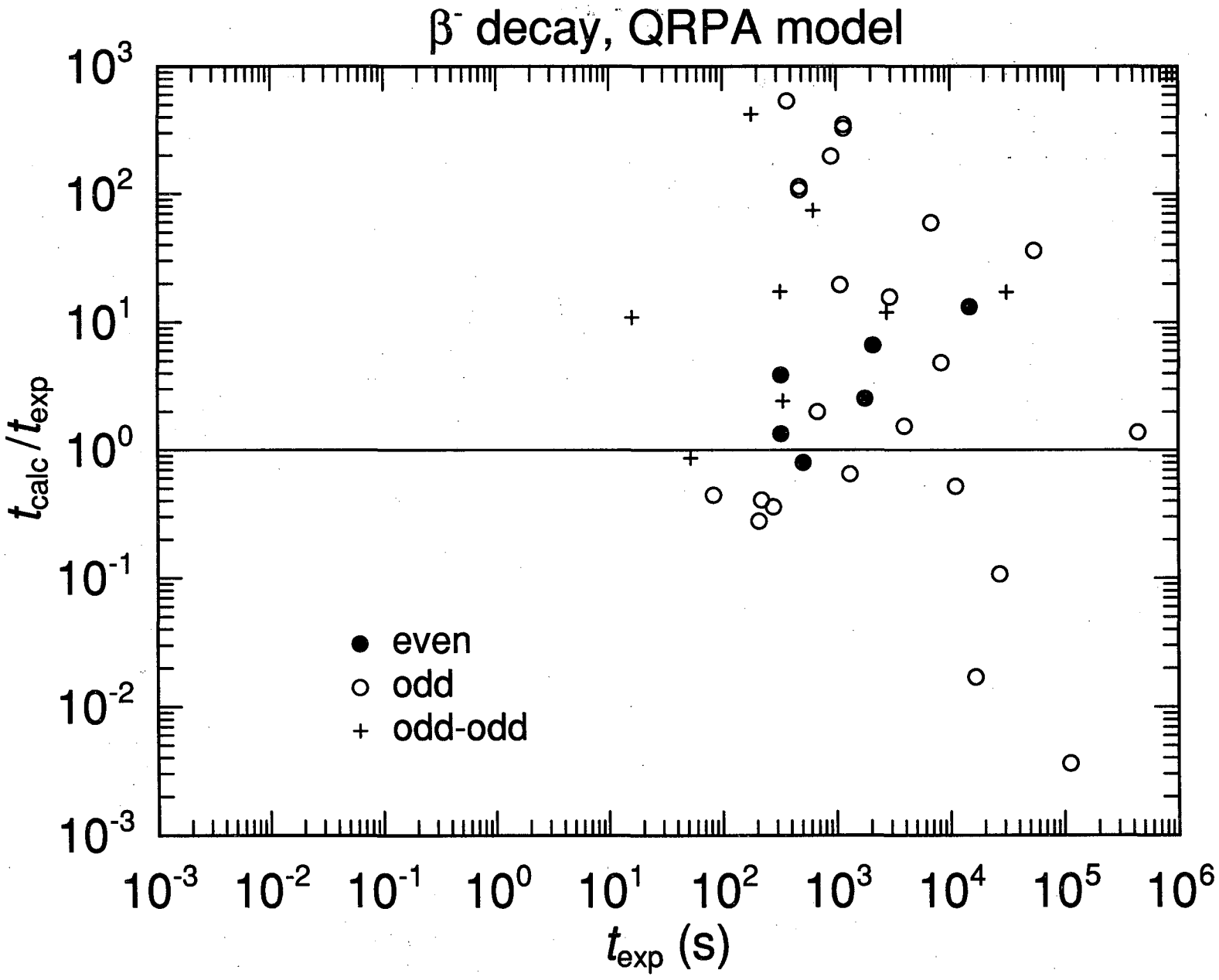
β⁻ decay, QRPA model
t_{calc}/t_{exp}
t_{exp} (s)
even
odd
odd-odd
10^{-3}
10^{-2}
10^{-1}
10^{0}
10^{1}
10^{2}
10^{3}
10^{4}
10^{5}
10^{6}

Figure 22

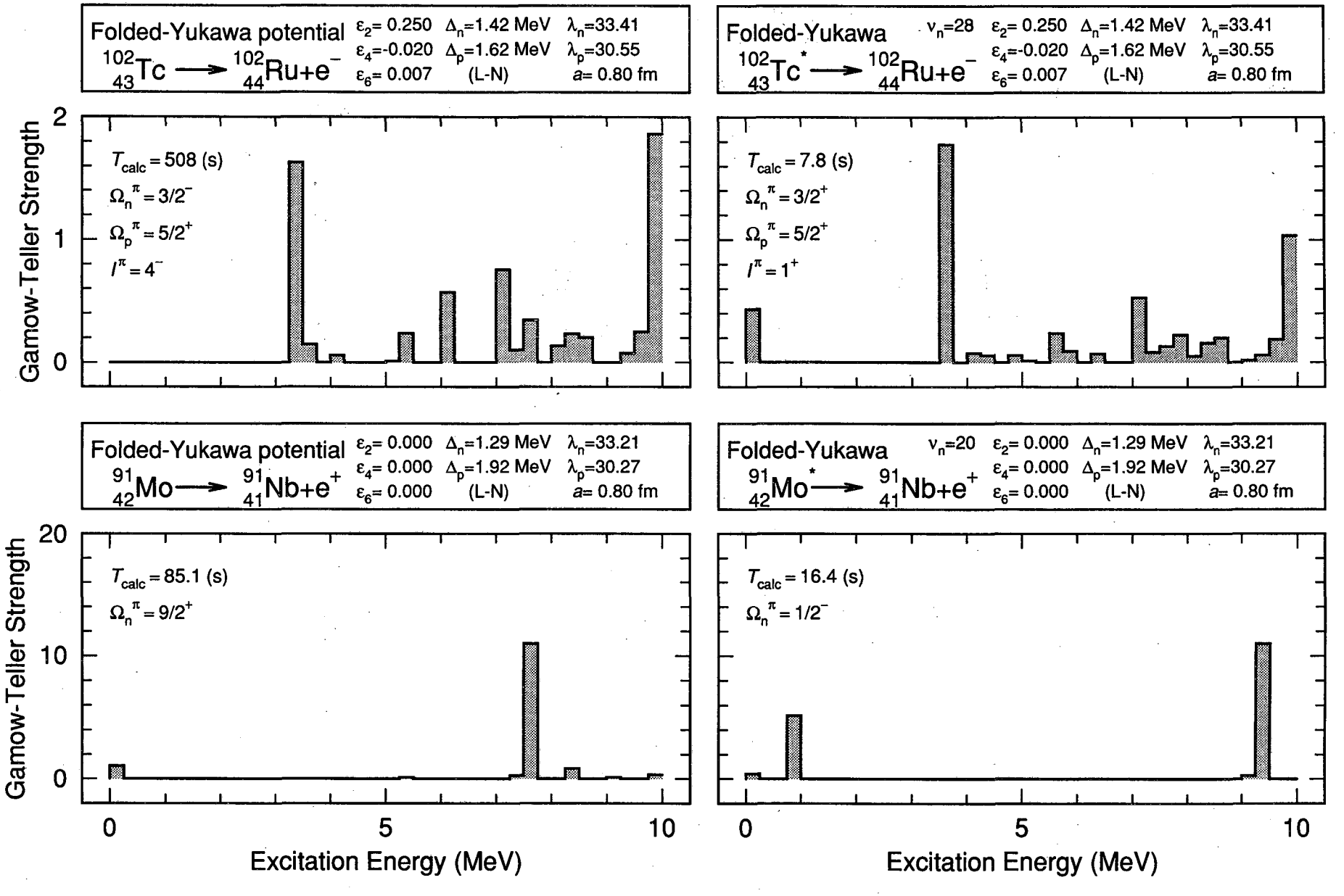
Folded-Yukawa potential
$^{102}_{43}Tc \rightarrow {}^{102}_{44}Ru+e^-$
ε_2= 0.250 Δ_n=1.42 MeV λ_n=33.41
ε_4=-0.020 Δ_p=1.62 MeV λ_p=30.55
ε_6= 0.007 (L-N) a= 0.80 fm
Folded-Yukawa
$^{102}_{43}Tc^* \rightarrow {}^{102}_{44}Ru+e^-$
ν_n=28
ε_2= 0.250 Δ_n=1.42 MeV λ_n=33.41
ε_4=-0.020 Δ_p=1.62 MeV λ_p=30.55
ε_6= 0.007 (L-N) a= 0.80 fm
T_{calc} = 508 (s)
$\Omega_n^{\pi} = 3/2^-$
$\Omega_p^{\pi} = 5/2^+$
$I^{\pi} = 4^-$
T_{calc} = 7.8 (s)
$\Omega_n^{\pi} = 3/2^+$
$\Omega_p^{\pi} = 5/2^+$
$I^{\pi} = 1^+$
Folded-Yukawa potential
$^{91}_{42}Mo \rightarrow {}^{91}_{41}Nb+e^+$
ε_2= 0.000 Δ_n=1.29 MeV λ_n=33.21
ε_4= 0.000 Δ_p=1.92 MeV λ_p=30.27
ε_6= 0.000 (L-N) a= 0.80 fm
Folded-Yukawa
$^{91}_{42}Mo^* \rightarrow {}^{91}_{41}Nb+e^+$
ν_n=20
ε_2= 0.000 Δ_n=1.29 MeV λ_n=33.21
ε_4= 0.000 Δ_p=1.92 MeV λ_p=30.27
ε_6= 0.000 (L-N) a= 0.80 fm
T_{calc} = 85.1 (s)
$\Omega_n^{\pi} = 9/2^+$
T_{calc} = 16.4 (s)
$\Omega_n^{\pi} = 1/2^-$
Gamow-Teller Strength
0
1
2
0
10
20
0
5
10
Excitation Energy (MeV)

Figure 23

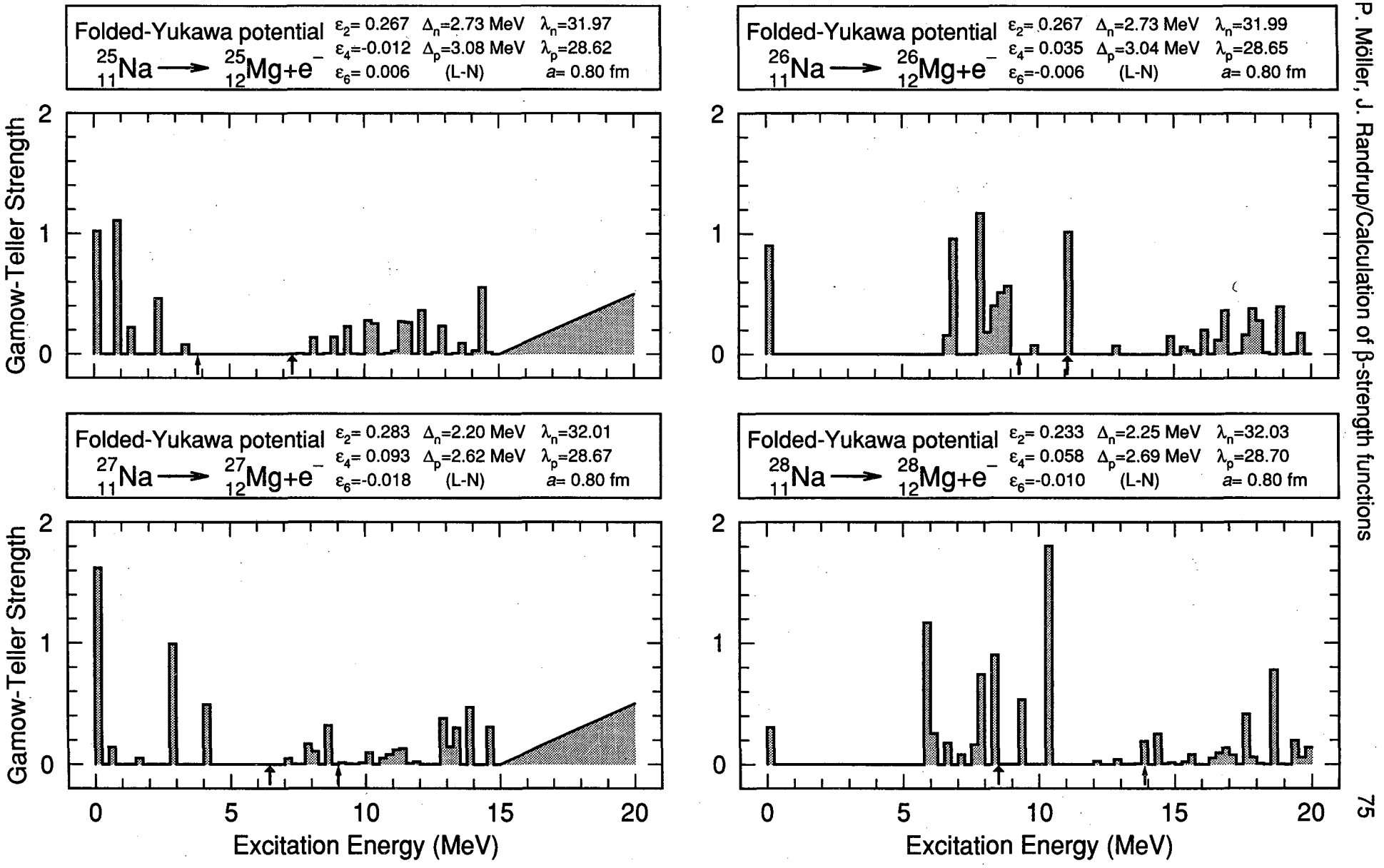
Folded-Yukawa potential
$^{25}_{11}Na \rightarrow {}^{25}_{12}Mg+e^-$
ε_2= 0.267 Δ_n=2.73 MeV λ_n=31.97
ε_4=-0.012 Δ_p=3.08 MeV λ_p=28.62
ε_6= 0.006 (L-N) a= 0.80 fm
Folded-Yukawa potential
$^{26}_{11}Na \rightarrow {}^{26}_{12}Mg+e^-$
ε_2= 0.267 Δ_n=2.73 MeV λ_n=31.99
ε_4= 0.035 Δ_p=3.04 MeV λ_p=28.65
ε_6=-0.006 (L-N) a= 0.80 fm
Folded-Yukawa potential
$^{27}_{11}Na \rightarrow {}^{27}_{12}Mg+e^-$
ε_2= 0.283 Δ_n=2.20 MeV λ_n=32.01
ε_4= 0.093 Δ_p=2.62 MeV λ_p=28.67
ε_6=-0.018 (L-N) a= 0.80 fm
Folded-Yukawa potential
$^{28}_{11}Na \rightarrow {}^{28}_{12}Mg+e^-$
ε_2= 0.233 Δ_n=2.25 MeV λ_n=32.03
ε_4= 0.058 Δ_p=2.69 MeV λ_p=28.70
ε_6=-0.010 (L-N) a= 0.80 fm
Gamow-Teller Strength
0
1
2
0
5
10
15
20
Excitation Energy (MeV)

Figure 24

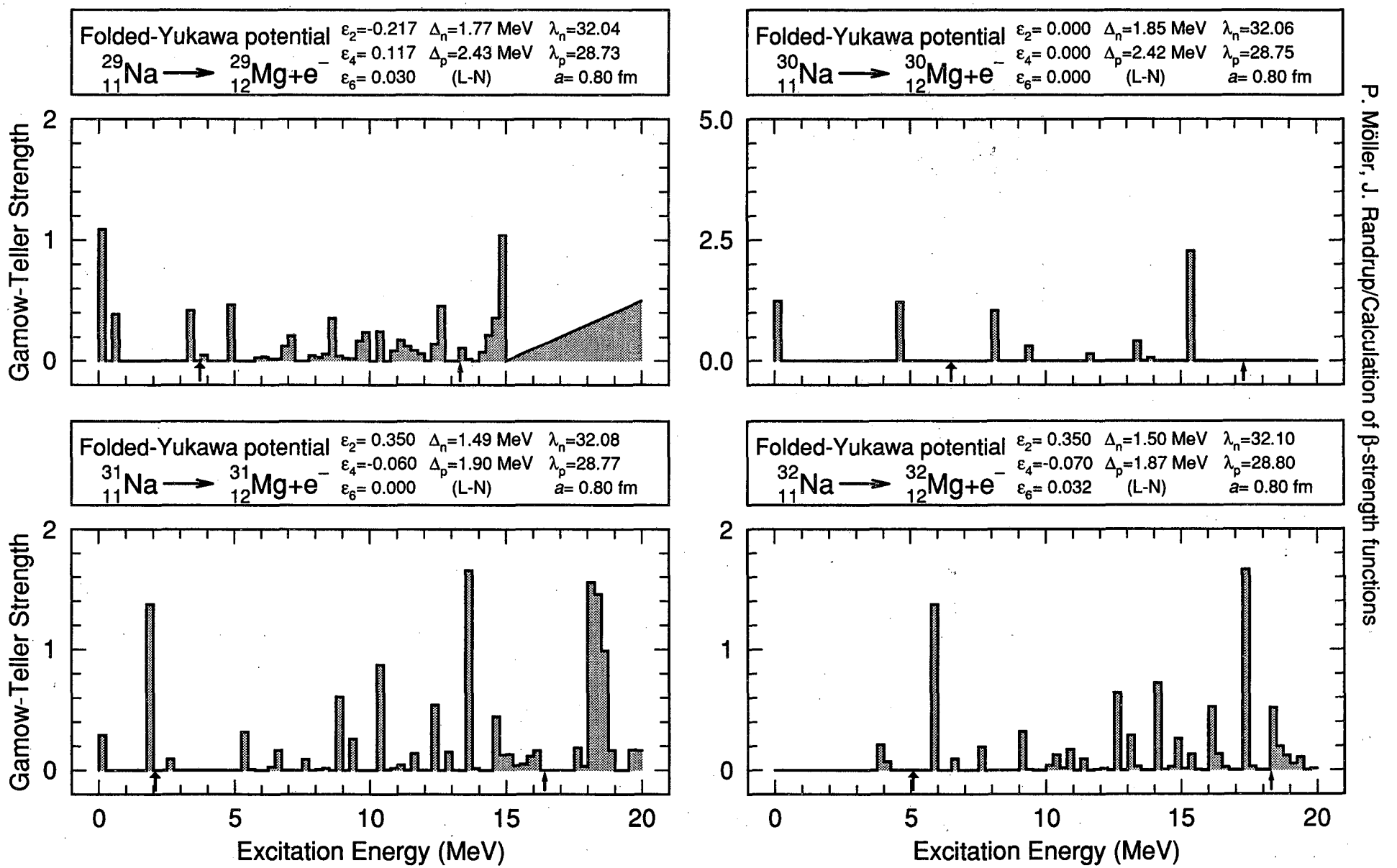
Folded-Yukawa potential
29 11Na → 29 12Mg+e−
ε2=-0.217 Δn=1.77 MeV λn=32.04
ε4= 0.117 Δp=2.43 MeV λp=28.73
ε6= 0.030 (L-N) a= 0.80 fm
Folded-Yukawa potential
30 11Na → 30 12Mg+e−
ε2= 0.000 Δn=1.85 MeV λn=32.06
ε4= 0.000 Δp=2.42 MeV λp=28.75
ε6= 0.000 (L-N) a= 0.80 fm
Folded-Yukawa potential
31 11Na → 31 12Mg+e−
ε2= 0.350 Δn=1.49 MeV λn=32.08
ε4=-0.060 Δp=1.90 MeV λp=28.77
ε6= 0.000 (L-N) a= 0.80 fm
Folded-Yukawa potential
32 11Na → 32 12Mg+e−
ε2= 0.350 Δn=1.50 MeV λn=32.10
ε4=-0.070 Δp=1.87 MeV λp=28.80
ε6= 0.032 (L-N) a= 0.80 fm
Gamow-Teller Strength
Excitation Energy (MeV)

Figure 25

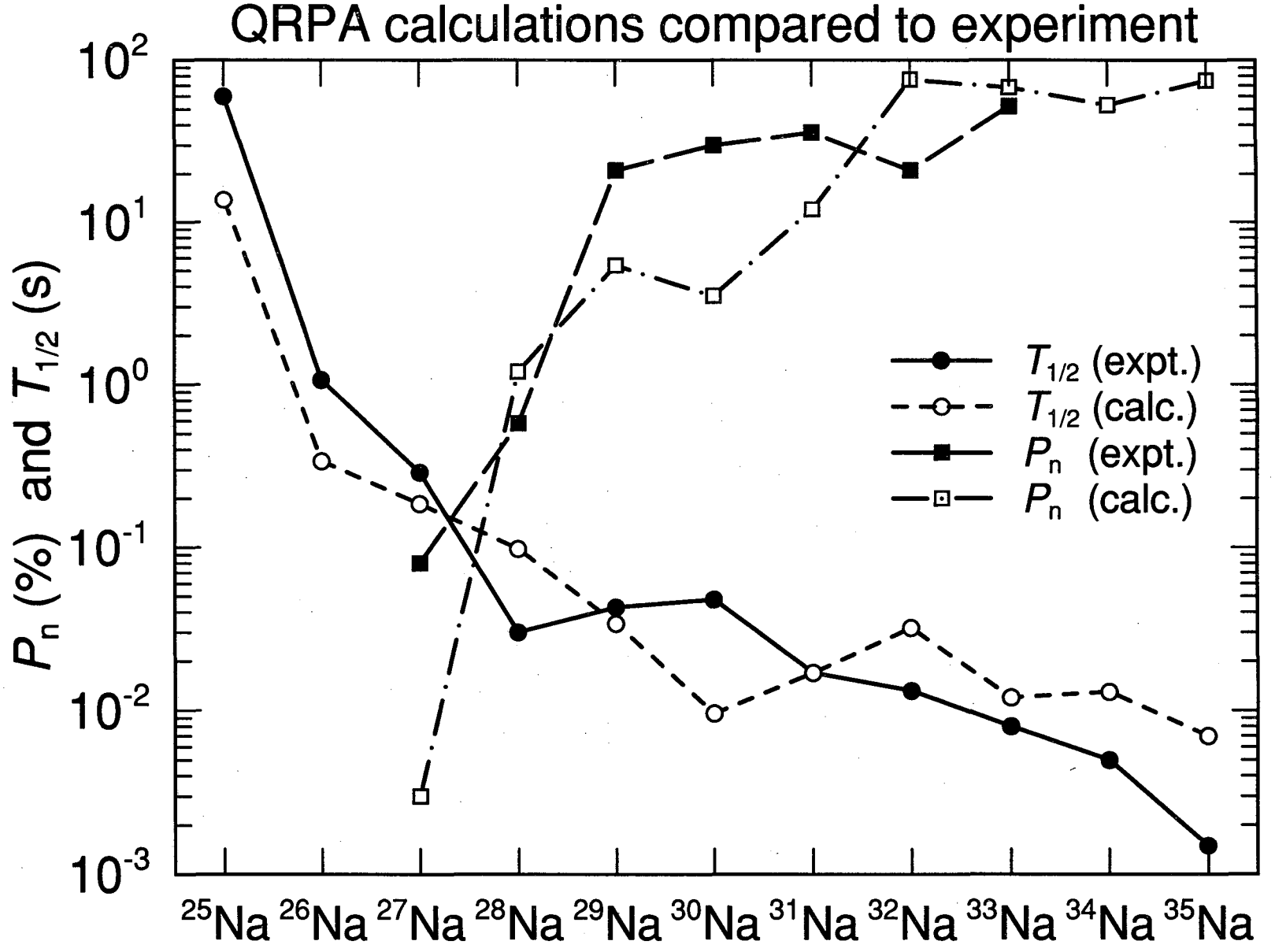
QRPA calculations compared to experiment
P_n (%) and $T_{1/2}$ (s)
10^2
10^1
10^0
10^{-1}
10^{-2}
10^{-3}
$T_{1/2}$ (expt.)
$T_{1/2}$ (calc.)
P_n (expt.)
P_n (calc.)
^{25}Na ^{26}Na ^{27}Na ^{28}Na ^{29}Na ^{30}Na ^{31}Na ^{32}Na ^{33}Na ^{34}Na ^{35}Na

Figure 26

LAWRENCE BERKELEY LABORATORY
TECHNICAL INFORMATION DEPARTMENT
1 CYCLOTRON ROAD
BERKELEY, CALIFORNIA 94720